Design and Development of High Gain Wideband Microstrip Antenna and DGS Filters Using Numerical Experimentation Approach

Dissertation

zur Erlangung des akademischen Grades

Doktoringenieur

(Dr.-Ing.)

von **MSc. Adel Bedair Abdel-Mooty Abdel-Rahman**

geb. am 05.08.1968 in Aswan

genehmigt durch die Fakultät Elektrotechnik und Informationstechnik der Otto-von-Guericke-Universität Magdeburg

Gutachter: Prof. Dr. A. S. Omar

Prof. Dr. B Michaelis

Doc. Ing. J. Machac, DrSc.

Promotionskolloquium am 01.06.2005

ACKNOWLEDGEMENTS

All gratitude is due to " *ALLAH* " who guides me to bring forth to light this thesis.

Pursuing Ph.D in Microstrip antennas and DGS compact Microstrip filters is one of the most valuable and exciting experiences in my education. The knowledge I learned and confidence I gained during the study years will be beneficial to my whole life.

I am greatly indebted to my supervisor, Prof. Dr.-Ing. A. S. Omar, who takes so much effort and patience in mentoring me to become a qualified researcher. From leading me at the beginning into the Maxwell domain and then step by step to its actual application in Antennas and Filters, to revise my poorly written papers and edited presentations. Prof. Omar gave me direction in every step of my thesis work, while never forgetting trivial details. It is his insight and wide knowledge that guided me to the completion of this thesis work. Due to his broad research interests, he gave me the opportunity to explore many interesting antennas, low-pass and band-pass filters.

I am also grateful to Prof. Dr.-Ing. Habil. Bernd Michaelis, University of Magdeburg, and Prof. Doc., Ing., DrSc. Jan Machac, Czech Technical University, for kindly agreeing to be referees for this thesis in spite of their hectic schedules.

I also want to thank Prof. A. K. Verma who is with the Department of Electronic Science, University of Delhi, New Delhi, India for his interest in Microstrip antennas and filters and helpful discussion even face to face or by e-mail.

Great of thanks and very deep appreciation to Assist Prof. G. Kirov for his guide and deeply discussion in antennas.

Deep thanks to Prof. G. Nadim, Cairo University, Cairo, Egypt for his help and support.

I would like to thank Dr. H. Holub, Dr. H. Bresch, Dr. A. Jöstingmeyer and Dr. T. Meyer for their continuous help.

I also appreciate the support I received from all engineers and technicians in the workshop, in particular, Mr. H. Rodiek and Mr. D. Salbert.

I always feel lucky to be with so many excellent researchers in Prof. Omar's group. I sincerely thank A. Boutejdar for being a good partner in the filter part work and earnest colleague with whom I had so many intensive discussions. Many thanks go to Nick, whose enormous contributions to the measurement lab greatly facilitated the progress of my work.

Finally, I would like to thank my family and friends. I am very grateful to my father and my mother who encourage and support me during their life time. I owe all my achievement to my wife and children, who share all my joy and bitterness every day and night. Again, thanks to all my friends: Omar Ali, Ehab Hamad, A. Bandyopadhyay, M. Anis, A. Teggatz, F. Abu-Jarad, Ali Aassie, A. Slavova and A. R. Ali for their support.

Abstract

This work covers two aspects of microwave communication technology. The first is the analysis and design of new wideband high gain microstrip antennas and the second aspect is the design of compact high performance low-pass and band-pass filters. We have introduced the resonating coupling slot in the aperture coupled microstrip antenna to increase its bandwidth. A new method is reported for impedance matching of the antenna structure with 50-Ohm microstrip feed line. Also we have developed the concept of the short surface mounted horn to increase the gain without adversely affecting its bandwidth. By inserting the horn into the substrate, the gain of the patch antenna has been increased by more than 6 dB. The surface mounted horn has been applied around the four and eight element arrays. An increase of 3.5 dB in gain has been obtained with the horn frame around the array elements. For the compact microstrip based filter design we have adopted the defected ground structure (DGS). We have shown that proper selection of the shape and position of DGS slot is important for the improved performance of the low-pass filter in the stop and transition bands. We have also introduced the band-pass structure in the DGS configuration and used it to design a new compact band-pass filter.

Table of Contents

1. Introduction 1

1.1 Antennas 6

1.2 Filters 12

1.3 Organization of the Thesis 15

2. Single Element Aperture Coupled Microstrip Antenna 17

2.1 Introduction 17

2.2 Microstrip Antenna Feeds 18

2.3 Aperture Coupled Microstrip Antennas 21

2.3.1 Linearly Polarized Microstrip Antenna 22

2.3.1.1 Antenna Design 23

2.3.2 Analysis and Simulation 41

2.3.2.1 Matching Characteristics 41

2.3.2.2 Far-Field Characteristics 42

2.3.3 Practical Implementation 43

2.3.4 Experimental Results 46

2.3.4.1 Measured Matching Characteristics 46

2.3.4.2 Measured Radiation Characteristics. 48

2.4 Impedance Matching Improvement for a Class of Wideband Antennas 50

2.4.1 Description of The Proposed Solution 50

2.4.1 Results 54

3. Defected Ground Structure Low-pass and Band-pass Filters 57

3.1 Introduction 57

3.2 Filter Implementation 59

3.2.1 Illustration Example 60

3.3 Defected Ground Structure Filters 62

3.3.1 Frequency Characteristics of DGS Unit Section 62

3.3.2 Modeling and Parameter Extraction 63

3.4 Study of Different DGS Slots Configuration 66

3.4.1 Rectangular Slot 68

3.4.2 Dumb-bell Slot. 70

3.4.3 Square Head Slot 74

3.4.4 Arrow Head Slot 78

3.5 Stepped-Impedance Low-Pass Filter 86

3.6 Stepped Impedance Low-Pass Filter Using DGS Slots 88

3.6.1 Study of DGS Slot Position on 3-Pole Hi-Lo LPF 88

3.6.2 Fabrication and Measurement of 3-Pole Hi-Lo LPF 91

3.7 Frequency Characteristics of DGS Unit Section with Cutting Gap in the 50 Ω Line 95

3.7.1 Modeling of DGS Based Band- Reject and Band- Accept (Band-Pass) Components 96

3.7.2 The 3-Pole Band-Pass Filter 98

3.7.3 Fabrication and Experimental Results 99

4. Microstrip Antenna Gain Enhancement Technique Using Quasi-Planar Surface Mounted Horn 103

4.1 Introduction 103

4.2 Aperture Coupled Microstrip Antenna with Quasi-Planar Surface Mounted Horn 105

4.2.1 Numerical Experimentation 105

4.2.2 Fabrication and Measurement 109

4.3 Aperture Coupled Microstrip Antenna with Quasi-Planar Conical Surface Mounted Horn 113

4.4 High Gain Wideband Probe Feed Compact Microstrip Antenna With Quasi- Planar Surface Mounted Horn 117

4.4.1 Numerical Experimentation 117

4.4.2 Fabrication and Measurement 120

4.4.3 Gain Behavior of Inserted Horn 125

5. Gain Enhancement of Microstrip Antenna Array Using Surface Mounted Horn 127

5.1 Patch Antenna Array 127

5.1.1 Array Feeds 128

5.1.2 T-junction 129

5.1.3 Power Divider 131

5.1.4 Aperture Coupled Microstrip Antenna Array with Surface Mounted Horn 132

5.1.5 Fabrication and Experimental Results 132

5.2 Gain Enhancement of Microstrip Antenna Array Using Surface Mounted Horn 136

5.2.1 Numerical Experimentation 137

5.2.2 Fabrication and Experimental Results 140

6. Summary and Suggestions for Future Work 145

6.1 Antennas 145

6.2 Filters 146

6.3 Suggestions for Future Work 147

CHAPTER 1

Introduction

This work presents two aspects of microwave communication technology. The first is the design of new wideband high gain microstrip antenna and the second is that of compact high performance low-pass and band-pass filters.

In this brief introduction we describe the basic RF stages of wireless transmitters and receivers, and provide an introductory discussion of the main RF and microwave components that are used in these systems. Applications of microwave components such as microstrip *antennas* and *filters* will be considered. In the next chapters we will introduce the analysis and design of these components in much more detail, so the purpose here is simply to provide an initial broad view. In this way it will be easy to see the larger context in which these individual components are used in practical microwave communication systems. The function of an antenna is to convert an RF signal from a transmitter to a propagating electromagnetic wave or, conversely, convert a propagating wave to an RF signal in a receiver as shown in Fig. 1.1.

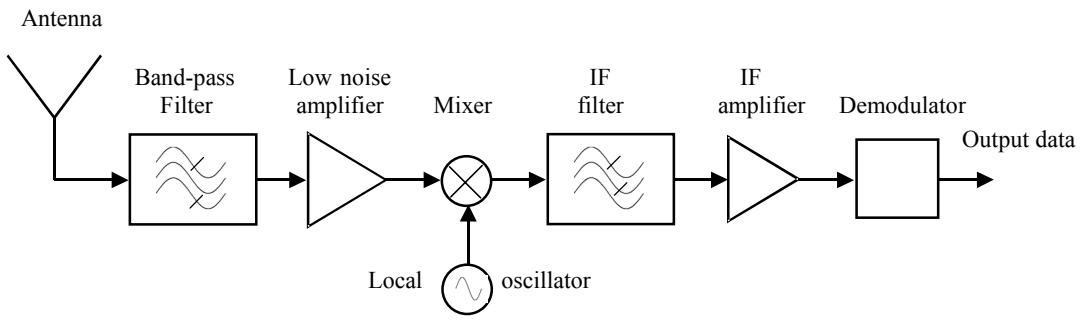

Figure 1.1 Block diagram of a basic radio receiver

One of the antennas that can be used is shown in Fig. 1.2 e.g., Fig. 1.3 shows a metallic high gain circular Ku-band horn antenna and an equivalent aperture coupled microstrip antenna (ACMA) with PVC horn. The latter is advantageous, as waveguide technology elements are typically heavy, bulky, and difficult to integrate with other elements such as amplifiers.

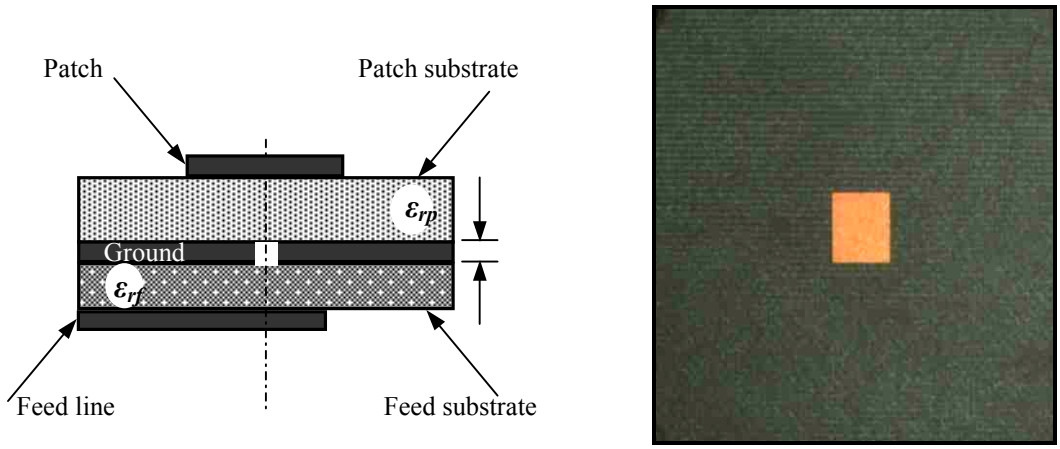

Microstrip antenna geometry

Photograph of a microstrip antenna

Figure 1.2 Single element microstrip antenna

As may be noticed from Fig. 1.3, the ACMA is much more compact despite the fact that the gain and bandwidth of both antennas are comparable. The ACMA is one of the topics which will be considered in details in this thesis.

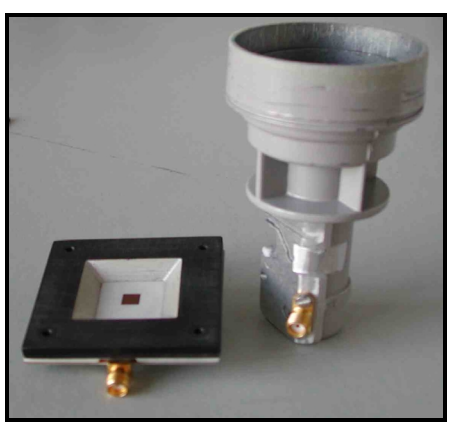

Figure 1.3 Photograph of metallic Ku-band horn and ACMA with PVC horn

More sophisticated antennas are able to change the direction of their main beam electronically. Such antennas are called phased arrays, and in the past have generally been limited to use in military systems because of their high cost. In e.g. mobile communication phased array antenna beam can be directed towards a given user, while avoiding interference with other users. Such systems are called adaptive arrays, or sometimes smart antennas. Fig. 1.4 shows a photograph of a 4x4 element antenna array which can be steered in this way. Fig. 1.5 shows a patch antenna array on a laptop, which represents another application of microstrip antennas.

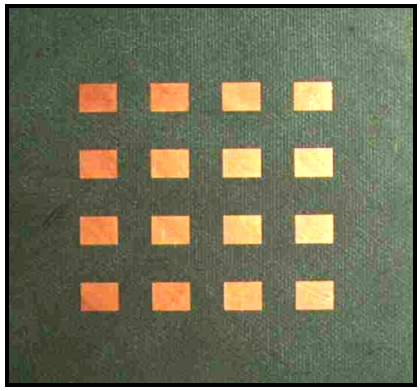

Figure 1.4 Photograph of a 4x4 element microstrip antenna array

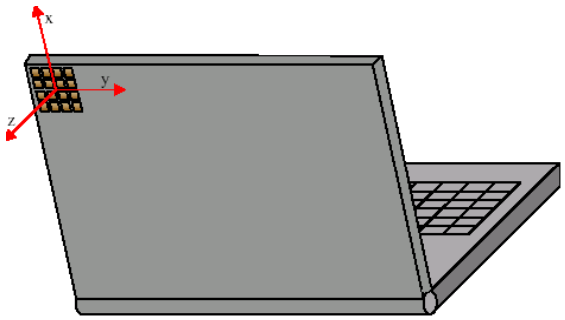

Figure 1.5 Microstrip antenna array on a laptop

As an example for antenna array with steerable beams, we consider a mobile satellite communication system as shown in Figure 1.6. The system consists of a satellite, a gateway earth station, and various mobile earth stations such as aircraft, ships, land vehicles, and portable terminals. The communication from the earth to the satellite is called uplink, and that from a satellite to the earth is called downlink. On the other hand a communication link between a gateway earth station and a satellite is called a feeder link. Some frequency

ranges used in mobile satellite communications are C, Ku, Ka-bands with the frequencies shown in Table 1.1. The vehicular satellite communication and automotive radar applications require lightweight and low cost antennas with the possibility of conformal integration. As shown in Fig. 1.6, The microstrip antenna array is a good choice for these applications.

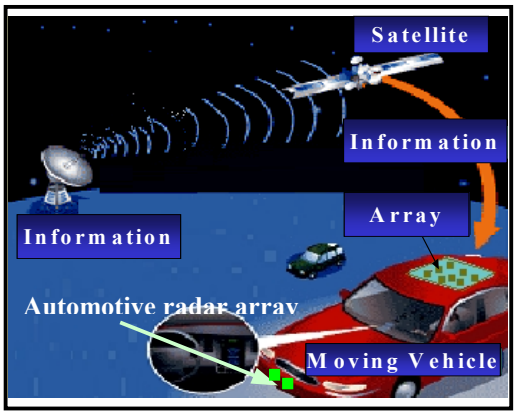

Figure 1.6 The concept of mobile satellite communication system

Table 1.1 Broadcast Electromagnetic Spectrum

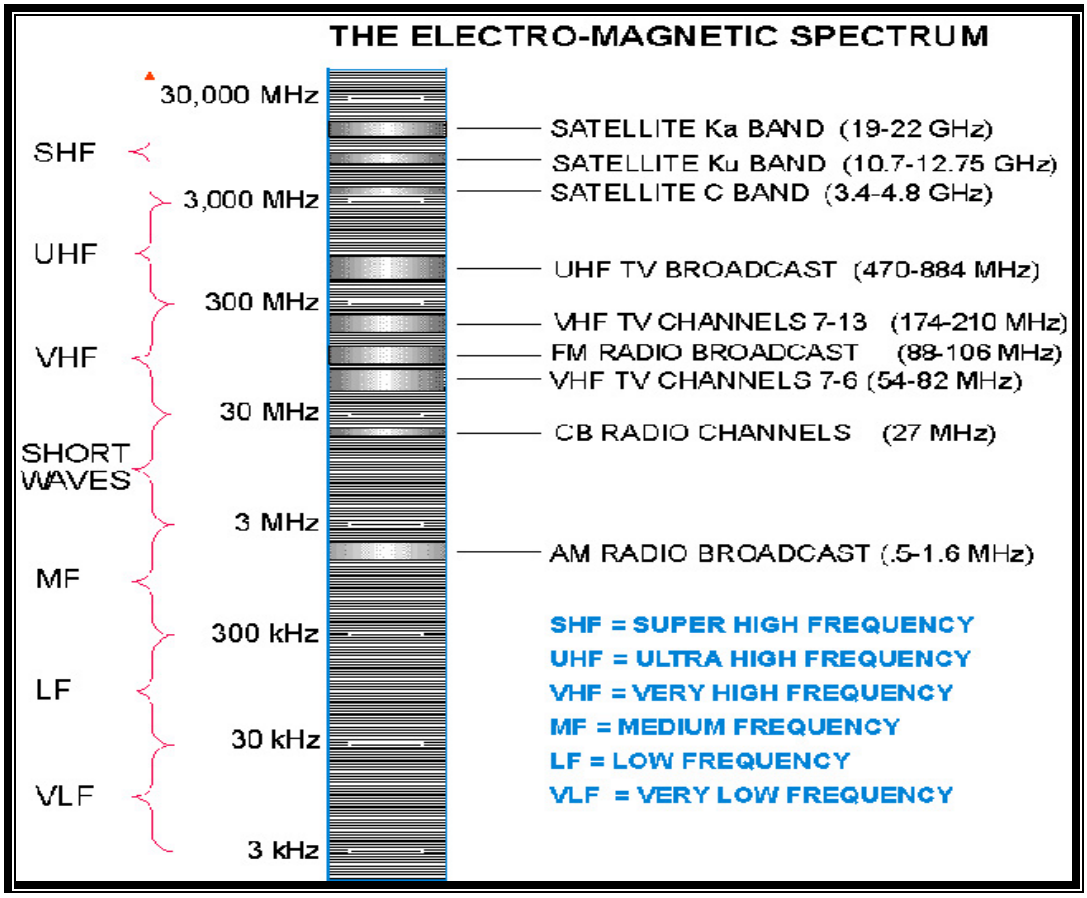

Besides the antenna issue, the filter topic is considered in details in this work. Filters are used to pass or eliminate specific frequency bands. Filters are classified as low-pass (LP), high-pass (HP), band-pass (BP), and band-stop (BS). Some applications of filters are:

LPF: are used, e.g.,

at the output of an oscillator to eliminate the harmonics generated by the nonlinearity of the oscillator;

at the output of a mixer to pass only the intermediate frequency;

at the input of a receiver to reject the unwanted higher frequencies;

in conjunction with a HPF to realize a wideband band-pass filter.

BPF: are used, e.g., at

the output of an oscillator to pass the required frequency band only;

the input of a receiver and the amplifier to pass the required frequency band only.

HPF: are used, e.g., at

the output of a multiplier to eliminate the lower frequencies;

the input of a receiver to reject the unwanted lower frequencies.

BSF: are used, e.g., at

the output of an oscillator to eliminate the harmonic frequencies together with LPF.

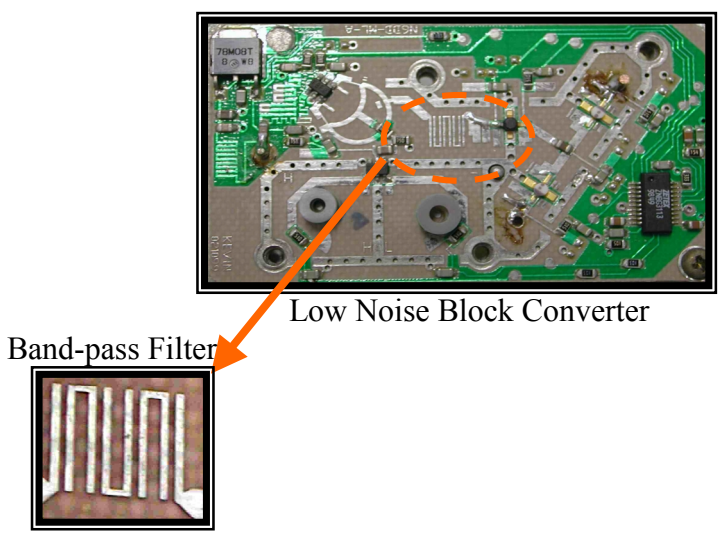

Figure 1.7 Photograph of Ku-band LNB with microstrip band-pass filter

As an example for a BPF, Fig. 1.7 shows a low noise block converter (LNB) which is usually used as a front end in satellite receiver systems. The filter suppress or filter out all frequencies except the required frequency. Fig. 1.8 shows a photograph of the used C-band band-pass filter.

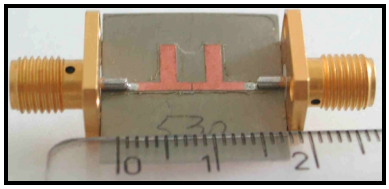

Figure 1.8 Photograph of a compact C-band band-pass filter

In the previous brief introduction we described some applications of microstrip *antennas* and *filters.* The following two sections introduce the antennas and filters state of the art.

1.1 Antennas

An antenna serves as the "transition" between the RF front-end circuitry and the radiation and propagation of electromagnetic waves in free space. Antennas play a critical role in microwave and other wireless applications systems. Planar oriented antennas, such as microstrip patch and printed dipole have attracted significant attention among antenna engineers due to the tremendous benefits they bring to modern wireless systems in comparison to more conventional designs.

Since the late 1970s, the international antenna community has devoted much effort to the theoretical and experimental research on the microstrip patch antennas. The microstrip antenna is probably the simplest yet most popular planar antenna. In its simplest form, the patch antenna can be realized by etching a rectangular metal pattern on a dielectric substrate. These antennas are:

- low profile;
- lightweight antennas;
- most suitable for aerospace and mobile applications;
- easily integrated with electronic components;
- easily integrated into arrays.

Microstrip antennas have matured considerably during the past 25 years. The results of the research have contributed to overcome many of their limitations and to the success of these antennas not only in military applications such as aircraft, missiles, and rockets but also in commercial areas. During the past few years there has been an explosion in commercial applications involving RF and microwave systems. Industrial applications such as satellite data transfer, vehicle tracking, and personal paging have been among the first to be developed. Another early application is the mobile telephone. The future will see even further penetration of RF and microwave systems into both the workplace and personal lives. Direct broadcast television (DBS) and digital audio broadcast (DAB) allow reception of entertainment virtually anywhere. Wireless local area networks (WLANs) and personal communications systems (PCS) provide untethered data transfer and communications. The intelligent vehicle highway of the future will guide us through traffic jams and tell us about services along the way. Finally, systems using GPS and other techniques not only tell us where we are going but where we should be going.

Most of these commercial systems must be low-cost, easy to use, small in size, and rugged to achieve wide acceptance. Low cost demands easily produced components. The drive for smaller systems pushes not only the integrated circuit technology but also antenna technology. Small, conformal antennas are aesthetically pleasing and increase product ruggedness by avoiding antenna breakage. Many applications currently use straightforward antennas (for example reflectors) partly because they are well understood and relatively easy to design. Reflector systems have been used in optical devices (telescopes, microscopes, etc.) for centuries. They are simple means of generating a large radiating aperture, which results in a high gain and narrow beamwidth. The most common is the "satellite dish" a single surface parabolic reflector.

The advantages are:

- Simple
- Broadband (provided that the feed antenna is broadband)
- Very large apertures possible

The disadvantages are:

- Slow beam scanning
- Mechanical limitations (wind resistance, gravitational deformation, etc.)

- Surface roughness must be controlled
- Limited control of aperture illumination

As customers demand smarter, smaller lower cost products, more innovative antennas will be required. Microstrip antennas are ideal for these applications. They are very thin. They are compatible with IC technology in the sense that they readily interface with IC interconnects. They can even be made part of the chip. Most importantly, microstrip antennas are manufactured with printed circuit techniques and, therefore, are very low in cost.

Two parameters usually come first in relation with the design and analysis of any antenna structure. The first is its radiation patterns, which essentially determine how the radiated electromagnetic fields can be controlled by antenna. Other important parameters to describe the antenna radiation properties include directivity, gain, radiation efficiency, front-to-back ratio, cross polarization level, axial ratio (for circularly polarized antenna), as well as side lobes for the case of an array antenna.

The other important parameter in antenna analysis is the input impedance, or equivalently the input return loss, which describes how well the antenna, is matched with its feeding network. The impedance bandwidth is another important parameter. As wireless communication applications require more and more bandwidth such as high data rate communication systems, the demand for wideband antenna increases as well. One of the major disadvantages of microstrip antennas is their inherent narrow bandwidth. The narrow impedance bandwidth is ultimately a consequence of its electrically thin ground- plane-backed dielectric substrate, which leads to a high-resonance behavior. Bandwidth improves as the substrate thickness is increased. A thick substrate will support surface waves, which will deteriorate the radiation patterns as well as reduce the radiation efficiency. Also problems with the feeding technique of the antenna appear. The impedance bandwidth of a typical microstrip patch radiator is less than 1% to several percent for substrates satisfying the criteria $h/\lambda_0<0.023$ for $\varepsilon_r=10.2$ to $h/\lambda_0<0.07$ for $\varepsilon_r=2.3$, where h is the substrate thickness, ε_r is the relative substrate permittivity, and λ_0 is the free space wave length [1].

The variety of methods proposed for impedance bandwidth enhancement may be categorized according to the following three approaches [2]:

- Multiple resonances (Stacked patch configuration)

This approach has been applied to various shapes of microstrip antennas. Some of the implementations of these techniques employ two or more resonant elements, with slightly different resonant frequencies, proximity coupled to each other. Coupling is controlled to increase the bandwidth. Usually only one element (a driven element) is fed directly, with the other elements (parasitic elements) being coupled by proximity effects. The parasitic elements can be disposed in the same level as a driven element [3]-[4] or in different levels (parasitic stacked elements). Impedance bandwidths of 18 % to 67 % have been achieved with aperture-coupled stacked patches [5]-[12]. It is possible to excite two independent modes in the same patch or in the patch and the feed network. A nearly square patch has been used to obtain almost three times the bandwidth by exciting two modes with orthogonal polarizations [13]. To excite both the modes, the feed in this case, is located along the diagonal. Other configuration consists of a rectangular patch with a U slot embedded in it [14]-[17]. The patch and the slot are designed to produce resonances close to each other. Utilizing a foam substrate of thickness 16.5 mm a 10-dB return loss bandwidth of about 32 % near 1.5 GHz is achieved. Dubost [18] also has developed a wideband patch loaded with an H-shaped slot.

- Impedance matching

The second method is by means of a wideband matching network. This is the most common and direct technique to influence the impedance behavior in a frequency range. The matching devices must be mounted as close as possible to the radiating patch to increase the total antenna efficiency. A bandwidth of about 10 % to 12 % is obtained by Pues and Van Capelle [19] using a passive coplanar matching network. Similar techniques by Paschen [20] produce a bandwidth of more than 25 %. Using a 3-D tapered transition between a probe feed and a suspended rectangular patch an impedance bandwidth of about 90 % is obtained [21].

- The use of lossy materials

It is possible to increase an impedance bandwidth by introducing loss into antenna system, but at the expense of decrease in radiation efficiency [2]. The losses can be in the form of lossy substrate materials, layer of lossy film, or a discrete chip resistor. For instance, a 1 ohm chip resistor mounted at the edge of the patch increases the bandwidth by 4.9 times [22]. The reduction in antenna gain due to resistive loading is estimated to be about 2 dB.

By introducing losses into the antenna system, the bandwidth can be increased but the efficiency will also reduce.

The patch antenna can be fed either by a coaxial cable from the backside, or by a microstrip line fabricated on the same side of the substrate [23]. The patch antenna can also be fed through a coupling aperture using a multi-layer substrate configuration. This type of feed arrangement allows physical separation of the two functions and the use of optimal substrates for the radiator and transmission line. The characteristics of the microstrip antennas can be significantly improved by using multi-layered structures with thick substrates and low-permittivity materials, which usually leads to a significant increase in its frequency bandwidth [24]. By using a more complex structures, a bandwidth in excess of 20 % can be achieved [25]-[26]. These antennas use the SSFIP (Strip-Slot-Foam-Inverted-Patch) principle and have a complex configuration and deterioration of characteristics, such as size, high and radiation patterns.

In [27] we introduced a wide bandwidth aperture coupled microstrip antenna. By choosing the suitable substrates relative permittivity and thickness, a bandwidth of 12.4 % has been obtained from a simple aperture coupled microstrip antenna. This bandwidth is the maximum that one can get from the non multilayer structures.

For many applications such as satellite communications and mobile radio, for which printed antennas are otherwise well-suited, low gain may be a serious disadvantage.

The electromagnetically coupled stacked patch antenna has been investigated to improve the gain and bandwidth the microstrip antenna. An experimental study of a two layer electromagnetically coupled rectangular patch antenna excited in the TM_{01} mode has been reported in [28]. The two layers are separated by a distance, s. Depending on the spacing s, the characteristics of the antenna can be divided into three regions. The first one occurring when s is between 0 and 0.14 λ_0, the radiation patterns have good broadside features and the beams are not symmetrical in E and H-planes. The bandwidth rises to 13 % at s =0.017 λ_0 and the gain is about 7 dB. The second one occurring when s is between 0.158 λ_0 and 0.2966 λ_0, the E-plane patterns show a dip at broadside and the bandwidth is less than 2 %. Little advantage is gained in operating the antenna in this region. The third region which begins at 0.31 λ_0, the patterns return to the normal shape and the gain increased to 8.9 dB and the bandwidth is about 1.3 %. In conclusion, the electromagnetically coupled

rectangular patch antenna structure can be optimized either for the gain or for the bandwidth but not for both. A method that improves gain significantly for printed antennas is discussed in [29], [30]. This method involves the addition of a superstrate or cover layer over the substrate. It is referred to as the resonance gain method, and it utilizes a superstrate with either $\varepsilon >>1$ or $\mu >>1$. By choosing the layer thickness and patch position properly, a very large gain may be realized at any desired angle θ. The gain varies proportionally to either ε or μ, depending on the configuration. However, the bandwidth is seen to vary inversely to gain so that a reasonable gain limit is actually established for practical antenna operation. A theoretical investigation of the resonance gain conditions has been done in [31]. To achieve directive gain of about 20 dB, impractical superstrate permittivity and or permeability values are needed. An extension of the results found in [31] has been done in [32] so that a practical low loss material can be implemented using multiple superstrates. The narrow-bandwidth resonance gain phenomenon is shown to be attributable to the excitation of weakly attenuated leaky waves on the structure [33].

More efforts have been made to increase both the gain and bandwidth with the help of stacked parasitic patch. However, this structure can be optimised either for the gain or for the bandwidth. Likewise, the cavity backed microstrip antenna with multiple layers of dielectric can improve the gain, however the bandwidth is very limited [34]. There is need to increase the gain of radiating patch element without sacrificing the bandwidth.

We have introduced in this thesis the resonating coupling slot for the aperture coupled microstrip antenna to increase the bandwidth and the short surface mounted horn to increase the gain of the patch antenna [35]. This new combination of the aperture coupled microstrip antenna and the quasi-planar surface mounted short horn is demonstrated to increase the gain of the patch antenna by 4.2 dB. The structure has a fractional bandwidth of 12.4 % at a center frequency of 11.8 GHz. The horn improves the gain without adversely affecting the bandwidth. The presence of the quasi-planar surface mounted horn has improved the back-lobe level by 5.4 dB.

The vehicular satellite communication and automotive radar applications require lightweight, compact, and low cost antennas with possibility of conformal integration. As we know, the microstrip antenna is a good choice. However, they have typical gain of about 6dBi only. Thus high gain array requires more number of elements. The losses associated

with the feed network will increase by increasing the array elements. The measured gain of single element aperture coupled microstrip antenna is around 6 dB. In case of four element, the theoretical gain will be 6 dB+6 dB =12 dBi. The measured gain of the four elements is 10.5 dBi. I.e. 1.5 dB has been lost. The surface mounted horn has been applied around the four element linear array. 3.5 dB more gain has been obtained with the horn frame around the array elements [36].

1.2 Filters

Filters play important roles in many RF/microwave applications. They are used to separate or combine different frequencies. The electromagnetic spectrum is limited and has to be shared; filters are used to select or confine the RF/microwave signals within assigned spectral limits. Emerging applications such as wireless communications continue to challenge RF/microwave filters with ever more stringent requirements higher performance, smaller size, lighter weight, and lower cost. Depending on the requirements and specifications, RF/microwave filters may be designed as lumped element or distributed element circuits; they may be realized in various transmission line structures, such as waveguide, coaxial line, and microstrip.

The recent advance of novel materials and fabrication technologies, including MMIC and MEMS has stimulated the rapid development of new microstrip and other filters. In the meantime, advances in computer-aided design (CAD) tools such as full-wave electromagnetic (EM) simulators have revolutionized filter design. Many microstrip filters with advanced filtering characteristics have been appeared.

The lumped-element filter design generally works well at low frequencies, but two problems arise at microwave frequencies. First, lumped elements such as inductors and capacitors are generally available only for a limited range of values and are difficult to implement at microwave frequencies, but must be approximated with distributed components. In addition, at microwave frequencies the distances between filter components is not negligible.

The lumped-element filter design can be approximated with the transmission line structure. However, agreement of filter response is only in the pass band. In the stop band the transmission line based LPF departs from the response of the lumped element LPF and the stop bands response of the transmission line based LPF degrades. A quasi-lumped element

based on the photonic band gap (PBG) ground plane and the defected ground structures (DGS) have been proposed to improve the stop band characteristics of the low-pass filter [37]-[44].

Several compact and high performance components have been reported by using the generic structure called the defected ground structure (DGS) for the microstrip line. Another type of structures, known as electromagnetic bandgap (EBG) or alternatively called photonic band gap (PBG) structures have periodic structure are also reported in the literature. These structures are etched as the defects in metallic ground plane of the microstrip line. Recently, there has been an increasing interest in microwave and millimeter wave applications of PBG in antennas, filters, and other devices [45]-[54]. Not only the PBG structures, which have a periodic structure [46], [50], [55]-[57], have been known as providing rejection of certain frequency bands but also non periodic structures have been suggested. Since DGS cells have inherently resonant property, many of them have been applied to filter circuits [37], [42], [58], [59], [60]. So, various shapes of DGS structures, such as rectangular [37], [58]-[59], square [61]-[62], circular [46], modified dumbbell [37], [43], [63], and combined structures [46], [62]-[64] have been appeared in the literature.

However, it is difficult to use a PBG structure for the design of the microwave or millimeter wave components due to the difficulties of the modeling. There are many design parameters, which have an affect on the bandgap property, such as the number of lattice, lattice shapes, lattice spacing, and relative volume fraction. Another difficulty in using the PBG circuit is caused by the radiation from the periodic etched defects.

Many etched shapes for the microstrip could be used as a unit DGS. An etched defect in ground plane disturbs the shield current distribution in the ground plane. This disturbance can change the characteristics of the microstrip transmission line by modifying the line capacitance and inductance. Thus an LC equivalent circuit can represent the unit DGS circuit. The physical dimensions of the DGS unit affect the equivalent circuit parameters. It is one the purposes of this thesis to study different DGS slots and the effect of its shape on the equivalent circuit parameters and the response of the circuits. To design a circuit with DGS section, the equivalent circuit and parameters of the DGS section should be extracted. Using the 3D-EM Simulator derives the equivalent circuit of the DGS section. The equivalent circuit parameters are extracted from the response of the EM Simulator. A DGS

section can be used as a series element of a low-pass filter. The shunt capacitance can be implemented either by stub or low-characteristic impedance section [65].

The low-pass filter using the DGS slot in the ground plane has a number of attractive features that include the following:

- The structure is very simple and compact.
- The stopband is very wide and the rejection is better than that of a conventional low-pass filter.
- The insertion loss is low.

The researchers have commented that for the equal area of slot head, any shape of slot can be used [37]. However, equal area only ensures equal equivalent inductance at the cutoff frequency and not the identical response of the DGS circuit elements. Also a particular shape of the slot in the ground plane could be more appropriate to design a complete circuit on the same substrate. The shape, size and orientation of a slot can have influence on performance of the circuit. In this thesis, the response of four shapes of the DGS slot like rectangular, dumb-bell, square head slot and arrow head slot will be studied and parameters are defined to characterize them. A method to design low-pass filters using DGS on microstrip substrate has been proposed already by [37]. In this thesis the DGS will be used to improve the stop band characteristics of the stepped impedance microstrip LPF. By controlling the separation between the slots, we can improve the stop band characteristics. Thus a judicious choice of the separation between slots and offset of the slot head can improve the performance of the LPF with DGS [66], [67].

The exiting DGS configuration provides only the band-reject (band-stop) characteristic. In this thesis, a new DGS based band-pass configuration in a microstrip line will be introduced. Not only an etched lattice shape can achieve this new band-pass DGS unit element ground plane of the microstrip but also by providing a gap in the microstrip line. The characterization of a gap in a microstrip is useful in the design of dc blocks; end coupled filters, and coupling elements to resonators. The microstrip band-pass filter can be designed by the use of a cascade of half-wave resonators or by using the parallel coupled microstrip lines [68]-[80]. However, due to the periodicity of the distributed microstrip

lines with respect to frequency, these filters suffer from the spurious response in not desired passbands, as well as narrow bandwidth and radiation losses in the pass band [81].
The defected ground plane structures (DGS) have been proposed for suppression of spurious response in the LPF [37], [82] as well as in the coupled microstrip line band-pass filters [83], [84]. The new DGS unit section with cutting gap in the 50 Ω line has been used to design a band-pass filter [85]. This band-pass filter is based on creation of a series-resonance in the main 50Ω microstrip line and creation of attenuation pole in the shunt arm. A compact BPF based on this concept is reported in this thesis

1.3 Organization of the Thesis:

Chapter 1 gives an introduction and describes the associated problems with the microstrip antenna and also the associated problems with the microstrip filters. It presents a general review for the previous work and states the suggested new methods to overcome these associated problems.

Chapter2 presents a quick review of microstrip antenna feed structure and a summary of design equations. A wide band aperture coupled microstrip antenna is designed, simulated and measured in the Ku-band. We achieved wide band by a resonating slot in the common ground plane and a new method is reported for impedance match of the antenna structure with 50-Ohm microstrip feed line. The design is achieved by systematic application of the 3D EM-Simulator, Microwave studio.

Chapter 3 concentrates on basic limitations of classical microstrip line based low-pass and band-pass filters and way to improve the design by using the defected ground plane structures. New investigations are presented on the choice of geometrical shapes for the DGS structure as an element for the LPF. We have also introduced the new band-pass structure in DGS and used it for the development of a new compact BPF.

Chapter 4 introduces the surface mounted short horn with wideband aperture coupled microstrip antenna of chapter two in order to improve the gain by 4.5 dB without degrading the bandwidth and the return loss. It also presents the inserted horn, which improves the gain by 5.5 dB in case of thick substrate.

Chapter 5 gives an extension of the application of the surface mounted horn to 4x1 element linear array, 2x2 element planar array, and 4x2 element planar array to improve the gain of the array by 3.5 dB.

In chapter 6, summary and suggestions for future work are presented.

CHAPTER 2

Single Element Aperture Coupled Microstrip Antenna

This chapter presents a quick review of microstrip antenna feed structure and a summary of design equations. A wide band aperture coupled microstrip antenna is designed, simulated and measured in the Ku-band. The wide bands is achieved by a resonating slot in the common ground plane and a new method is reported for impedance match of the antenna structure with 50 Ohm microstrip feed line. The design is achieved by systematic application of the 3D EM-Simulator, Microwave studio.

2.1 Introduction

The demand for applications of the microstrip antenna has been increasing rapidly since its invention in 1953 [86],[87]. Because of their extremely thin profile (0.01 to 0.05 free-space wavelength), printed antennas have found main applications in military aircraft, missiles, rockets, and satellites. In the commercial sector, the adoption of the microstrip antenna has not been as rapid, primarily due to the cost of the substrate material, design, and manufacturing processes. In addition, the earlier popular terrestrial communication system's configuration and environment did not warrant the use of the Microstrip antenna. During the last decade, however, the cost to develop and manufacture the microstrip antenna has dropped significantly, because of the reduction in cost of substrate material and manufacturing process, and the simplified design process using newly developed computer aided design (CAD) tools. At present the CAD tools can help the designer to complete a microstrip element or array design in short time, while the old "cut and try" method may take several weeks to arrive the required characteristics. Furthermore, the current satellite communication applications benefit from the small size and low profile of the microstrip antenna. In the UHF cellular terrestrial communication system, with large amount of RF

power, the mobile unit can perform adequately with a very simple low-gain monopole antenna. However such monopole in L-band mobile satellite communications is not suitable because of the limited spacecraft solar-battery power and spacecraft antenna size. In this case, the mobile vehicle terminal requires a higher gain antenna, on the order of 10 dBi, to ensure an adequate system link margin. An antenna such as horn, helix or monopole array will be too bulky to cover a wide elevation angular region from 20 degrees to 60 degrees above the horizon with such a gain. However a low-profile printed microstrip array is suitable for such application.

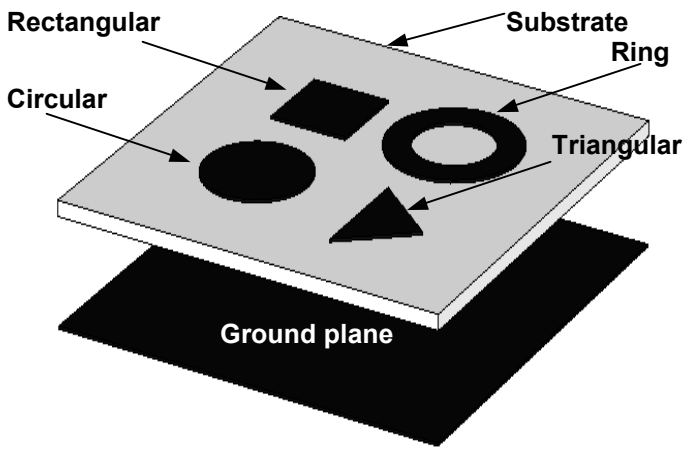

Figure 2.1 Exploded view of microstrip patch antenna

Fig. 2.1 shows several kind of microstrip patch antenna printed on a thin sheet of low-loss insulating dielectric substrate. It is completely covered with metal on one side, called the ground plane. The patch can be made into different shapes, however, rectangular and circular patches are popular. The relative permittivity and thickness of the substrate determine the electrical characteristics of the antenna. Low dielectric constant substrate enhances the radiation efficiency of the antenna and thicker substrate gives more bandwidth.

2.2 Microstrip antenna feeds

A single microstrip patch element can be excited in many ways. The more popular feed networks are summarized below:

A. Microstrip line feed

The simplest way to feed a microstrip patch is to connect a microstrip line directly to the edge of the patch. In this case both the patch and lines are located on the same substrate. The matching between the characteristic impedance of the microstrip feed line and the patch can be done by selecting the right depth of the inset as shown in Fig. 2.2.a. [88]. A microstrip structure with the line and patch on the same level cannot be optimized simultaneously as an antenna or as a transmission line because the specific requirements for both are contradictory. A low dielectric constant is needed for the efficient radiation from the patch. However, it will result in spurious radiation from line and the step discontinuities.

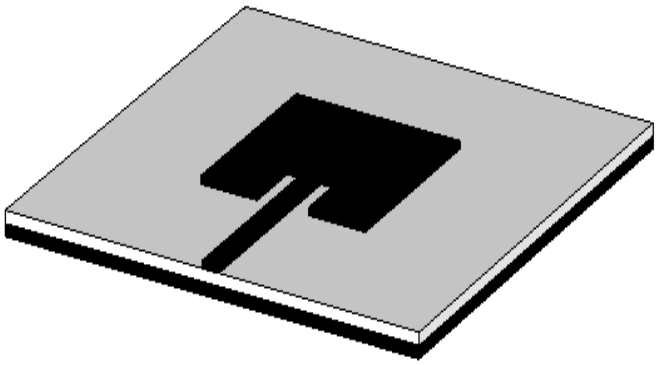

Figure 2.2.a Patch antenna with microstrip line feed

This spurious radiation increases both the sidelobe level and the cross-polarization. The patch behaves like a cavity due to the accumulated reactive power below it. To reduce the radiation from the microstrip line if we use high dielectric constant substrate, it will degrade the radiation efficiency of the patch and increase the surface wave loss.

B. Coaxial feed

The coaxial feed is the simplest feed structure for the microstrip antennas and remains among the most popular one. It is a quite different way to feed a patch by means of a coaxial line that is set perpendicular to the ground plane as shown in Fig. 2.2.b. In this case the inner conductor of the coaxial line is attached to the radiating patch while the outer conductor is connected to the ground plane. The input impedance depends on the position

of the feed so that the patch can be matched to the coaxial line by properly positioning the feed. It has low spurious radiation because the radiating and feeding systems are disposed on the two sides of the ground plane and shielded from each other. However, it is not suitable for antenna array applications.

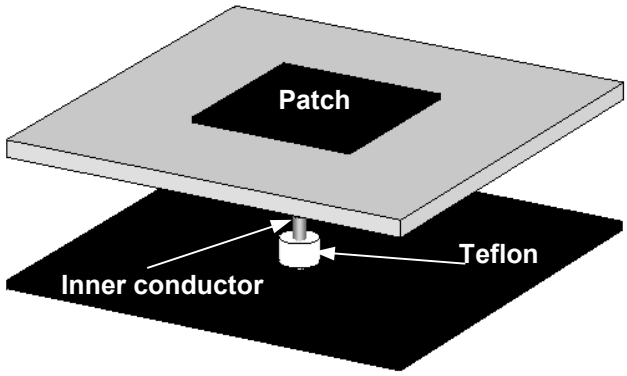

Figure 2.2.b Patch antenna with coaxial line feed

C. Proximity coupling

Proximity coupling of the patch to the feed line is obtained by placing the patch and the feed at different levels as shown in Fig. 2.2.c. Using this feed, the frequency bandwidth of batch resonator could be significantly widened (around 13%) and it gives low spurious radiation [89]. Using a thin substrate of high relative permittivity can considerably reduce the radiation from the feed. The upper dielectric layer is thicker and has a low relative permittivity, so that the radiation of the patch is enhanced. However, the feed line is no longer located on an open surface, so there is no direct access to it and one can not easily connect components within the feeding circuit.

D. Aperture coupling feed

The further step is to achieve the complete separation of the radiation and guided transmission functions. This separation can be achieved by placing the ground plane between the radiating patch and the feed system as shown in Fig. 22.d. Coupling between the microstrip feed line and the radiating patch is provided by a slot (aperture) in the ground

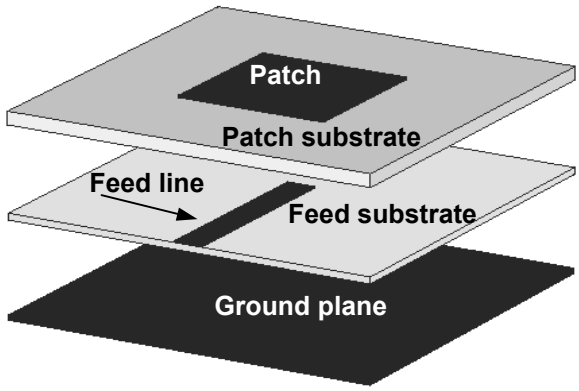

Figure 2.2.c Patch antenna with proximity coupling feed

plane between the radiating patch and the feed system as shown in Fig. 22.d. Coupling between the microstrip feed line and the radiating patch is provided by a slot (aperture) in the ground plane. Radiation from the open end feed line does not interfere with the radiation pattern of the patch because of the shielding effect of the ground plane. Possible radiation from the feed line can be completely avoided by enclosing the bottom part within a shielded enclosure. The aperture coupling is not so simple to fabricate. However, it is preferred in our investigation because of its high performance in antenna array applications [25]. There is no need to drill holes in the substrate to connect the feed to the patches. The aperture coupling feed method has the advantages that one can easily integrate active components in the feed structure.

2.3 Aperture Coupled Microstrip Antennas

"The demand is the mother of invention", let me start with this sentence and give the history of the aperture coupled microstrip antenna. The aperture coupled microstrip antenna (ACMSA) was proposed by Pozar for its application the integrated phased array systems [90]. Several major drawbacks are found in the direct application of a microstrip antenna to integrated phased array systems. Firstly, there is generally not enough space on a single layer to hold antenna elements, and other components such as active phase shifters, amplifiers, bias lines, and RF feed lines. Secondly, the high permittivity of a semiconductor substrate such as GaAs is a poor choice for antenna bandwidth, since the bandwidth of a

microstrip antenna is best for low dielectric constant substrates. If we increase the substrate thickness to improve bandwidth, the spurious feed radiation increases and also power loss in the surface wave increases. This leads to scan blindness, where the antenna is unable to receive or transmit at a particular scan angle. Because of these and another issues, the aperture coupled microstrip antenna configuration was proposed. It consists of two different layers separated by a common ground plane. A slot is used to couple a microstrip feed line to a resonant microstrip patch antenna as shown in Fig. 2.2.d.

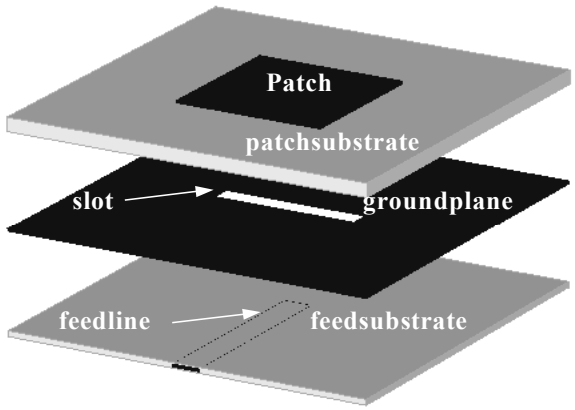

Figure 2.2.d Exploded view of aperture coupling feed

2.3.1 Linearly polarized microstrip antenna

In this section an aperture coupled single element Microstrip antenna is designed, simulated, fabricated and measured. It is used as an element of an antenna array. We have focused our attention to obtain a large bandwidth [27]. The major advantages of the aperture coupling feed technique is that it allows an independent optimization of both radiating patch and feed line of the microstrip antenna. The bandwidth of the linearly polarized antenna is widened by selection of substrates and combination of two resonances. One resonance is due to the patch and the other resonance results from the slot and its combination with the patch.

The main starting data for the design of a single element microstrip antenna are shown in Table 2.1. These requirements are suitable to the Eurobird ™ satellite [91].

Table 2.1 Main Starting data for design of a single element microstrip antenna

No.	Characteristic	Data
1.	Polarization	Linear
2.	Frequency range f_{min}/f_{max}, *GHz*	11.2 – 11.7
3.	Central frequency f_o, *GHz*	11.45
4.	Central wavelength λ_o, mm	26.201
5.	Fractional bandwidth bw, %	4.4

In this work, substrates produced by Rogers Corporation are used. Some of their properties are given in Table 2.2 [92].

2.3.1.1 Antenna Design

Fig. 2.3 shows the geometry of the linearly polarized aperture coupled microstrip antenna. The following items are chosen to obtain the maximum bandwidth:

- Aperture coupling feed technique.
- Low permittivity of the patch substrate.
- Thick patch substrate.
- Thin feed substrate.
- Resonant slot.

(i) Substrate Choice:

We have selected RT/Duroid 5880 substrate as for the patch antenna and RT/Duriod 6006 for the microstrip feed line. Their characteristics are given in Table 2.2.

(ii) Design Frequency:

The patch dimensions are found using a CAD programme called PATCH9 [93]. The effect of the aperture (slot) in the ground plane of the patch substrate is to reduce its resonance frequency. For thin substrates ($h_p = 0.01\lambda_o - 0.02\lambda_o$) this reduction is between 2 % to 4 %. For patch substrate thickness h_p =0.06 λ_o , the optimum design frequency is found by some iterations for different values of the ratio (patch resonance frequency/Antenna resonance frequency)

$$Q_P = f_{op} / f_o = 1 + \Delta f_{op} / f_o \tag{2.1}$$

The results are given in Table 2.3 for values of Q_P, 1 to 1.5.

Table 2.2. Properties of high frequency circuit materials produced by Rogers Corporation @ 10 GHz.

Product	Composition	Dielectric Constant (ε_r)	Tanδ_p	Standard Thickness in (mm)	
RT/duroid 5870	PTFE Glass Fiber	2.33 ± 0.020	0.0012	0.127 0.254 0.381 0.508	0.787 1.575 3.175
RT/duroid 5880	PTFE Glass Fiber	2.20 ± 0.020	0.0009	0.127 0.254 0.381 0.508	0.787 1.575 3.175
ULTRALAM 2000	PTFE Woven Glass	2.40 – 2.60 ± 0.020	0.0019	0.101 0.256 0.373	0.482 0.762 1.524
RT/duroid 6002	PTFE Ceramic	2.94 ± 0.040	0.0012	0.127 0.254 0.508	0.762 1.524 3.048
RT/duroid 6006	PTFE Ceramic	6.15 ± 0.150	0.0019	0.254 0.635 1.270	1.905 2.540
RO4003C	PTFE /Ceramic	3.38 ± 0.05	0.0027	0.203 0.508	0.813 1.524

(iii) Dominant Mode :

The TM_{100} is chosen as a dominant mode ($h_p \ll W_P$, $L_P > W_P > h_p$) with resonant frequency given by

$$f_{0P} = (f_{0P})_{100} = \frac{150}{L_{Peff}[mm]\sqrt{\varepsilon_{rpeff}}}, \text{ GHz} \tag{2.2}$$

(iv) Aspect-Ratio (Patch width/patch length)

$$q_P = W_P / L_P \tag{2.3}$$

The aspect ratio affects the bandwidth of the patch. For high polarization purity, the value of q_P should be in the range from 0.750 to 0.875 [93]. A value of 0.8125 is chosen in this work.

(v) Patch length:

The patch length determines the resonance frequency of the patch and the antenna. It is given by

$$L_P = L_{Peff} - 2\Delta L_P \tag{2.4}$$

where,

$$L_{Peff} = \frac{150}{f_{0P}[GHz]\sqrt{\varepsilon_{rPeff}}} \text{ , mm} \tag{2.5}$$

is the effective patch length [94],

$$\varepsilon_{rPeff} = 0.5\left[\varepsilon_{rP} + 1 + \frac{\varepsilon_{rP} - 1}{\sqrt{1 + 12h_P / W_P}}\right] \tag{2.6}$$

is the effective dielectric constant, and

$$\Delta L_P = 0.412 h_P \frac{(\varepsilon_{rPeff} + 0.3)(W_P / h_P + 0.264)}{(\varepsilon_{rPeff} - 0.258)(W_P / h_P + 0.8)} \tag{2.7}$$

is the fringing patch length [95].

The replacement of (2.5) – (2.7) into (2.4) produces

$$L_P = \frac{150}{Q_P f_0 \sqrt{\varepsilon_{rpeff}}} - 0.824 h_p \frac{(\varepsilon_{rpeff} + 0.3)(B_P L_P + 0.264)}{(\varepsilon_{rpeff} - 0.258)(B_P L_P + 0.8)}, \tag{2.8}$$

where,

$$\varepsilon_{rpeff} = 0.5\left[\varepsilon_{rp} + 1 + \frac{\varepsilon_{rp} - 1}{\sqrt{1 + \frac{12}{B_P L_P}}}\right], \tag{2.9}$$

$$B_P = q_p / h_P \tag{2.10}$$

The patch length is defined by equation 2.8, and the results are shown in Table 2.3.

Table 2.3. Dimensions and Characteristics of a Linearly Polarized Microstrip Patch Antenna

Q_P	L_P (mm)	W_P (mm)	ε_{rPeff}	ΔL_P (mm)	L_{Peff} (mm)	W_{Peff} (mm)	$(f_{oP})_{010}$ (GHz)
1.00	7.949	6.459	1.9028	0.774	9.497	7.849	13.855
1.01	7.860	6.386	1.9015	0.773	9.406	7.776	13.989
1.02	7.772	6.315	1.9003	0.772	9.316	7.705	14.123
1.03	7.686	6.245	1.8990	0.772	9.230	7.635	14.257
1.04	7.602	6.176	1.8978	0.771	9.144	7.566	14.390
1.05	7.519	6.109	1.8965	0.770	9.059	7.499	14.524
1.06	7.438	6.044	1.8953	0.770	8.978	7.434	14.657
1.07	7.360	5.980	1.8941	0.769	8.898	7.370	14.789
1.08	7.280	5.915	1.8929	0.768	8.816	7.305	14.924
1.09	7.204	5.853	1.8918	0.767	8.738	7.243	15.057
1.1	7.129	5.792	1.8906	0.766	8.661	7.182	15.189
1.11	7.055	5.732	1.8894	0.766	8.587	7.122	15.322
1.12	6.982	5.673	1.8883	0.765	8.512	7.063	15.455
1.13	6.911	5.615	1.8872	0.764	8.439	7.005	15.587
1.14	6.841	5.558	1.8860	0.763	8.367	6.948	15.720
1.15	6.772	5.502	1.8849	0.763	8.298	6.892	15.852

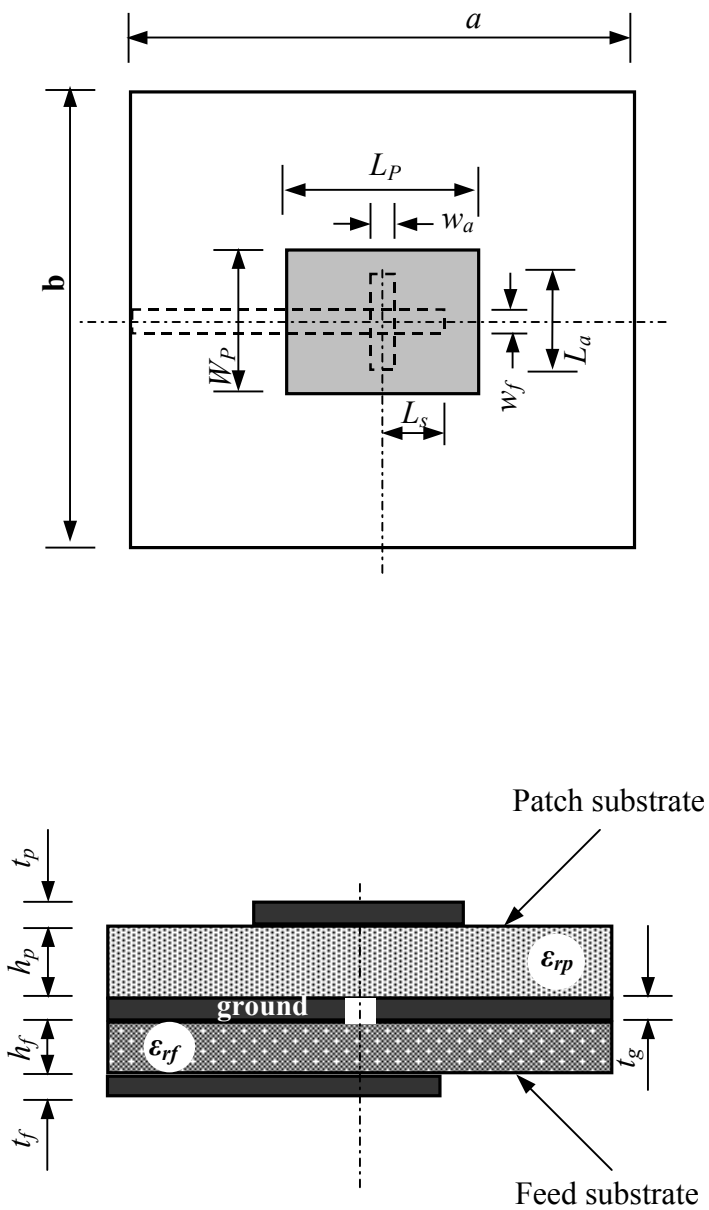

Figure 2.3 Linearly polarized aperture–coupled microstrip antenna geometry

(vi) Patch width:

Once length of the patch is known, its width is obtained by equation 2.3.

(vii) Effective dielectric constant:

The effective dielectric constant is obtained by equation-2.9 and it is given in Table 2.3.

(viii) Effective Patch width:

$$W_{Peff} = W_P + 2\Delta W_P, \tag{2.11}$$

Where the fringing width ΔW_P is given by [96]

$$\Delta W_P \sim (\ln 4/\pi) h_P, \text{ (=0.695 mm for } h_P \text{=1.575 mm)} \tag{2.12}$$

The values of the effective patch width are indicated in Table 2.3.

(viii) Resonant frequency of TM_{010} mode:

Since $L_P > W_P > L_P/2 > h_P$, the next higher order mode is the TM_{010} whose resonance frequency is

$$(f_{0P})_{010} = \frac{150}{W_{Peff}[mm]\sqrt{\varepsilon_{rpeff}}}, \text{ GHz} \tag{2.13}$$

and it is indicated in Table 2.3.

(x) Patch bandwidth:

The bandwidth of the patch is given in [97], [1] by

$$bw = \left(\frac{16}{3\sqrt{2}} \frac{p}{\eta_P} \frac{1}{\varepsilon_{rp}} \frac{h_P}{\lambda_0} \frac{W_P}{L_P} C_1 \right) \times 100, \ \% \tag{2.14}$$

Where,

$$\eta_P = \frac{P_r}{P_r + P_c + P_d + P_{sw}} \sim \frac{P_r}{P_r + P_{sw}} = \frac{1}{1 + 0.75\pi k_0 h_P (1 - 1/\varepsilon_{rp})^3 / C_1} \tag{2.15}$$

is the radiation efficiency of the patch, $k_0 = 2\pi/\lambda_0$

$$p = 1 - \frac{0.16605}{20}(k_0 W_P)^2 + \frac{0.02283}{560}(k_0 W_P)^4 - 0.009142(k_0 L_P)^2 \tag{2.16}$$

$$C_1 = 1 - \frac{1}{\varepsilon_{rp}} + \frac{0.4}{(\varepsilon_{rp})^2} \tag{2.17}$$

The values of the patch radiation efficiency and the bandwidth of the central frequency are shown in Table 2.4. One expects that the patch bandwidth will increase by the aperture coupling feed technique.

Table 2.4 Radiation Efficiency and Bandwidth of the Patch Antenna

Q_P	f_0, GHz	ε_{rp}	h_P, mm	L_P, mm	W_P, mm	η_P %	bw_P %
1.0	11.45	2.20	1.575	7.949	6.459	81.30	6.13

(xi) Dimension of the ground plane:

The dimension of the ground plane must be chosen enough large to replace entirely the infinite ground plane. In practice these dimensions are in order of some wavelengths. Finite ground plane gives rise to diffraction of radiation from the edges of the ground plane resulting in changes in radiation patter, radiation conductance, and resonance frequency [1]. The experimental investigations on the resonant frequency of a rectangular patch as a function of the size of the ground plane show that the influence on the resonance frequency is negligible if the ground plane size exceeds the patch sizes with about $\lambda_0/2$ from all sides [98]. A theoretical study shows that the influence on the radiation pattern can be neglected if the size of the ground plane exceeds two-wave length [99]. According to the above recommendations, dimensions of the ground plane of the linearly polarized Microstrip antenna are chosen as follows

$$a = b \sim 2\lambda_0, \ (a = b = 53\,mm) \tag{2.18}$$

(xii) Patch position:

To obtain maximum magnetic coupling, the patch is placed at the center of the antenna. The coupling slot is also located at the center. The center of the patch is the center of the square patch substrate (26.5mm, 26.5mm)

(xiii) Feed microstrip line

The general structure of a microstrip is illustrated in Fig. 2.4. A microstrip line is used to feed the aperture coupled microstrip antenna. Basic concepts and design equations for microstrip lines are briefly described.

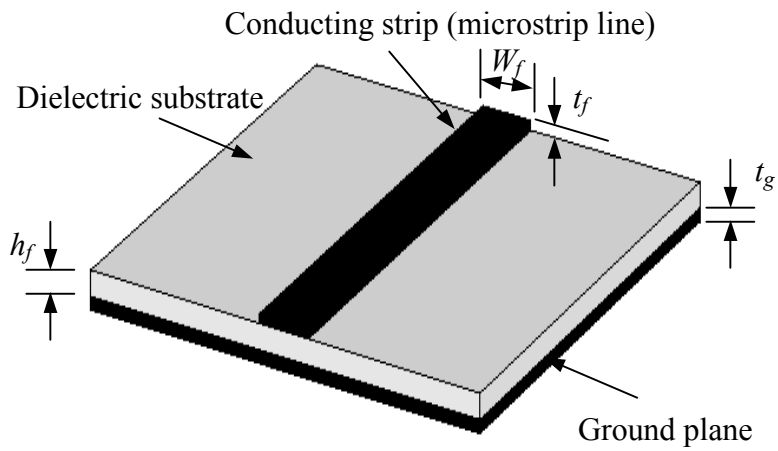

Figure 2.4 Microstrip feed structure

(xiv) Substrate choice:

According to the recommendations in the top of this section and the available data in Table 2.2, the substrate RT/duroid 6006 with relative permittivity ε_{rf} = 6.15 ± 0.15, $\tan\delta_f$ = 0.0019, substrate thickness h_f = 0.635 mm (0.024λ_0) and copper layer thickness $t_g = t_f$ =17.5 μm has been chosen as a feed substrate. The dimension of the 50 Ω microstrip line is taken suitable for fabrication .It is around 1mm at 11.45 GHz.

(xv) Waves in microstrips:

The fields in the microstrip extend within two media, air above and dielectric below. Thus, the structure is inhomogeneous. Due to this inhomogeneous nature, the microstrip does not support a pure TEM wave. This is because that a pure TEM wave has only transverse components, and its propagation velocity depends only on the material properties, namely the permittivity ε and the permeability μ. However, with the presence of the two guided-wave media (the dielectric substrate and the air), the waves in a microstrip line will have no

vanished longitudinal components of electric and magnetic fields, and their propagation velocities will depend not only on the material properties, but also on the physical dimensions of the microstrip.

***Quasi-TEM approximation**:*

When the longitudinal components of the fields for the dominant mode of a microstrip line remain very much smaller than the transverse components, they may be neglected. In this case, the dominant mode then behaves like a TEM mode, and the TEM transmission line theory is applicable for the microstrip line as well. This is called the quasi-TEM approximation and it is valid over most of the operating frequency ranges of microstrip.

Quasi-Static values of the effective dielectric constant

In the quasi-TEM approximation, a homogeneous dielectric material with an effective dielectric permittivity replaces the inhomogeneous dielectric-air media of microstrip. Transmission characteristics of microstrips are described by two parameters, namely, the effective dielectric constant ε_{rfeff} and characteristic impedance Z_0, which may then be obtained by quasi-static analysis and closed form expression [93]-[94], [100]

$$\varepsilon_{rfeff}(0) = 0.5\left[\varepsilon_{rf} + 1 + (\varepsilon_{rf} - 1)F\left(\frac{W_f}{h_f}\right)\right] - \frac{(\varepsilon_{rf} - 1)t_f}{4.6\sqrt{h_f W_f}} \tag{2.19}$$

where,

$$F\left(\frac{W_f}{h_f}\right) = \left(1 + 12\frac{h_f}{W_f}\right)^{-0.5} + 0.04\left(1 - \frac{W_f}{h_f}\right)^2 \quad for\ \frac{W_f}{h_f} \le 1 \tag{2.20}$$

$$F\left(\frac{W_f}{h_f}\right) = \left(1 + 12\frac{h_f}{W_f}\right)^{-0.5} \quad for\ \frac{W_f}{h_f} \ge 1 \tag{2.21}$$

The values of the feed line characteristics and dimensions are shown in Table 2.5.

Table 2.5. Dimensions and Characteristics of Antenna Feed Line

Input data									
f_0 (GHz)	λ_0 (mm)	$Z_0(f)$ Ω	ε_{rf}	h_f (mm)	$\tan\delta_f$	t_f (μm)	t_g (μm)	σ_f (S/m)	l (mm)
11.45	26.201	50	6.15	0.635	0.0019	17.5	17.5	$5.813\text{x}10^7$	26.5
Output data									
$\varepsilon_{rfeff}(0)$	$Z_0(0)$ Ω	$\varepsilon_{rfeff}(f)$	W_f (mm)	ΔW_f (mm)	W_{feff} (mm)	α_d (dB/mm)	α_c (dB/mm)	α (dB/mm)	αl (dB)
4.415	48.27	4.622	0.970	0.018	1.006	0.0040	0.0032	0.0072	0.191

(xvi) Effective feed line width:

$$W_{feff} = W_f + 2\Delta W_f \tag{3.22}$$

where the fringing width ΔW_f is given by [95], [101]

$$\Delta W_f = \frac{0.625}{\pi} t_f \left[1 + \ln\left(\frac{4\pi W_f}{t_f}\right)\right] \quad for \ \frac{W_f}{t_f} \le \frac{1}{2\pi} \tag{2.23}$$

$$\Delta W_f = \frac{0.625}{\pi} t_f \left[1 + \ln\left(\frac{2h_f}{t_f}\right)\right] \quad for \ \frac{W_f}{t_f} \ge \frac{1}{2\pi} \tag{2.24}$$

(xvii) Quasi-Static values of the characteristic impedance:

The closed-form expressions that provide an accuracy better than one percent are given by [95, 101] as follows:

$$Z_0(0) = \frac{60}{\sqrt{\varepsilon_{rfeff}(0)}} \ln\left\{\frac{8h_f}{W_{feff}} + 0.25\frac{W_{feff}}{h_f}\right\} \quad for \ \frac{W_f}{h_f} \le 1 \tag{2.25}$$

$$Z_0(0) = \frac{120\pi}{\sqrt{\varepsilon_{rfeff}(0)}} \ln\left\{\frac{W_{feff}}{h_f} + 1.393 + 0.667\ln\left[\frac{W_{feff}}{h_f} + 1.444\right]\right\}^{-1} \quad for \ \frac{W_f}{h_f} \geq 1 \qquad (2.26)$$

***(xviii) Dispersion in microstrip**:*

Generally, there is dispersion in microstrips. This means that its phase velocity is not a constant but depends on frequency. It follows that its effective dielectric constant ε_{rf} is a function of frequency and can in general be defined as the frequency dependent effective dielectric constant $\varepsilon_{rf}(f)$. An empirical expression is proposed in [102]. It gives an upper frequency, which above the quasi-static formulas are no longer accurate which is

$$f_{stat} = \frac{0.04 Z_0(0)}{h_f[mm]\sqrt{\varepsilon_{rfeff}(0)}}, \quad GHz \qquad (2.27)$$

The value of this frequency for the selected feed substrate is $f_{stat} \sim 1.5\,GHz$. At this frequency the dispersion is negligible. Above about 8 GHz, when the dispersion can not be ignored, the design accuracy may be improved using full-wave analysis. A full wave solutions for electromagnetic fields on a microstrip line as a function of frequency are fitted to empirical frequency-dependent expressions [93]-[103].

The frequency-dependent effective dielectric constant value is given by [104] as,

$$\varepsilon_{rfeff}(f) = \varepsilon_{rf} - \frac{\varepsilon_{rf} - \varepsilon_{rfeff}(0)}{1+P} \qquad (2.28)$$

where,

$$P = P_1 P_2 \left[(0.1844 + P3P4)10 f_0[GHz] h_f[cm]\right]^{1.5763} \qquad (2.29)$$

$$P_1 = 0.27488 + \frac{W_f}{h_f}\left[0.6315 + \frac{0.525}{(1+0.157 f_0[GHz] h_f[cm])^{20}}\right] \qquad (2.30)$$

$$P_2 = 0.33622\left[1-\exp(-0.03442\varepsilon_{rf})\right] \tag{2.31}$$

$$P_3 = 0.0363\exp\left(-4.6\frac{W_f}{h_f}\right)\left\{1-\exp\left[-\left(\frac{f_0\,[GHz]h_f\,[cm]}{3.87}\right)^{4.97}\right]\right\} \tag{2.32}$$

$$P_4 = 1+2.751\left[1-\exp\left(-\frac{\varepsilon_{rf}}{15.916}\right)^{8}\right] \tag{2.33}$$

The frequency-dependent characteristic impedance is given by [105] as,

$$Z_0(f) = Z_0(0)(R_{13}/R_{14})^{R_{17}} \tag{2.34}$$

$$R_1 = 0.0389\left(\varepsilon_{rf}\right)^{1.4} \tag{2.35}$$

$$R_2 = 0.267\left(\frac{W_f}{h_f}\right)^{7} \tag{2.36}$$

$$R_3 = 4.766\exp\left[-3.228\left(W_f/h_f\right)^{0.641}\right] \tag{2.37}$$

$$R_4 = 0.016+\left(0.0514\varepsilon_{rf}\right)^{4.524} \tag{2.38}$$

$$R_5 = \left(f_0[GHz]h_f[mm]/28.843\right)^{12} \tag{2.39}$$

$$R_6 = 22.2\left(\frac{W_f}{h_f}\right)^{1.92} \tag{2.40}$$

$$R_7 = 1.206-0.3144\exp(-R_1)\left[1-\exp(-R_2)\right] \tag{2.41}$$

$$R_8 = 1 + 1.257\left\{1 - \exp\left[-0.004625 R_3 (\varepsilon_{rf})^{1.674}\left(f_0[GHz] h_f[mm] / 18.365\right)^{2.745}\right]\right\} \quad (2.42)$$

$$R_9 = \frac{5.086 R_4 R_5 (\varepsilon_{rf} - 1)^6 \exp(-R_6)}{(0.3838 + 0.386 R_4)(1 + 1.2992 R_5)\left[1 + 10(\varepsilon_{rf} - 1)^6\right]} \quad (2.43)$$

$$R_{10} = 0.00044(\varepsilon_{rf})^{2.136} + 0.0184 \quad (2.44)$$

$$R_{11} = (f_0[GHz] h_f[mm] / 19.47)^6 \Big/ \left[1 + 0.0962(f_0[GHz] h_f[mm] / 19.47)^6\right] \quad (2.45)$$

$$R_{12} = 1 \Big/ \left[1 + 0.00245(W_f / h_f)^2\right] \quad (2.46)$$

$$R_{13} = 0.9408\left[\varepsilon_{rfeff}(f)\right]^{R_8} - 0.9603 \quad (2.47)$$

$$R_{14} = (0.9408 - R_9)\left[\varepsilon_{rfeff}(0)\right]^{R_8} - 0.9603 \quad (2.48)$$

$$R_{15} = 0.707 R_{10} (f_0[GHz] h_f[mm] / 12.3)^{1.097}$$

$$R_{16} = 1 + 0.0503(\varepsilon_{rf})^2 R_{11}\left\{1 - EXP\left[-(W_f / h_f)^6\right]\right\} \quad (2.49)$$

$$R_{17} = R_7\left\{1 - 1.1241(R_{12} / R_{16}) \exp\left[-0.026\,(f_0[GHz] h_f[mm])^{1.15656} - R_{15}\right]\right\} \quad (2.50)$$

(xix) Feed line width:

The width of the feed line can be calculated from expressions 2.28 – 2.50 using some iteration with a programme Micro [93]. By adjusting the feed line width W_f , the characteristic impedance $Z_0(f)$ of the microstrip line at the central frequency can be set to 50 Ω.

The loss components of a single microstrip line include conductor loss α_c and dielectric loss α_d , while the magnetic loss plays a role only for magnetic substrates such as ferrites. The propagation constant on a lossy transmission line is complex; namely, $\gamma = \alpha + j\beta$, where the real part α in nepers per unit length is the attenuation constant, which is the sum

of the attenuation constants arising from each effect. The attenuation constants are given in decibels per unit length by [106]

$$\alpha_d = 8.686\pi\left(\frac{\varepsilon_{rf}}{\varepsilon_{rf}-1}\right)\left(\frac{\varepsilon_{rfeff}(f)-1}{\sqrt{\varepsilon_{rfeff}(f)}}\right)\left(\frac{\tan\delta_f}{\lambda_0}\right) \tag{2.51}$$

$$\alpha_c = 1.38A_f\frac{R_S}{h_f Z_0(f)}\left(\frac{(32-W_{feff}/h_f)^2}{(32+W_{feff}/h_f)^2}\right) \quad for\ \frac{W_f}{h_f}\le 1 \tag{2.52}$$

$$\alpha_c = 6.1\times10^{-5}A_f\frac{R_S Z_0(f)\varepsilon_{rfeff}(f)}{h_f}\left[\frac{W_{feff}}{h_f}+\frac{0.667(W_{feff}/h_f)}{(W_{feff}/h_f)+1.444}\right] \quad for\ \frac{W_f}{h_f}\ge 1 \tag{2.53}$$

where,

$$A_f = 1+\frac{h_f}{W_{feff}}\left\{1+\frac{1.25}{\pi}\ln\left(\frac{2\pi W_f}{t_f}\right)\right\} \quad for\ \frac{W_f}{h_f}\le\frac{1}{2\pi} \tag{2.54}$$

$$A_f = 1+\frac{h_f}{W_{feff}}\left\{1+\frac{1.25}{\pi}\ln\left(\frac{2h_f}{t_f}\right)\right\} \quad for\ \frac{W_f}{h_f}\ge\frac{1}{2\pi} \tag{2.55}$$

$$R_S = \sqrt{\frac{\pi f_0\mu_0}{\sigma_c}} \quad \text{is the surface conductor impedance, and} \tag{2.56}$$

$\sigma_c = \sigma_f$ is the copper conductivity.

All feed line losses are $\sigma_{c,d}l$, where l=26.5 mm = length of the feed line from the connector reference plane to the antenna centre as shown in Fig. 2.3. The length, L_s is called the stub length and it will be investigated with the slot (aperture).

(xx) Coupling aperture

In order to investigate the frequency characteristics of the aperture (slot) in the contribution in the equivalent circuit model of the aperture coupled microstrip antenna, the structure shown in Fig. 2.5 has been simulated. The substrate RT/duroid 6006 with relative permittivity ε_{rf} = 6.15 ± 0.15, tanδ_f = 0.0019, substrate thickness h_f = 0.635 mm (0.024λ_0) and copper layer thickness t_g = t_f=17.5 μm has been used. A 50 Ω microstrip line has been

etched on one of the substrate sides. On the other side, a slot with length 4.45 mm and width 0.44 mm has been removed from the copper layer. The simulation results is modeled by a parallel LC resonant circuit [66]. The capacitance C_{ap} in picofarads and the inductance L_{ap} in nanohenrys are given by [66] as

$$C_{ap} = \frac{5 f_c}{\pi\left[f_0^2 - f_c^2\right]} \quad pF \tag{2.56}$$

$$L_{ap} = \frac{250}{C_{ap}(\pi f_0)^2} \quad nH \tag{2.57a}$$

where f_c, in gigahertz, is the cutoff frequency of the slot response at 3 dB and f_0, in gigahertz is its pole (resonance). At any frequency $f < f_0$, the parallel circuit behaves as an inductor and its value in nanohenrys is given by [85] as

$$L_{ae} = \frac{L_{ap}}{[1-(\frac{f}{f_0})^2]} \quad \text{nH} \tag{2.57b}$$

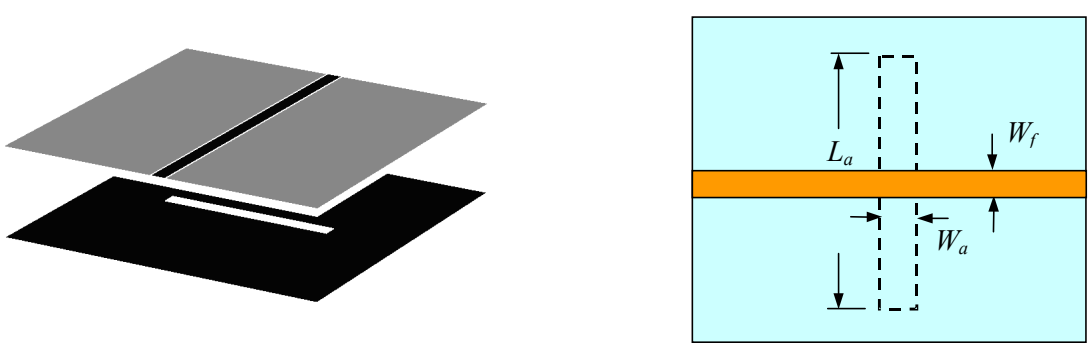

Figure 2.5 50 Ω microstrip line feed slot (DGS)

The equivalent circuit of the aperture coupled microstrip antenna is shown in Fig 2.6. L_{ae} is the equivalent inductance associated with the below resonance aperture (slot). The patch is the parallel R_pL_pCp circuit. The stub is an open circuited transmission line with the same

characteristic impedance as the feed line. The stub compensates for the inductance of the slot and the patch to create a real input impedance for the antenna at resonance frequency.

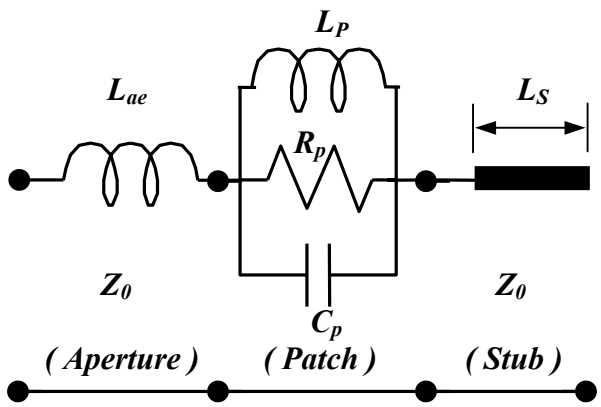

Figure 2.6 Linearly polarized aperture coupled microstrip antenna equivalent circuit

a. Position of the coupling aperture:

For maximum coupling, the slot is placed below the patch centre. Where the magnetic field is maximum. The feed line is positioned at right angle to the centre of the slot.

b. Slot length:

The slot length affects the coupling level and the back radiation level. Based on the results in [107], [108], the slot length should be chosen to be about

$$L_a \sim (0.1-0.2)\lambda_0 \tag{2.58}$$

In practice, this value is chosen between 2.5 mm to 5 mm ($0.095\lambda_0$ to $0.190\lambda_0$). Using commercial software package Micro Wave Studio [109], several iterations have been carried out for different values of the patch and slot dimensions to obtain an optimum antenna performance (minimum return loss, maximum bandwidth, and acceptable level of the back radiation due to the slot). The optimum values of L_a, W_a, and L_S in this design are given in Table 2.6.

c. Slot width:

It is chosen as tenth of the slot length

$$W_a = 0.10 L_a \tag{2.59}$$

Table 2.6. Aperture and Stub Dimensions of A Linearly Polarized Microstrip Antenna

Input data				
f_0 **(GHz)**	ε_{rf}	h_f **(mm)**	W_f **(mm)**	$\varepsilon_{rfeff}(f)$
11.45	6.15	0.635	0.970	4.622
Output data				
L_a **(mm)**	W_a **(mm)**	L_S **(mm)**	ΔL_S **(mm)**	L_{Seff} **(mm)**
4.450	0.440	1.600	0.2274	1.8274

d. Effective stub length:

The stub length L_S is adjusted until the input impedance at the design frequency becomes purely real

$$Z_{in} = R_{in} + jX_{in} = R + jX - jZ_0 \cot(2\pi L_{Seff} / \lambda_f) \tag{2.60}$$

where R is the real part, and X is the imaginary part of the input impedance without stub. The effective stub length can be defined by (2.60) for $X_{in} = 0$

$$L_{Seff} = \frac{\lambda_0}{2\pi\sqrt{\varepsilon_{rfeff}(f)}} \arctan\left(\frac{X}{Z_0}\right) \tag{2.61}$$

e. Stub length:

The stub length is given by

$$L_S = L_{Seff} - \Delta L_S \tag{2.62}$$

where the fringing stub length can be calculated by the following expressions [1], [110]

$$\Delta L_S = h_f g_1 g_2 g_3 g_5 / g_4 \tag{2.63}$$

$$g_1 = 0.434907 \frac{\left[\varepsilon_{rfeff}(f)\right]^{0.81} + 0.26}{\left[\varepsilon_{rfeff}(f)\right]^{0.81} - 0.189} \left(\frac{(W_f / h_f)^{0.8544} + 0.236}{(W_f / h_f)^{0.8544} + 0.87} \right) \tag{2.64}$$

$$g_2 = 1 + \frac{(W_f / h_f)^{0.371}}{2.358\varepsilon_{rf} + 1} \tag{2.65}$$

$$g_3 = 1 + \frac{0.5274 \arctan\left[0.084 (W_f / h_f)^{1.9413/g_2}\right]}{\left[\varepsilon_{rfeff}(f)\right]^{0.9236}} \tag{2.66}$$

$$g_4 = 1 + 0.0377 \arctan\left[0.067 (W_f / h_f)^{1.456}\right]\left\{6 - 5\exp\left[0.036(1-\varepsilon_{rf})\right]\right\} \tag{2.67}$$

$$g_5 = 1 - 0.218 \exp(-7.5 (W_f / h_f)) \tag{2.68}$$

For frequencies up to about 10 GHz, the quasi-static approach gives also reasonably good results [1]. For this ase the quasi-static approach gives $\Delta L_S = 0.2287\, mm$ (a difference of 1.3 μm, or an error of 0.57 %).

Table 2.7. Dimensions and Properties of the Designed Linearly Polarized Aperture Coupled Microstrip Antenna

Antenna element	**Dimensions/parameters**
Antenna	Length a = 53 mm, width b = 53 mm
Patch	Length L_P = 7.42 mm, width W_P = 6.029 mm thickness t_p = 17.5 μm
Patch substrate (RT/duroid 5880)	Thickness h_p = 1.575 mm (0.026λ_o), relative dielectric constant ε_{rp} = 2.20, loss tangent tanδ_p = 0.0009
Ground	Thickness t_g = 17.5 μm
Aperture	Length L_a = 3.49 mm, width W_a = 0.35 mm
Feed substrate (RT/duroid 6006)	Thickness h_f = 0.635 mm (0.025λ_o), relative dielectric constant ε_{rf} = 6.15, loss tangent tanδ_f = 0.0019
Microstrip feed line	Length l = 26.5 mm, width W_f = 0.972 mm, stub length L_S = 1.6 mm, thickness t_f = 17.5 μm

The dimensions of the complete antenna according to the previous design investigation are shown in Table 2.7. A bandwidth of 12.2 % in the frequency range from 11.06 GHz to 12.5 GHz is obtained.

2.3.2. Analysis and simulation

Simulation is an important step, which saves time and money before fabrication. It is an intermediate step between design and fabrication. To use a simulator, it is very important to test your knowledge with it. Simulating a test structure and then measuring it can improve the design. There may be a difference between simulated and measured results. One of the error sources is the accuracy of fabrication and it is another domain. Thus, to remove the doubt one must measure the actual dimensions after the fabrication process and re-simulate the structure with this new dimensions. The result will be your experience and knowledge with the simulator. Any antenna structure is characterized by its matching and far-field characteristics .

2.3.2.1. Matching characteristics

The analysis and simulation of the designed antenna in this work is carried out using the available commercial software package MicroWave Studio [109]. It is a general-purpose electromagnetic simulator based on the Finite Integral Technique (FIT), first proposed by weiland in 1976-1977 [111]. In addition a Perfect Boundary Approximation (BPA) technique, particularly extended by the thin sheet technique is used. In this way the software package ensures a good geometry approximation and high simulation speed. It is suitable for accurate modelling of curved and complex 3D structures.

The simulated impedance locus of the designed linearly polarized aperture coupled microstrip antenna is shown in Fig. 2.10 (dashed line). The resonance at the lower frequency is due to the patch, and the resonance at the higher frequency is due to the slot. These two resonant frequencies can be seen also in Fig. 2.10 which indicates the return loss versus frequency. Due to the magnetic coupling between the patch and the slot, the resonance frequency of the antenna has been shifted. It is clear from data of Tables 2.7 and 2.3. The optimum dimensions of the patch obtained from the design procedure are L_P=6.91 mm, and W_P =5.6 mm. According to table 2.3, the resonance frequency belongs to these

dimensions of the patch is f_{0P} =12.938 GHz. At the same time, the patch resonance frequency of the coupled structure is f_{02} as shown in Fig. 2.10. The resonance frequency of the slot having length of 4.45 mm and width of 0.443 is 20.84 GHz and it is very far from any one of the two resonances shown in Fig. 2.10. Thus, the resulting first frequency is due to the inductance of the slot combined with the capacitance due to the stub and the coupling action with the patch which introduces the matching at this resonance.

The simulated results are:

$f_{\min} = 11.060\ GHz,\ f_{\max} = 12.5\ GHz,\ f_0 = 11.78\ GHz,\ BW = 1440\ MHz,$ and $bw = 12.2\ \%.$

The central frequency f_0 =11.78 GHz is not the designed central frequency f_0 =11.78 GHz but the required bandwidth (11.2 – 11.7 GHz) is within the achieved bandwidth (11.06 – 12.5 GHz).

2.3.2.2. Far-field characteristics

The radiation patterns of the antenna can be defined according to the model based on a two slot array [1] by

$$E_\theta(\theta) = -jk_0 V_0 W_P \frac{e^{-jk_0 r}}{2\pi r} F_E(\theta) F_1(\theta) \quad \text{for the E-plane} \tag{2.69}$$

$$E_\varphi(\theta) = -jk_0 V_0 W_P \frac{e^{-jk_0 r}}{2\pi r} F_H(\theta) F_2(\theta) \quad \text{for the H-plane} \tag{2.70}$$

where,

$$F_E(\theta) = \sin c\left[k_0 h_P \sin(\theta/2)\right]\cos\left[k_0 L_P \sin(\theta/2)\right] \tag{2.71}$$

$$F_H(\theta) = \sin c\left[k_0 W_P \sin(\theta/2)\right]\cos\theta \tag{2.72}$$

$$F_1(\theta) = \frac{2\cos\theta\sqrt{\varepsilon_{rp} - \sin^2\theta}}{\sqrt{\varepsilon_{rp} - \sin^2\theta} - j\varepsilon_{rp}\cos\theta\cot\left(k_0 h_P\sqrt{\varepsilon_{rp} - \sin^2\theta}\right)} \tag{2.73}$$

$$F_2(\theta) = \frac{2\cos\theta}{\cos\theta - j\sqrt{\varepsilon_{rp} - \sin^2\theta}\,\cot\left(k_0 h_P \sqrt{\varepsilon_{rp} - \sin^2\theta}\right)} \tag{2.74}$$

V_0 is the voltage across either radiating slot. Similar expressions are given in [93]. Unfortunately, they are very approximate for the aperture coupled microstrip antenna because in this theory the ground is assumed to be infinite. By this assumption, the back radiation from the antenna has not been taken into account. The simulated radiation patterns in both E and H-plane are shown in Fig. 2.11 and Fig. 2.12 (dashed lines). The 3 dB beam widths in the E and H-planes are 96° and 88° respectively. The simulated back radiation of the antenna is shown in Fig. 2.9. It varies from –8 dB to –11 dB in the frequency bandwidth.

2.3.3 Practical Implementation

The dimensions of the antenna will be small at high frequency (Ku-band). Thus, the fabrication accuracy becomes the main requirement in practical implementation of the designed antenna. If the achieved accuracy in the antenna implementation is not enough, all the design will be for nothing. It is seen from Table 2.3 that a variation about 80 µm of the patch length L_P shifts the resonant frequency of the patch f_{0P} with approximately 1%. The study indicated that the companies known to us in Germany, which work in the field of printed circuit technology, could ensure a tolerance of ± 10 µm for substrates with metal thickness of 17.5 µm, and ± 20 µm for metal thickness of 35 µm in the photo etching process. Three samples were fabricated by S & H Electronic Leiterplatten GmbH (Werigerode, Sachsen Anhalt) according to the dimensions of the designed antenna in Table 2.7. Dimension measurements have been accomplished by the Laboratory of high accuracy measurements at the Magdeburg University. The average margin tolerance of the three antenna dimensions are shown in Table 2.8. It is seen that the maximum margin tolerance has a value of 75 µm. The matching characteristics of the antennas have been measured using the vector network analyser as shown in Fig. 2.8.

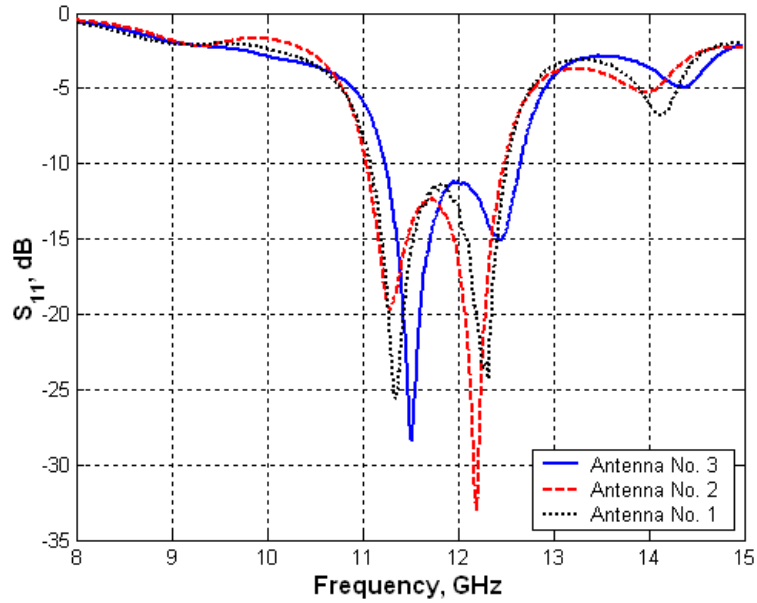

Figure 2.7 Measured Return Loss of Three Antenna Samples

The resonance frequencies are listed in Table 2.8. It is noticed that the maximum difference between the values of the central frequencies is

$$\Delta f_{0\max} = f_{03} - f_{01} = 128 MHz\ (\sim 1\%\ shift) \tag{2.69}$$

Table 2.8. Average Margin Tolerances and Central Frequencies of Three Antennas

Antenna / Parameter	Antenna No. 1	Antenna No. 2	Antenna No. 3	Average value
Patch length change $\lvert\Delta L_P\rvert_{avg}, \mu m$	30	23	63	39
Patch width change $\lvert\Delta W_P\rvert_{avg}, \mu m$	22	52	75	50
Slot length change $\lvert\Delta L_a\rvert_{avg}, \mu m$	12	2	12	9
Slot width change $\lvert\Delta W_a\rvert_{avg}, \mu m$	13	13	16	14
Feed line width change $\lvert\Delta W_f\rvert_{avg}, \mu m$	12	3	4	6
Central frequency f_0, GHz	11.805	11.766	11.933	-

In the second implementation, the accuracy has been improved and a maximum change from the designed dimensions in the order of 30 – 40 μm has been achieved. Within these implementation conditions, the designed antenna has been fabricated. Fig. 2.9 shows the photograph of the fabricated antenna.

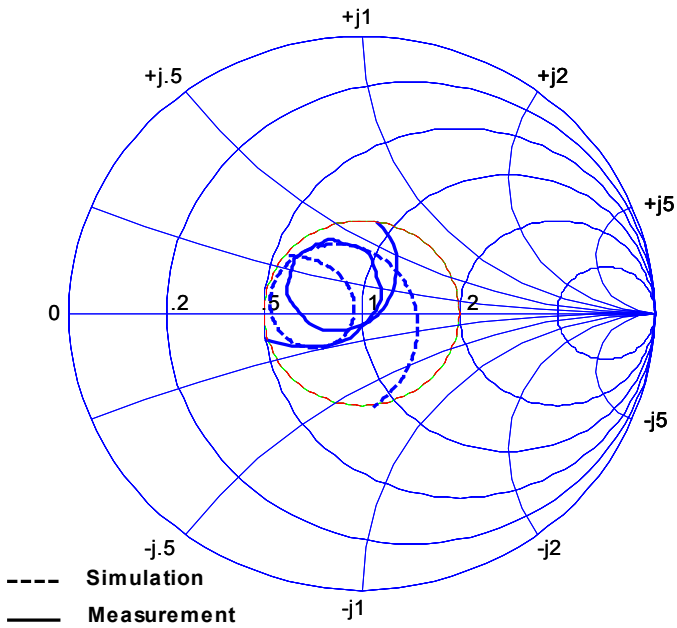

Figure 2.8 Impedance locus of a linearly polarized microstrip antenna

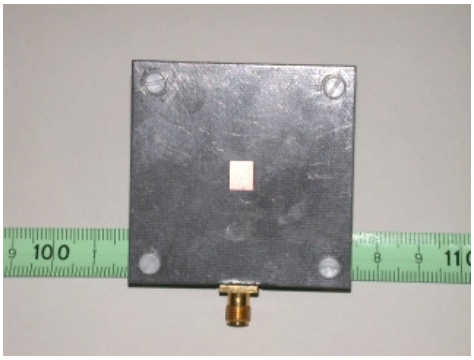

Figure 2.9 Photograph of a linearly polarized microstrip antenna

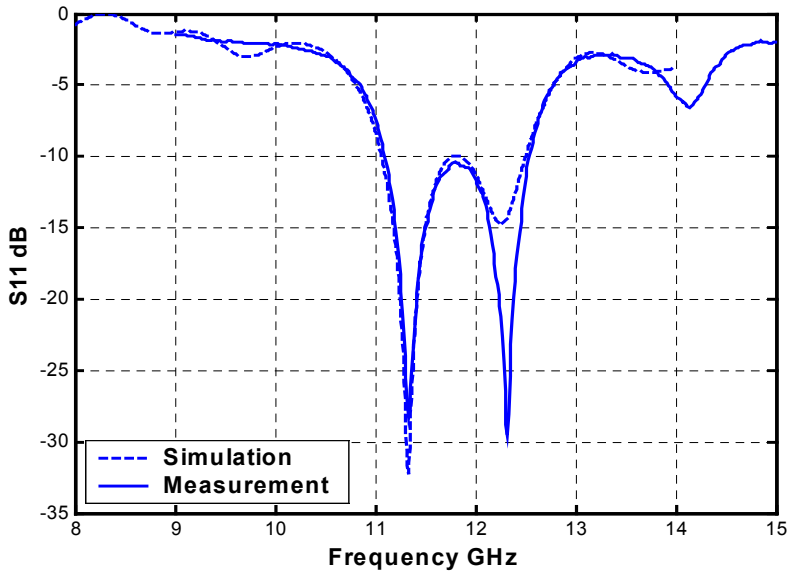

Figure 2.10 Return loss of a linearly polarized microstrip antenna

2.3.4. Experimental Results

The Performance of the antenna has been characterized using the following input and radiation characteristics of the antenna.

2.3.4.1 Measured Matching characteristics

The input characteristics of the fabricated aperture coupled microstrip antenna have been measured using a Wiltron 37347A Vector Network Analyser. The measured impedance locus of the antenna as a function of frequency is displayed in Fig. 2.8 where it can be compared with the simulated behaviour. It is seen from the figure that both the simulated and measured impedance locus have a similar behaviour in the frequency band width. The measured return loss is shown in Fig.2.10. A good agreement is indicated. A 10 dB return loss bandwidth of 12.4% (11.08 -12.55 GHz) with a center frequency f_o = 11.815 GHz is obtained. The difference between the computed and measured central frequencies is only 0.3 % (35 MHz). The fractional bandwidth of 12.4% represents a very good result for this antenna construction. In fact, it is known, that there is similar aperture coupled microstrip antennas with larger bandwidth from 20 % to 70 % [7]-[8], [112] but these antennas have a complex configuration, using stacked elements and foam material. Our is the maximum

bandwidth reported for the simple aperture coupled microstrip antenna on the thin substrate.

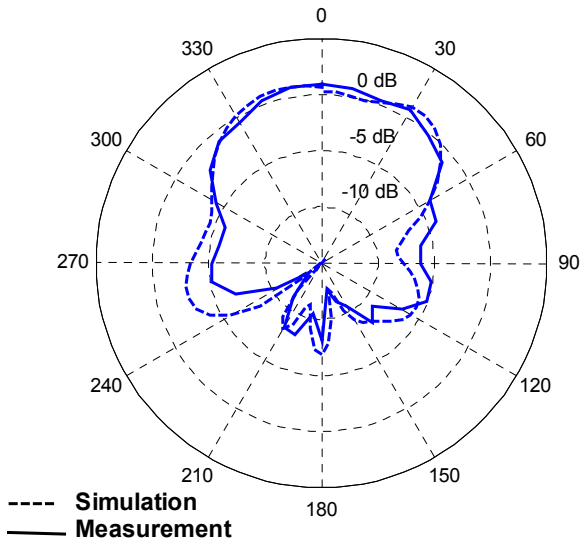

Figure 2.11 Radiation pattern of a linearly polarized microstrip antenna in E-plane

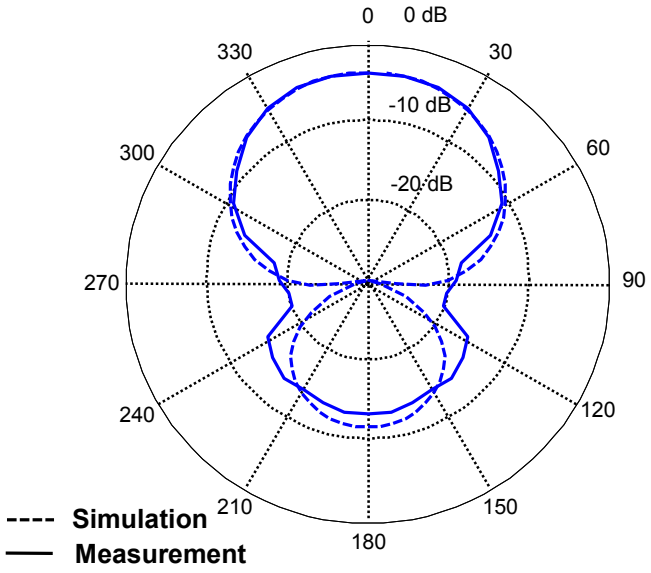

Figure 2.12 Radiation pattern of a linearly polarized microstrip antenna in H-plane

2.3.4.2 Measured Radiation characteristics

The radiation characteristics of the antenna are measured in the fare-zone in an anechoic chamber, using a HP 53152A receiver. Solid lines of Fig. 2.11 and Fig. 2.12 show the measured E- and H-plane radiation patterns of the antenna at frequency 11.8 GHz. The 3-dB beamwidth is equal to 93° in E-plane, and 83° in H-plane. The measured back radiation is – 9.1 dB. It is seen a good agreement between the computed and the measured E- and H-plane radiation patterns. The asymmetry in the E-plane diagrams is caused by the presence of a connector.

The measured back radiation of the antenna versus frequency is shown in Fig. 2.13. It remains between – 8 and – 20 dB over the interested bandwidth of the antenna and is in relatively good agreement with the simulation results.

The directivity of the antenna calculated by an integration of the E-plane and H-plane radiation patterns is D = 6.4 dB.

Table 2.9. Comparison of Simulated and Measured Characteristics of A Linearly Polarized Microstrip Antenna

Characteristic	f_0 **GHz**	f_{min}/f_{max} **GHz**	BW **MHz**	bw **%**	$(2\theta_{3dB})_E$ **degree**	$(2\theta_{3dB})_H$ **degree**	BRL **dB**
Simulation	11.780	11.06/12.50	1440	12.2	96	88	-7.5
Measurement	11.815	11.08/12.55	1470	12.4	93	83	-9.1

The gain of the antenna measured by the gain-comparison method is shown in Fig. 2.13. It is higher than 5.9 dB over a 12.4% bandwidth. The radiation efficiency at f = 11.8 GHz (G = 5.9 dB) is η_e = 89 %. The loss of 0.5 dB includes both the surface wave loss and the feed loss. The radiation efficiency increases with the frequency. The measured efficiency at the maximum frequency of the bandwidth f = 12.55 GHz is η_e = 94% (G = 6.84 dB, D = 7.1 dB). Fig. 2.14 shows also measured VSWR of the antenna. The excellent symmetry of the VSWR behaviour as a function of frequency widens also the antenna bandwidth.

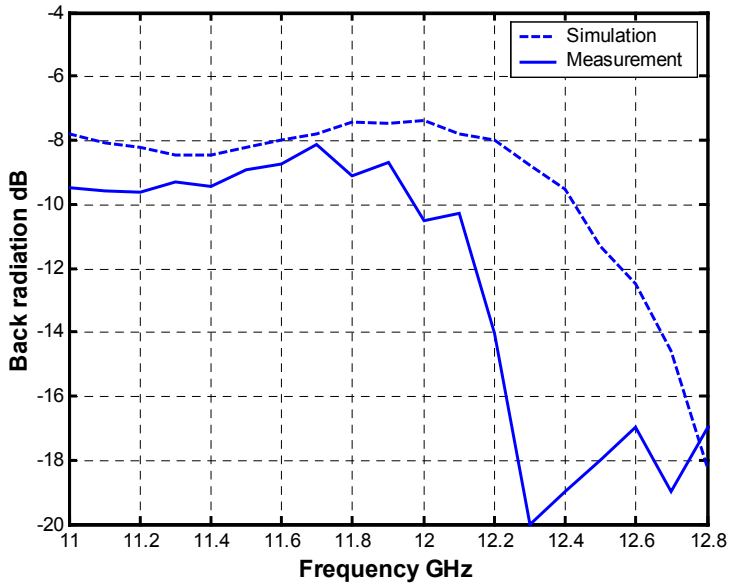

Figure 2.13. Backward radiation of a linearly polarized microstrip antenna

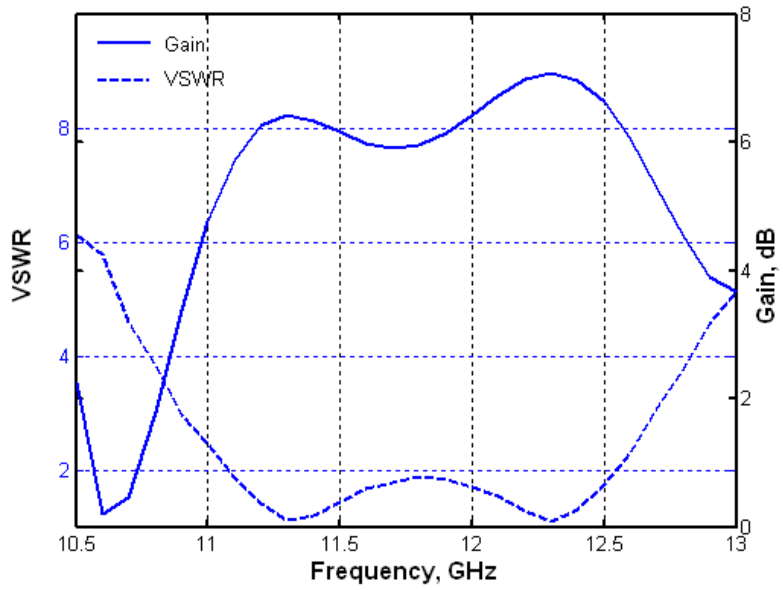

Figure 2.14. Measured gain and voltage standing wave ratio of a linearly polarized microstrip antenna

Table 2.10. Measured Characteristics of A Linearly Polarized Microstrip Antenna

Char.	f_0 GHz	f_{min}/f_{max} GHz	BW MHz	bw %	$(2\theta_{3dB})_E$ degree	$(2\theta_{3dB})_H$ degree	BRL dB	G dB	D dB	η_e %
Value	11.815	11.08/12.55	1470	12.4	93	83	-9.1	5.6	6.4	89

2.4 Impedance Matching Improvement for a Class of Wideband Antennas

The narrow impedance bandwidth is the most serious limitation factor of the linearly polarized antennas. One of the possible solutions of the impedance bandwidth problem consists of introducing dual (or multiple) resonances in the impedance characteristic. Typical examples of this bandwidth enhancement technique are aperture-coupled microstrip antennas with a resonant slot [26], stacked antennas [7], backfire antennas [113], and other types of antennas with similar impedance characteristics.

The basic problem in this class of antennas is the high value of the return loss within the antenna bandwidth. In addition, in antennas with an even number of resonances, the impedance matching is the worst at the design (operating) frequency. The use, in this case, of a usual (classic) quarter-wavelength transformer improves the impedance matching at the mid-frequency, but unfortunately decreases the bandwidth (with more than 30% for an antenna with two resonances).

In this section, a simple and efficient technique for impedance matching improvement within the antenna bandwidth has been proposed. These antennas have two resonances. The quarter-wavelength transformer will be used to match the antenna to the feed line.

2.4.1 Description of The Proposed Solution

The proposed solution has been applied to the wideband aperture-coupled microstrip antenna having a resonating slot. This resonating slot has the effect of approximately doubles the antenna bandwidth, but decreases the impedance matching within the antenna bandwidth [27]. The return loss of the antenna is shown in Fig. 2.16 (solid line). The patch is responsible for the low frequency resonance f_1 and the aperture (the slot) is responsible for the high frequency resonance f_2. In fact, these two resonances involve also the mutual influence between the patch and the slot.

Fig. 2.15 shows the microstrip feed line and its equivalent circuit. We assume that the origin of the coordinate system is at point *(z*=0)* on the line below the patch and slot centre. If the input to the line is at $z^* = l$,

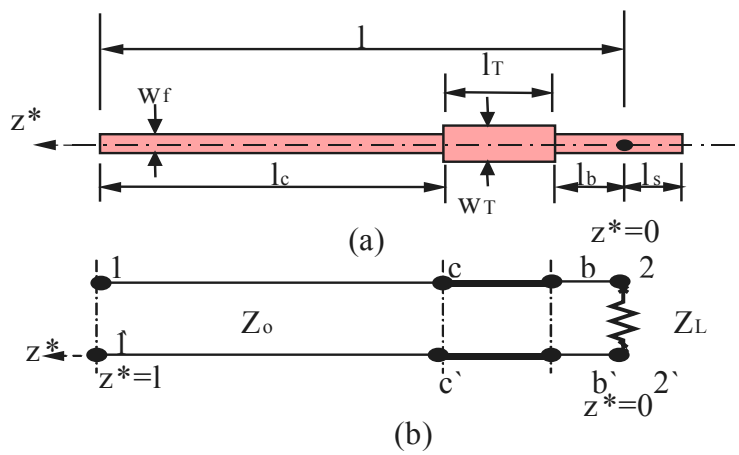

Figure 2.15. Microstrip feed line (a) and its equivalent circuit (b).

the normalized input impedance ($z = r + jx = Z/Z_0 = R/Z_0 + jX/Z_0$) is [114]

$$Z = \frac{Z_L + \tanh(\gamma l)}{1 + Z_L \tan(\gamma l)} \tag{2.75}$$

where,

$z_L = r_L + jx_L$ is the normalized load impedance (the antenna impedance at point *(z*=0)*);

$z_L = Z_L/Z_0$, $r_L = R_L/Z_0$, and $x_L = X_L/Z_0$,

Z_0 is the characteristic impedance of the feed line,

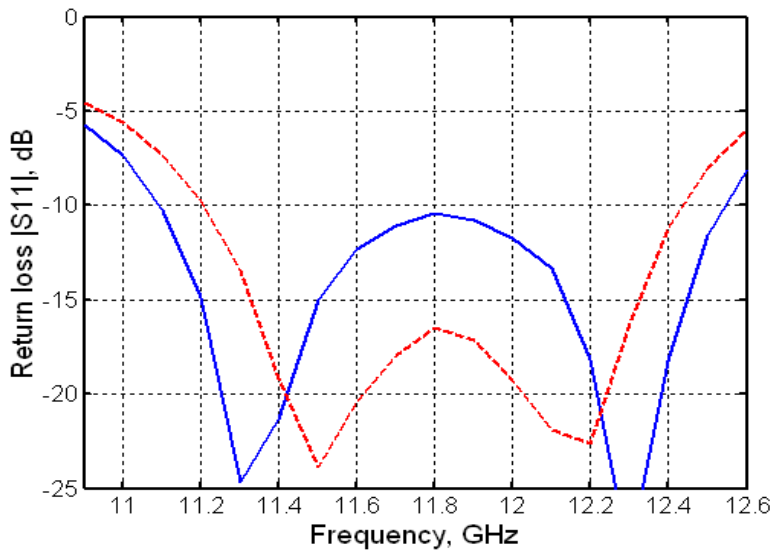

Figure 2.16. Return loss of aperture-coupled microstrip antenna: without matching (—); (b) with matching (----).

$\gamma = \alpha + j\beta$ is the complex propagation constant, where α is the attenuation constant, and β is the phase constant,

l is the length of the feed line.

The expression (2.75) can also be written as follows:

$$r = \frac{[r_L M + \sinh(2\alpha l)]Q + [x_L M + \sin(2\beta l)]U}{Q^2 + U^2},$$

$$x = \frac{[x_L M + \sin(2\beta l)]Q - [r_L M + \sinh(2\alpha l)]U}{Q^2 + U^2}, \tag{2.76}$$

where,

$$M = \cosh(2\alpha l) + \cos(2\beta l),$$
$$Q = M + r_L \sinh(2\alpha l) - x_L \sin(2\beta l),$$
$$U = r_L \sin(2\beta l) + x_L \sinh(2\alpha l).$$

If the return loss $S_{11}(f)$ or the normalized input impedance $z(f)$ at $z^* = l$ are known (by simulation or measurement), the normalized load impedance in (2.75) can be expressed as:

$$r_L = \frac{[rM - \sinh(2\alpha l)]A - [xM - \sin(2\beta l)]B}{A^2 + B^2},$$
$$x_L = \frac{[xM - \sin(2\beta l)]A + [rM - \sinh(2\alpha l)]B}{A^2 + B^2}, \tag{2.77}$$

where,

$$A = M - r\,sinh(2\alpha l) + x\,sin(2\beta l),$$

$$B = r\,sin(2\beta l) + x\,sinh(2\alpha l).$$

The quarter-wavelength transformer must be placed a distance l_b away from the load at point *(z*=0)*, where the input impedance toward the load at $z^* = l_b$ is real. The distance l_b can be found from equation (2.76)

$$x(l_b) = 0 \tag{2.78}$$

The same result, but in a closed-form expression may be obtained in the case of lossless feed line ($\alpha = 0$):

$$l_{b1,2} = \frac{\lambda_{g0}}{2\pi}\arctan\frac{\left(1 - r_{L0}^2 - x_{L0}^2\right) \pm \sqrt{\left(1 - r_{L0}^2 - x_{L0}^2\right)^2 + 4x_{L0}^2}}{2x_{L0}}, \tag{2.79}$$

where,

$l_b = l_{b1}$, $x_{L0} > 0$, and $l_b = l_{b2}$, $x_{L0} < 0$

λ_g is the wavelength in the feed line, and the index 0 denotes the mid-frequency f_0 of the operating frequency range.

The expression used to calculate the characteristic impedance of the quarter-wavelength transformer at $z^* = l_b$ and $f = f_0$ is

$$Z_{0T} = \sqrt{Z_0 R_{b0}}, \tag{2.80}$$

where R_{b0} is the impedance (real, $Z_{b0} = R_{b0}$, $X_{b0} = 0$) of the load seen at $z^*=0$.

Accordingly the impedance matching at $f = f_0$ improves. On the other hand, it leads to a matching degradation at both $f = f_1$ and f_2.

If the value of the λ/4 transformer characteristic impedance lies between the values of Z_0 (no transformer) and Z_{0T} (transformer in (2.80), the difference between the matching at $f = f_0$ and both $f = f_1, f_2$ will decrease. Thus, the choice of Z_{0T} to lie in this range would improve the impedance matching within the antenna bandwidth. The antenna-matching enhancement would as well, lead to an increase of the antenna gain and efficiency.

We propose to use the following expression to calculate the transformer characteristic impedance value

$$Z_{0T} = \sqrt[4]{Z_0^2 R_{b0} \sqrt{R_{b1} R_{b2}}}, \tag{2.81}$$

where R_{b1} and R_{b2} are the impedances of the feed line at $z^* = l_b$ at $f = f_1$ and f_2 respectively. One may see that in the case where $f_1 = f_2 = f_0$ and $R_{b1} = R_{b2} = R_{b0}$ the expression (2.81) reduces to (2.80).

2.4.2 Results

In order to verify the validity of the proposed solution, we have applied it to the wideband aperture-coupled microstrip antenna [27] in the Ku – band. The following parameters are used (Fig. 2.15): length of the feed line l = 26.5 mm, width of the feed line w_f = 0.972 mm, stub length l_s = 1.6 mm, feed substrate RT/duroid 6006 with substrate thickness h_f = 0.635 mm, metal thickness $t_f = t_g$ = 0.0175 mm, relative dielectric constant ε_{rf} = 6.15, and loss tangent tan δ_f = 0.0019, characteristic impedance of the feed line Z_0 = 50 Ω, mid-frequency f_0 = 11.822 GHz, patch resonance frequency f_1 = 11.330 GHz, slot resonance frequency f_2 = 12.315 GHz, bandwidth BW = 1.470 GHz (11.08 to 12.55 GHz), and fractional impedance bandwidth bw = 12.4 %.

Fig. 2.16 (solid line) shows the measured return loss of the antenna at the connector section ($z^* = l$). The application of expression (2.77) gives the normalized load impedance $z_L(f) = r_L(f) + jx_L(f)$. The distance l_b is given by (2.79) for r_{L0} = 1.316 and x_{L0} = - 0.665; $l_b = l_{b2}$ = 2.152 mm. The value of the transformer characteristic impedance is calculated using (2.81). Its value is Z_{0T} = 42.477 Ω. for R_{b0} = 26.631 Ω, R_{b1} = 46.738 Ω, and R_{b2} = 51.156 Ω.

Using [93] one determines the transformer length l_T = 2.901 mm, and width w_T = 1.296 mm. Using expression (2.76), the values of the normalized impedance at $l = l_b$, l_T, and l_c (l_c

= 21.447 mm) were calculated taking $z_L = z_L$, z_b, and z_c as the load impedance respectively in Fig. 2.15. Finally, the normalized input impedance of the matched antenna $z(f) = r(f) + jx(f)$ is given by its value at $z^* = l_c$.

The return loss is calculated by the well known expression in [115]

$$\left|S_{11}\right| = 20\log\sqrt{\frac{(r-1)^2 + x^2}{(r+1)^2 + x^2}}, dB \tag{2.82}$$

and is shown in Fig. 2.16 (dashed line).

Fig. 2.17 shows the voltage standing wave ratio *VSWR* of the antenna without matching (solid line) and with the proposed matching (dashed line).

Table 2.11 shows the comparison between the antenna bandwidth values with and without matching conditions. It has been observed that the bandwidth of the matched antenna decreases from 12.4 % to 10.5 % (a 15 % decrease), but the bandwidth for *VSWR* < 1.35 increases more than twice the value (2.22 times). The bandwidth $bw_{1.35}$ presents 76 % of the whole bandwidth $bw_{2.0}$ in case of matching. This is considered a substantial improvement compared with the unmatched case (29 %).

Finally, the designed antenna with the proposed transformer was fabricated and tested with a Hewlett Packard 8722D Network Analyzer (50 MHz – 40 GHz). Fig. 2.18 shows graph of the voltage standing wave ratio *VSWR* of the antenna, both measured (solid line) and calculated (dashed line). These comparison curves confirm that there is a good agreement between the measured and the theoretical values.

Table 2.11. Comparison Values of The Antenna Bandwidths with and Without Matching

Type of the feed line	**VSWR < 2 ($bw_{2.0}$)**	**VSWR < 1.35 ($bw_{1.35}$)**	**$bw_{1.35}/bw_{2.0}$**
Feed line without matching	12.4 %	3.6 %	29 %
Feed line with proposed transformer	10.5 %	8 %	76 %

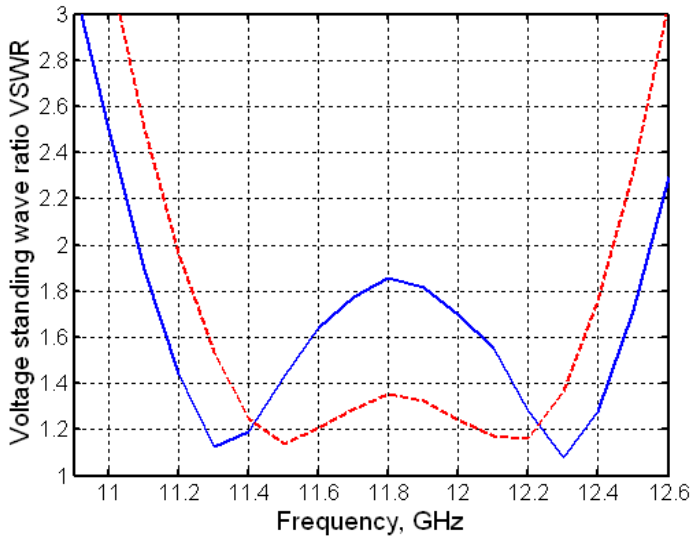

Figure 2.17. VSWR of aperture-coupled microstrip antenna:
(a) without matching (—); (b) with matching (----).

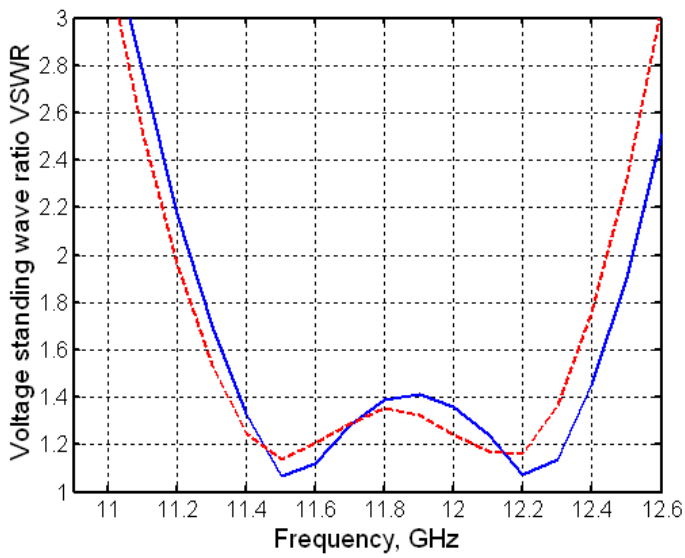

Figure 2.18. Comparison of aperture-coupled microstrip antenna bandwidth with the proposed matching: (a) measurement (—); (b) theory (----).

This approach can be carried out by Microwave Office [116], Mathcad, Matlab, or even by a programmable handheld calculator. Therefore, it is useful for a practical antenna designer.

CHAPTER 3

Defected Ground Structure Low-pass and Band-pass Filters

This chapter concentrates on basic limitations of classical microstrip line based low-pass and band-pass filters and way to improve the design by using the defected ground plane structures. New investigations are presented on the choice of geometrical shapes for the DGS structure as an element for the LPF. We have also introduced the band accept (band pass) structure in DGS and used it for the development of a new compact BPF.

3.1 Introduction

Several compact and high performance components have been reported by using the generic structure called the defected ground structure (DGS) for the microstrip line. Another type of structures, known as electromagnetic bandgap (EBG) or alternatively called photonic band gap (PBG)structures have periodic structure. These structures have been attractive to obtain the function of unwanted frequency rejection and circuit size reduction. Researches on the PBG had been originally carried out in the optical frequency. Recently, there has been an increasing interest in microwave and millimeter wave applications of PBG circuits. Various shapes of DGS structures have been appeared. Since DGS cells have inherently resonant property, many of them have applied to filter circuits. However, it is difficult to use a PBG structure for the design of the microwave or millimeter wave components due to the difficulties of the modeling. There are many design parameters, which have an effect on the bandgap property, such as the number of lattices, lattice shape and lattice spacing. Another difficulty in using the PBG circuit is caused by the radiation from the periodic etched defects.

Many etched shapes for the microstrip could be used as a unit DGS. An LC equivalent circuit can represent the unit DGS circuit. The physical dimensions of the DGS affect the

equivalent circuit parameters. It is one of the purposes of this chapter to study different DGS slots. To design a circuit with DGS section, the equivalent circuit and parameters of the DGS section should be extracted. Using the 3D-EM Simulator, one can derive the equivalent circuit of the DGS section.

The stepped impedance low-pass filter response can be improved by using the DGS. Also, the filter structure will be very simple and compact.

It has been commented that for the equal area of slot head, any shape of slot can be used [37]. However, equal area only ensures equal equivalent inductance at the cutoff frequency and not the identical response. Also a particular shape of the slot in the ground plane could be more appropriate to design a complete circuit on the same substrate. The shape, size and orientation of a slot can have influence on performance of the circuit. In this chapter, the response of four shapes of the DGS slot like rectangular, dumb-bell, square head slot and arrow head slot will be investigated. A method to design low pass filters using DGS on microstrip substrate has been proposed already by [37]. In this chapter the DGS will be used to control and improve the stopband characteristics of the stepped impedance microstrip LPF.

The DGS configuration provides only the band-reject (band stop) characteristic [37]. In this chapter, a new DGS based band accept (band pass) configuration in a microstrip line will be introduced. Not only an etched lattice shape can achieve this new band-accept DGS unit element ground plane of the microstrip but also by providing a gap in the microstrip line. The characterization of a gap in a microstrip is useful in the design of dc blocks; end coupled filters, and coupling elements to resonators. A microstrip gap is modeled by a series capacitance to the microstrip line and two shunt capacitances from the edges of the microstrip line to the ground plane. The etched defect in ground plane and a gap in the microstrip line disturb the current distribution in the ground plane. This disturbance can change characteristics of the transmission line such as line capacitance and inductance. The return loss response of this new configuration indicates two poles and one zero. The first pole comes from the series capacitance of the gap in the microstrip line, the zero can only come from series resonance behaviour and the second pole arises from a parallel LC resonance circuit. Thus, a series capacitance followed by a parallel LC circuit can represent the new DGS configuration. The DGS with and without gap in the microstrip line

configurations will apply to practical filter circuits. The equivalent circuit of the new DGS based band accepts configuration is derived by using the 3D-EM Simulator.

The microstrip band-pass filter can be designed by the use of a cascade of half-wave resonators or by using the parallel coupled microstrip lines. The defected ground plane structures (DGS) have been proposed for suppression of spurious response in the coupled microstrip line band-pass filters. In this chapter, the new DGS with gap in the 50 Ω. microstrip line configuration will be used to get both series and parallel resonance behavior simultaneously. By this new combination, a compact band pass filter has been designed using the DGS.

3.2 Filter implementation

This section will review the overall design strategy which may be followed for any microstrip filter.

Table 3.1 Microstrip filter design strategy

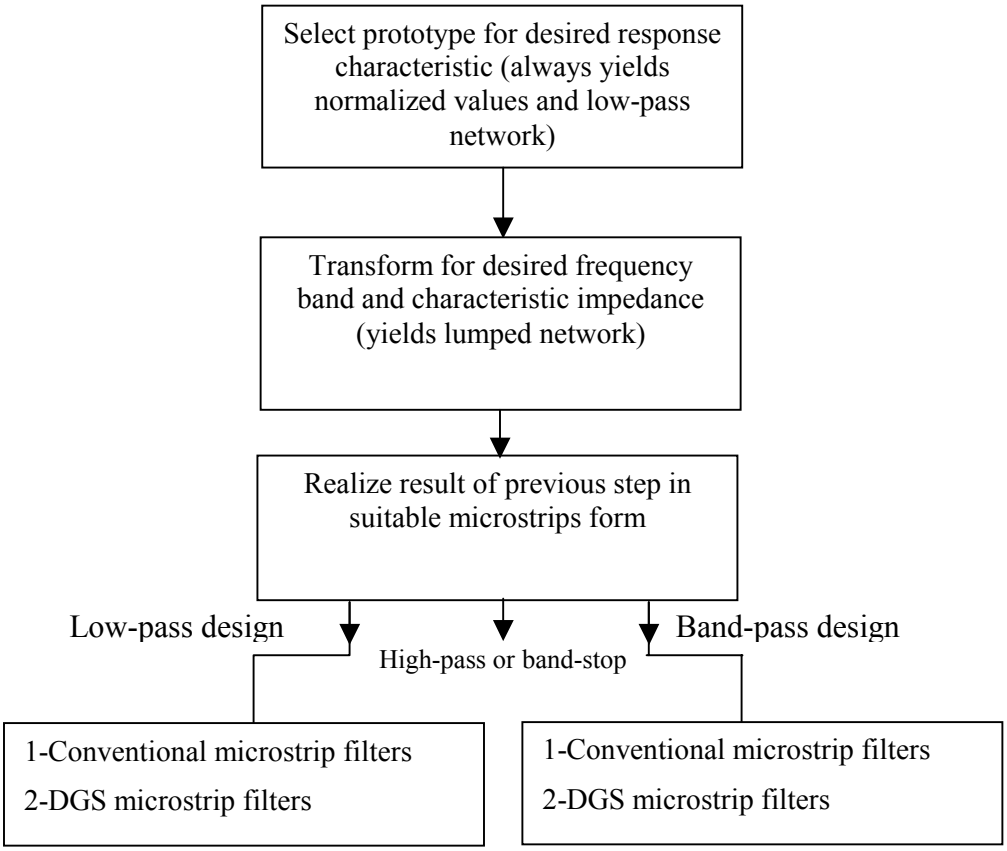

Table 3.1 shows the typical sequence which starts with a prototype specification (by insertion-loss approach) and finishes with a practical, fully dimensioned, microstrip circuit.

The lumped-element filter design generally works well at low frequencies, but two problems arise at microwave frequencies. First, lumped elements such as inductors and capacitors are generally available only for a limited range of values and are difficult to implement at microwave frequencies, but must be approximated with distributed components. In addition, at microwave frequencies the distances between filter components is not negligible. Richard's transformation is used to convert lumped elements to transmission line sections, while Kuroda's identities can be used to separate filter elements by using transmission line sections. Because such additional transmission line sections do not affect the filter response, this type of design is called redundant filter synthesis. It is possible to design microwave filters that take advantage of these sections to improve the filter response.

3.2.1 Illustration example

We present the design procedure for the conventional stub type three-pole low-pass filter. This example shows the problem associated with such LPF . Later on we will discuss the improvement achieved with the DGS patterns. The specifications for the filter under consideration are:

Cutoff frequency $f_c = 4$ GHz.

Passband ripple 0.1 dB (or return loss ≤-16.42 dB) and source/load impedance $Z_o = 50\ \Omega$

The normalized low-pass prototype with Chebyshev response is chosen, whose element values are

$$g_o = g_4 = 1,$$
$$g_1 = g_3 = 3.3487 = L_1, = L_3,$$
$$g_2 = 0.7117 = C_2$$

with the lumped-element circuit shown in Fig. 3.1. Its microstrip realization, using the stub is shown in Fig. 3.2. Finally, we impedance and frequency scale the circuit, which simply involves multiplying the normalized characteristic impedance by 50 Ω and choosing the line and stub lengths to be λ/8 at 4 GHz. The final microstrip layout is shown in Fig. 3.2.

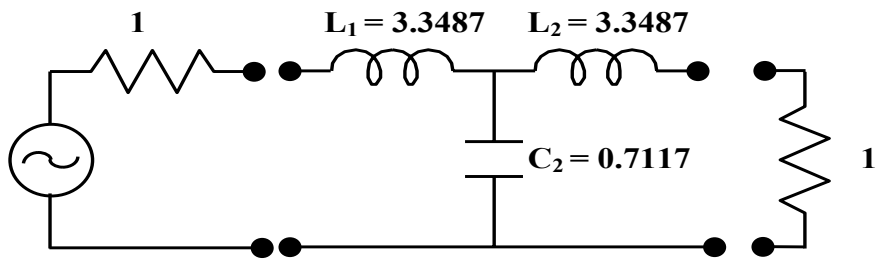

Figure 3.1 3 - pole proto type LPF

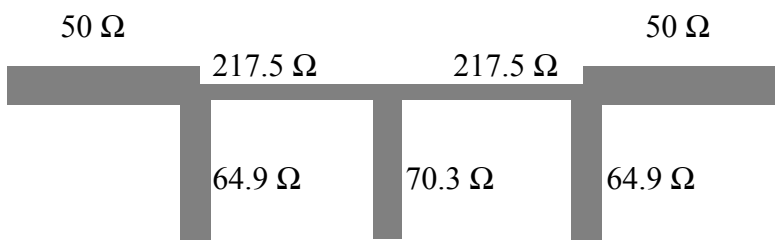

Figure 3.2 Microstrip final filter

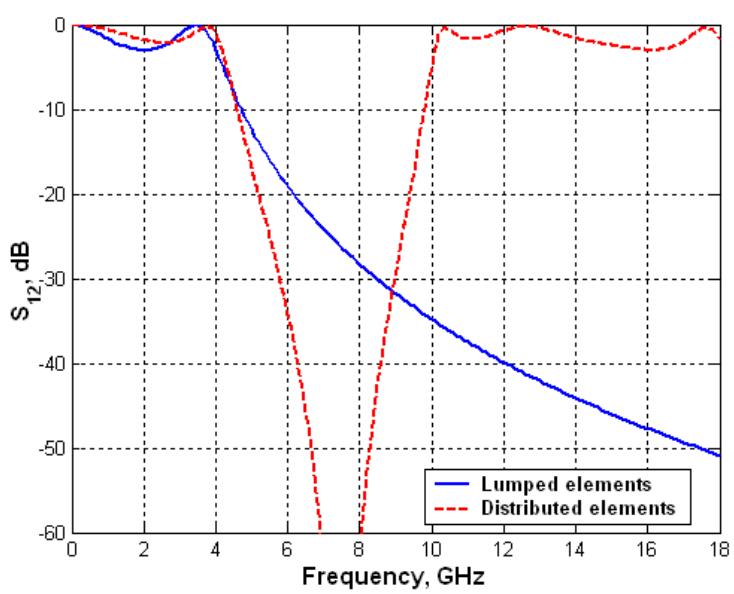

Figure 3.3 Amplitude response of lumped and distributed-element low-pass filter

The amplitude response of the low-pass filter is shown in Fig. 3.3 , along with the lumped element response using the electromagnetic and circuit simulator Microwave office. From the response, we note that the pass-band characteristics are very similar up to 4 GHz, but the distributed-element filter has a response, which repeats every 16 GHz, as a result of the periodic nature of Richard's transformation. Thus the stop band response of microstrip LPF is not satisfactory. Moreover the characteristic impedance values shown in Fig.3.2 cannot be realized in the microstrip structure.

3.3 Defected ground structure filters

In the previous section the lumped-element filter design has been approximated with the transmission line structure. Agreement of filter response is only in the pass band. In the stop band the transmission line based LPF departs from the response of the lumped element LPF and the stop bands response of the transmission line based LPF degrades. A quasi-lumped element based on the defected ground structures (DGS) has been proposed to improve the stop band characteristics of the low-pass filter

3.3.1 Frequency characteristics of DGS unit section

Fig. 3.4 shows the etched dumb-bell slot shape of the DGS section, which is located on the backside metallic ground plane. The DGS unit section can provide cutoff frequency and attenuation pole in some frequency without any periodicity of DGS. In order to investigate the frequency characteristics of the DGS section, the DGS unit section has been simulated by the 3-D EM-Simulator Microwave Studio.

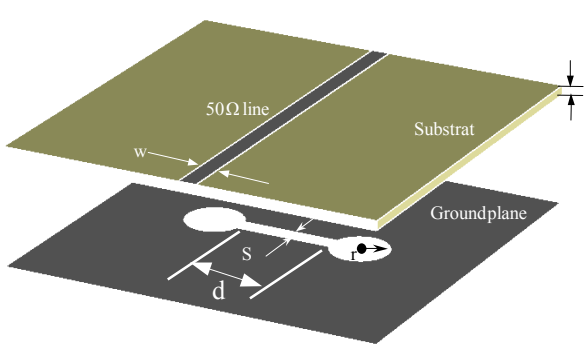

Figure 3.4 3-D view of the DGS

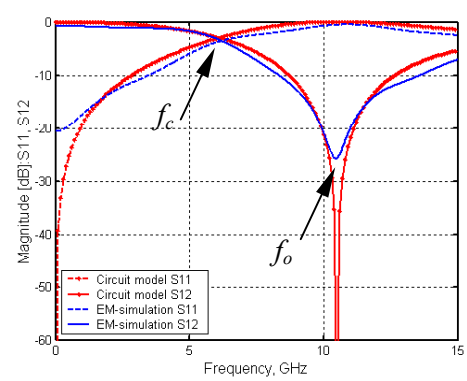

Figure 3.5 S_{11} and S_{12} of the DGS

unit section unit section

The simulation results show that one-pole low-pass filter characteristics. The presence of the DGS section operating at below its pole frequency increases the effective inductance of a microstrip line. The cutoff frequency is mainly dependent on the etched slot head area in the ground plane. There is also attenuation pole location, which is due to the etched slot width of the slot. Actually, it is well known that an attenuation pole can be generated by combination of the inductance and capacitance elements. Thus, the DGS section is fully described by the etched slot width, length and head area in case of slots with certain head shape.

3.3.2 Modeling and parameter extraction

A parallel LC circuit can represent the equivalent circuit of the DGS as shown from its response. From the application point of view, the DGS section can serve as replacement for a parallel LC resonator circuit in many applications. To apply the DGS section to a practical circuit design example, it is necessary to extract the equivalent circuit parameters. As an example of the parameter extraction procedure, Fig. 3.4 shows a 50 Ω microstrip line feeding the dumb-bell slot in the ground plane.

The dimensions of the DGS section shown in Fig. 3.4 are d, r, s and w have been chosen to be 6, 2, 0.6 and 1.9 mm respectively. The substrate RO4003C with 0.813 mm thick and a dielectric constant ε_r of 3.38 has been chosen for this study. The simulation result is shown in Fig. 3.5. There is an attenuation pole at 10.5 GHz. In order to explain the cutoff and attenuation pole characteristic of the DGS section simultaneously, the equivalent circuit should exhibit performances low-pass and band-stop filter at the same time. At frequency less than the resonance frequency, the circuit behaves like an inductor.

The circuit parameters for the equivalent circuit can be extracted from the simulation or from the measured results. The simulation result of the DGS section can be matched to the one pole maximally flat low pass response, which has 3-dB cutoff frequency at 6.25 GHz.

The equivalent inductive reactance can be easily calculated by using the prototype element value of the one-pole response. The parallel capacitance value for the given DGS section can be extracted from the attenuation pole location frequency.

The equivalent reactance value of the DGS unit can be expressed as follows:

$$jX_{LC} = \frac{j\omega L_P \times \frac{1}{j\omega C_P}}{j\omega L_P + \frac{1}{j\omega C_P}} = \frac{j\omega L_P}{1-\omega^2 L_P C_P} \tag{3.1}$$

$$\omega_o^2 = \frac{1}{L_P C_P} \tag{3.2}$$

$$X_{LC} = \frac{1}{\omega_o C\left(\frac{\omega_o}{\omega} - \frac{\omega}{\omega_o}\right)} \tag{3.3}$$

Using the prototype element value of the one-pole response network shown in Fig. 3.7, the parallel capacitance value for the DGS is given by

$$C_P = \frac{\omega_c}{Z_o g_1\left(\omega_o^2 - \omega_c^2\right)} = \frac{5 f_c}{\pi\left(f_o^2 - f_c^2\right)} \quad pf \tag{3.4}$$

$$L_P = \frac{250}{C_P\left(\pi f_o\right)^2} \quad nH \tag{3.5}$$

Where, f_c, in GHz is the cut-off frequency of the band-reject response of the slot at 3 dB and f_0, in GHz is its pole frequency. For the dumb-bell structure they are shown in Fig. 3.5. The Fig. 3.5 shows response of the circuit model obtained by feeding the model to the circuit simulator, Microwave Office [116]. The model follows results of the EM-simulator faithfully. The pole magnitude of the circuit simulator becomes infinite as the circuit model does not account for the losses in the DGS slot. At any frequency $f < f_0$ the parallel circuit behaves as an inductor and its equivalent inductance in nH is obtained from,

$$L_{eq} = \frac{L_P}{[1-(\frac{f}{f_0})^2]} \quad \text{nH} \tag{3.6}$$

Thus the slot in ground plane excited by the microstrip line behaves as parallel resonance.

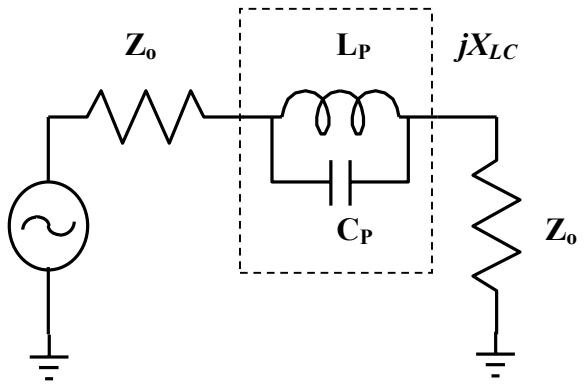

Figure 3.6 Equivalent circuit of the DGS circuit, where the dotted box shows the DGS Section

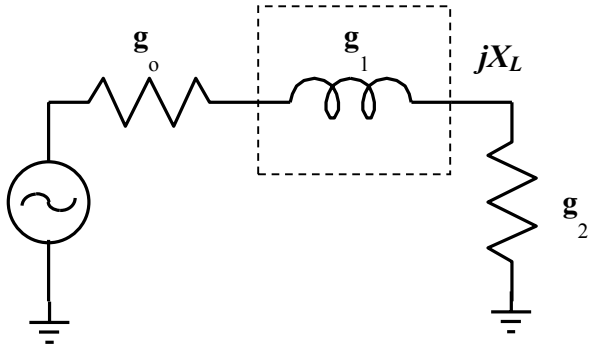

Figure 3.7 One-pole prototype low pass filter circuit

3.4 Study of different DGS slots configuration

One question arises. Does the shape of the slot affect the response of the DGS unit section?. To answer this question, we divided the slots into two categories. The first one is the rectangular slot Fig. 3.8.a, which has no head. The second category is the rectangular slots with different heads like circle, square, and arrow as shown in Fig. 3.8.b to Fig. 3.8.d respectively. At first, we selected three types of slots,

- Square head slot
- Arrow head slot
- Circular head slot or dumb-bell slot.

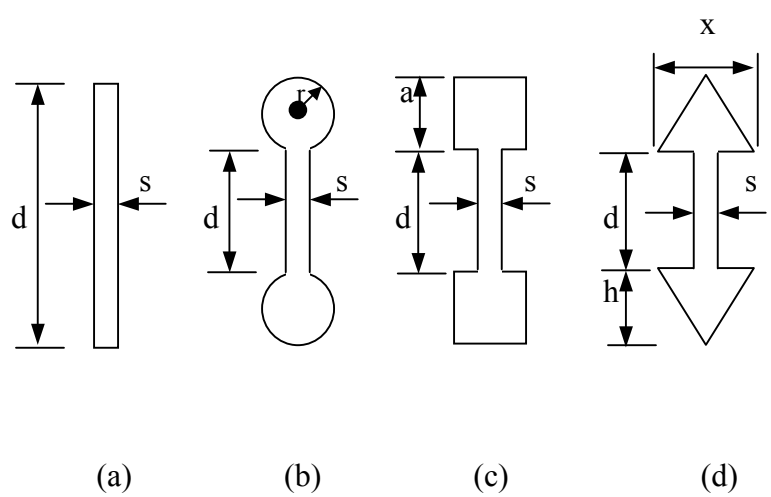

Figure 3.8 Shapes of DGS slots

We fixed the slot width, s = 600 μm and the slot lengths, d = 1.9 mm and also maintained the area of the slot heads constant and equal to 0.64 cm^2. We selected the square head dimension a = 0.8 cm, the radius of the dumb-bell slot circular head r = 0.4514 cm, and x = 1.2157 cm for the equilateral triangle which form the arrowhead. The response is shown in Fig. 3.9.a where, they have different response especially in the transition region. Fig. 3.9.b shows another comparison between the same square head with a = 0.8 cm and a triangular head with x = 1.4 cm, h = 0.9143 cm to keep the heads area at 0.64 cm^2. So, the shape of the DGS slot has an influence on the steepness of transition and stop-band rejection.

Another numerical experimentation has been done to understand the save in the length. Two different slots have been chosen, the rectangular and the arrow head slots. The response is shown in Fig. 3.9.c. For the same resonance frequency, the rectangular slot has 35 % more length than that of the arrow head slot. Fig. 3.9.d shows the comparison of dimensions.

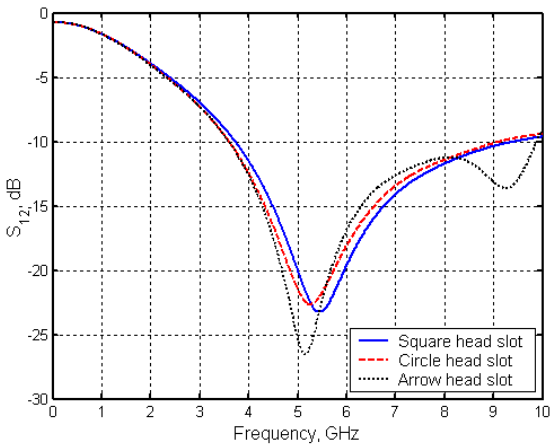

a. Square head, arrow head and dumb-bell slots

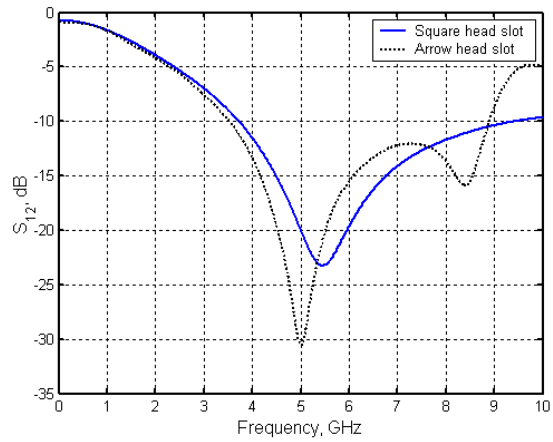

b. Square head and arrow head slots

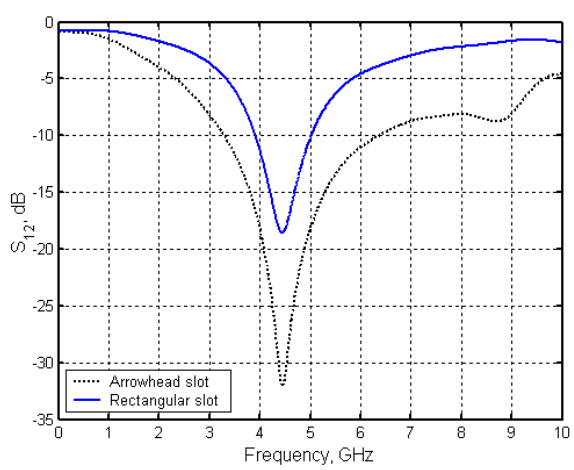

c. Comparison of rectangular and arrow head slots response

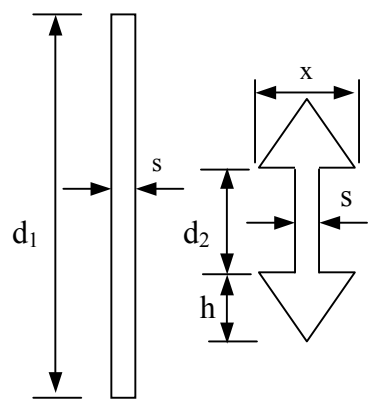

$(d_2+2h) = 0.65\ d_1$

d. Comparison of rectangular and arrow head slots

Figure 3.9 Comparison of DGS slots response

Thus, we decided to make more investigation for all four slot types parameters.

3.4.1 Rectangular slot

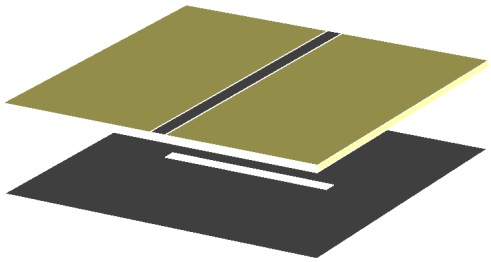

Figure 3.10.a 3-D view of the rectangular DGS slot

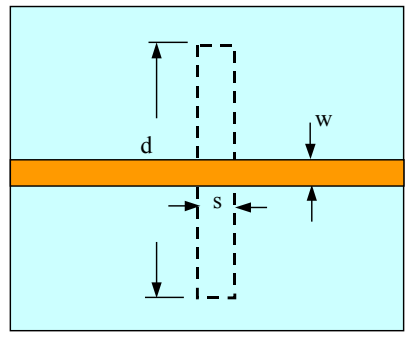

Figure 3.10.b Wire frame view of the rectangular DGS slot

A. Influence of the Slot Width

The influence of the etched slot width of the rectangular slot shown in Fig. 3.10 on the response will be examined. The slot length, d were kept constant to 10 mm for all the cases and the etched slot width, s was varied. The simulation results are shown in Fig. 3.11. The table 3.2 shows the variation in f_c, f_0 and extracted C_p and L_p of the rectangular slot respect to the change in the slot width, s. The nature of change in the f_c and f_0 are opposite to each other and f_c is more influenced by the increase in the gap as compared to f_0. So is the case for C_p.

Table 3.2 Rectangular slot characteristics for different slot widths S

S	f_c	f_o	C_P	L_P
0.2 mm	8.64 GHz	11.21 GHz	0.2696 pf	0.748 nH
0.4 mm	8.23 GHz	11.41 GHz	0.209 pf	0.928 nH
0.6 mm	8 GHz	11.62 GHz	0.179 pf	1.047 nh
0.8 mm	7.8 GHz	11.83 GHz	0.1569 pf	1.153 nH
1 mm	7.62 GHz	12 GHz	0.141 pf	1.247 nH

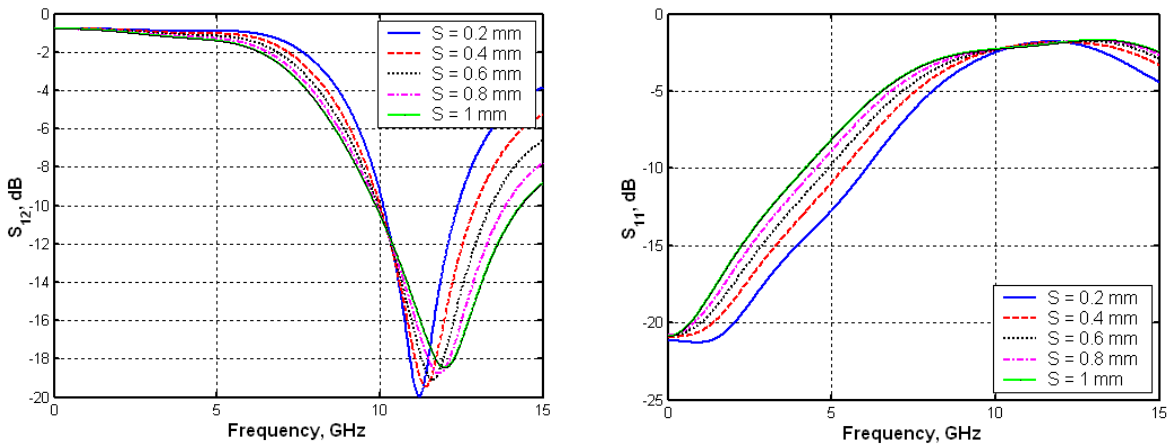

a. Transmission loss S_{12} b. Reflection loss S_{11}

Figure 3.11 Simulated S-parameters for rectangular slot for different slot widths S

B. Influence of the Slot Length

We extend our study to the influence of the slot length, d. The slot width, s was kept constant to 0.6 mm for all the cases and the slot etched length, d was varied. . The substrate with 0.813 mm thick and a dielectric constant of 3.38 was used for all simulations. The simulation results are illustrated in Fig. 3.12. The calculated capacitances and inductances are given in Table 3.3. From Fig. 3.12, by increasing the etched slot length, the series inductance will increase.

Table 3.3 Rectangular slot characteristics for different slot lengths d

d	f_c	f_o	C_P	L_P
1 cm	8.02 GHz	11.59 GHz	0.182 pf	1.034 nH
1.5 cm	5.51 GHz	7.77 GHz	0.292 pf	1.436 nH
2 cm	3.1 GHz	5.85 GHz	0.375 pf	1.975 nh
2.5 cm	3.18 GHz	3.69 GHz	0.426 pf	2.7 nH
3 cm	2.62 GHz	3.92 GHz	0.49 pf	3.36 nH

This effective series inductance introduces the cutoff characteristic at certain frequency. As the etched slot length d is increased, the effective series inductance increases, and increasing the series inductance gives a lower cutoff frequency, as seen in Fig. 3.12.

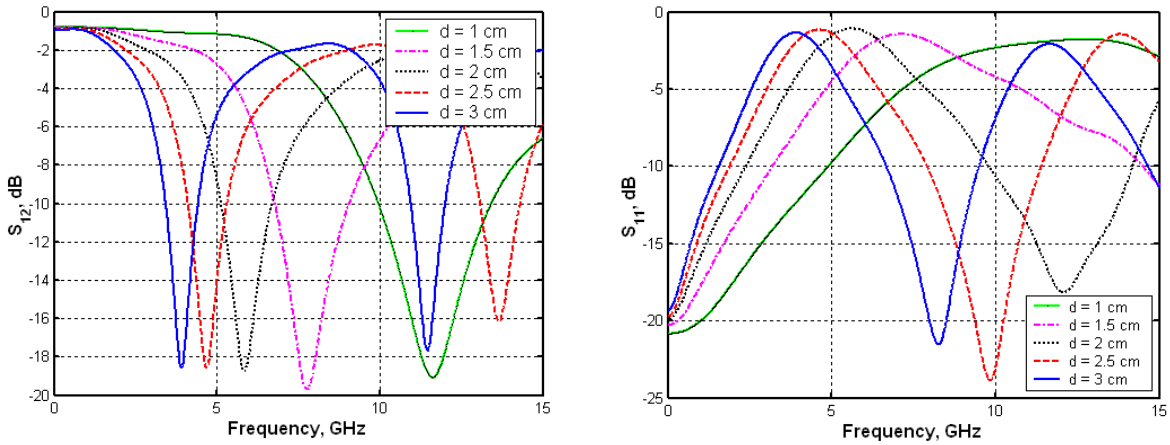

a. Transmission loss S_{12} b. Reflection loss S_{11}

Figure 3.12 Simulated S-parameters for rectangular slot for different slot lengths d

3.4.2 Dumb-bell slot

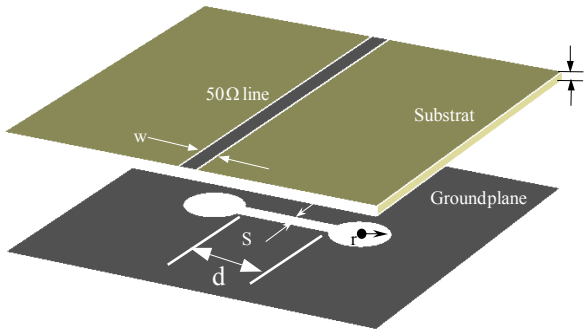

Figure 3.13.a 3-D view of the Dumb-bell DGS slot

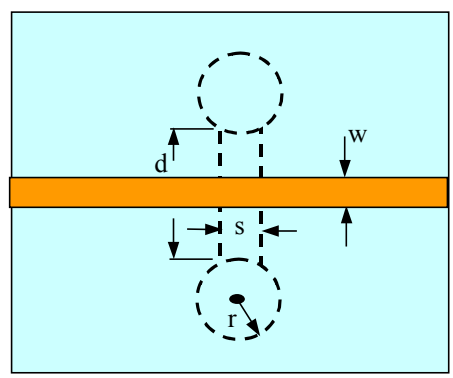

Figure 3.13.b Wire frame view of the dumb-bell DGS slot

A. Influence of the Dumb-bell Slot Head Dimension

The line width was chosen to be the characteristic impedance of the 50 Ω microstrip line for simulations. Five DGS unit circuits were simulated with different dimensions. In order

to investigate the influence of the dumb-bell slot head dimension, the etched slot width and the length were kept constant to 0.6 mm and 2 mm respectively for all five cases and the etched dumb-bell head was varied. The substrate with 0.813 mm thick and a dielectric constant of

3.38 was used for all simulations. The simulation results are illustrated in Fig. 3.14. The calculated capacitances and inductances are given in Table 3.4. From Fig. 3.14, one clearly observes that employing the etched dumb-bell slot head area increases the series inductance to the microstrip line. As the neck gap is kept constant so C_p does not change much.

This effective series inductance introduces the cut-off characteristic at certain frequency. As the etched area of the dumb-bell slot head is increased, the effective series inductance increases, and increasing the series inductance gives rise to a lower cut-off frequency, as seen in Fig. 3.14. There are attenuation poles in simulation results on the etched dumb-bell slot head area. These attenuation poles in simulation results can be explained by parallel capacitance with the series inductance, as indicated in the previous section.

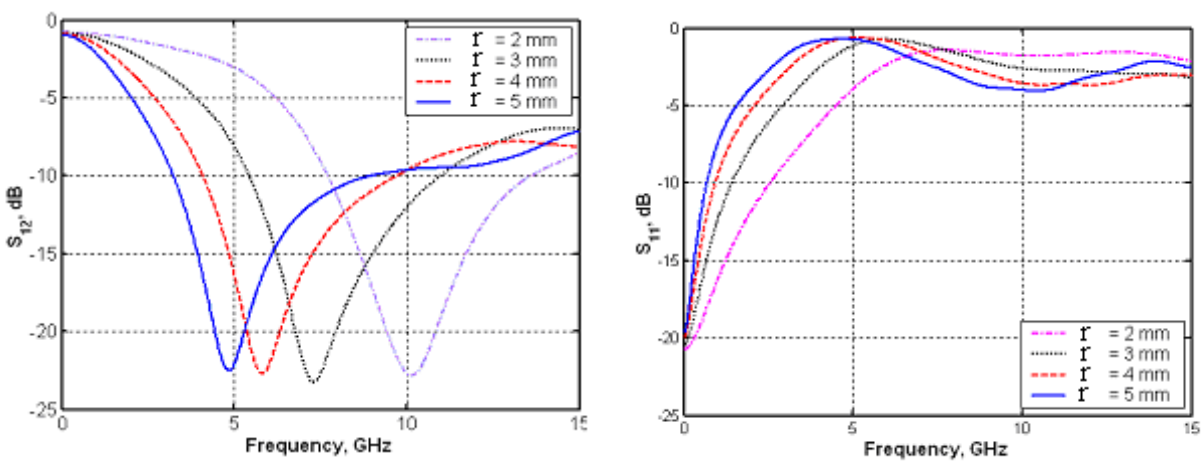

a. Transmission loss S_{12} b. Reflection loss S_{11}

Figure 3.14 Simulated S-parameters for Dumb-bell slot for different slot radiuses r

This capacitance depends on the etched gap below the conductor line, which is noted as s in Fig 3.13.b. The capacitance values are identical for all cases due to the identical slot width. However, the attenuation pole location, which corresponds to the resonance frequency of the parallel LC circuit, also becomes lower because as the series inductance increases, the resonance frequency of the equivalent parallel LC circuit decreases.

Table 3.4 Dumb-bell slot characteristics for different slot head radiuses r

r	f_c	f_o	C_P	L_P
2 mm	5.63 GHz	10.1 GHz	0.127 pf	1.949 nH
3 mm	3.25 GHz	7.31 GHz	0.121 pf	3.93 nh
4 mm	2.25 GHz	5.81 GHz	0.1248 pf	6.013 nH
5 mm	2.62 GHz	3.83 GHz	0.1245 pf	8.72 nH

B. Influence of the Slot Width

An investigation on the influence of the etched slot width will be employed. The dumb-bell slot head radius, r and slot length, d were kept constant to 2 mm and 6 mm respectively for all the cases and the etched slot width, s was varied. The simulation results are shown in Fig. 3.15. Due to the constant dumb-bell slot head dimensions, we can expect that the effective series inductances are also constant for all cases. Unlike the influence of the head dimension, there is no change in the cutoff frequency despite the variation of the slot width. This means that the slot width does not affect the effective series inductance of a microstrip. Variation of the effective capacitance only affects the attenuation pole location. As the etched slot width increases, the effective capacitance decreases so that the attenuation pole location moves up to higher frequency. The calculated capacitances and inductances are given in Table 3.5.

Table 3.5 Dumb-bell slot characteristics for different slot widths S

S	f_c	f_o	C_P	L_P
0.6 mm	3.02 GHz	6.41 GHz	0.2567 pf	2.4019 nH
0.7 mm	3.02 GHz	6.61 GHz	0.232 pf	2.495 nH
0.8 mm	3.02 GHz	6.77 GHz	0.2156 pf	2.563 nh
0.9 mm	3.02 GHz	6.88 GHz	0.2052 pf	2.607 nH

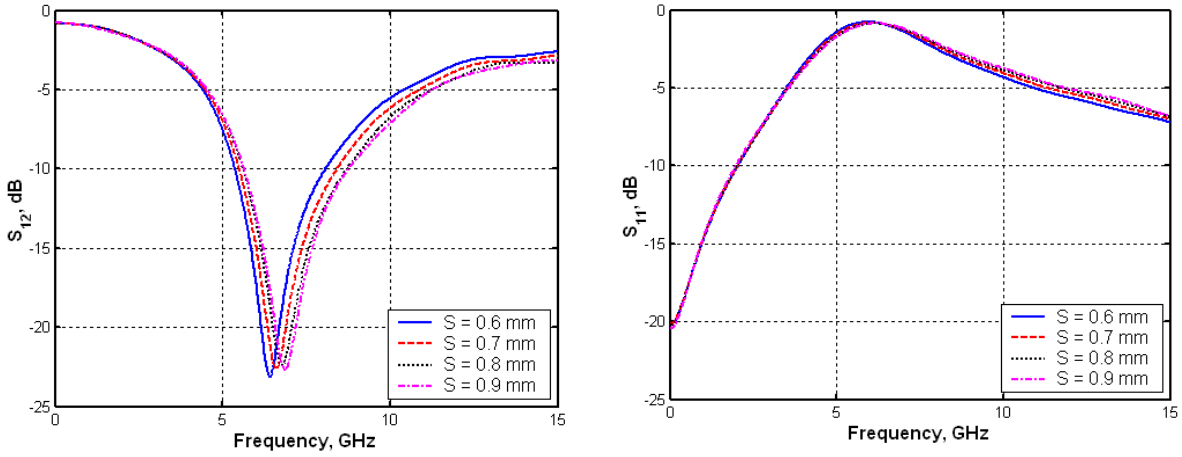

a. Transmission loss S_{12}

b. Reflection loss S_{11}

Figure 3.15 Simulated S-parameters for dumb-bell slot for different slot widths S

C. Influence of the Slot Length

We extend our study to the influence of the slot length, d. The dumb-bell head radius, r and the slot gap s, were kept constant to 2 mm and 0.6 mm respectively for all the cases and the slot etched length, d was varied. The substrate with 0.813 mm thick and a dielectric constant of 3.38 was used for all simulations. The simulation results are illustrated in Fig. 3.16. The calculated capacitances and inductances are given in Table 3.6. From Fig. 3.16, the slot-head separation d has almost identical effect on the cutoff frequency and the attenuation pole frequency. Where, increasing the etched slot length increases the series inductance to the microstrip line.

Table 3.6 Rectangular slot characteristics for different slot lengths d

d	f_c	f_o	C_P	L_P
0.25 cm	5.42 GHz	9.27 GHz	0.153 pf	1.933 nH
0.5 cm	3.32 GHz	6.98 GHz	0.229 pf	2.273 nH
0.75 cm	3.62 GHz	5.78 GHz	0.284 pf	2.67 nH
1 cm	3.18 GHz	5.00 GHz	0.340 pf	2.98 nh
1.25 cm	2.84 GHz	3.45 GHz	0.385 pf	3.322 nH
1.5 cm	2.58 GHz	1.01 GHz	0.4357 pf	3.615 nH

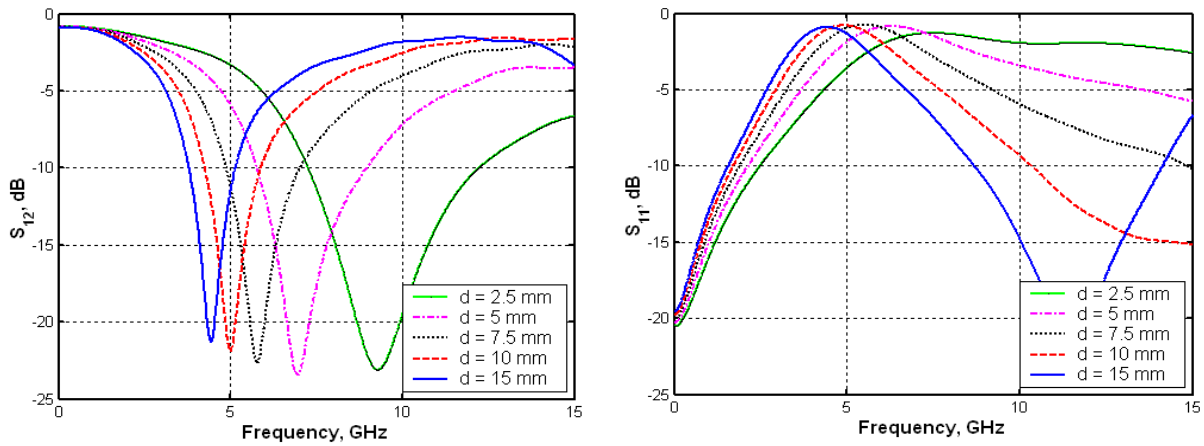

a. Transmission loss S_{12} **b. Reflection loss S_{11}**

Figure 3.16 Simulated S-parameters for dumb-bell slot for different slot lengths d

This effective series inductance introduces the cutoff characteristic at certain frequency. As the etched slot-head separation d is increased, the effective series inductance increases, and increasing the series inductance gives a lower cutoff frequency, as seen in Fig. 3.16.

3.4.3 Square head slot

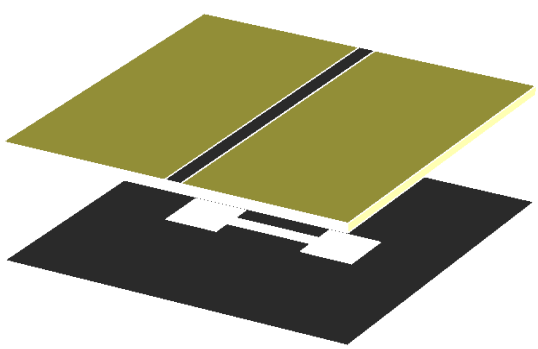

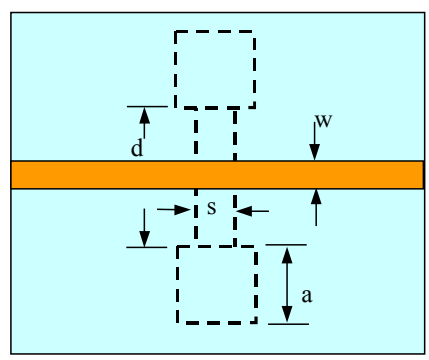

Figure 3.17.a 3-D view of the Square head DGS slot

Figure 3.17.b Wire frame view of the square head DGS slot

A. Influence of the Square Head Dimension

The line width was chosen to be the characteristic impedance of the 50 Ω microstrip line for simulations. Five DGS unit circuits were simulated with different dimensions. In order to investigate the influence of the square head dimension *a,* the etched slot width and the

length were kept constant to 0.6 mm and 4 mm respectively for all five cases and the etched square head was varied. The substrate with 0.813 mm thick and a dielectric constant of 3.38 was used for all simulations.

The simulation results are illustrated in Fig. 3.18. The calculated capacitances and inductances are given in Table 3.7. From Fig. 3.18, one clearly observes that employing the etched square head area increases the series inductance to the microstrip line. This effective series inductance introduces the cutoff characteristic at certain frequency. As the etched area of the square head is increased, the effective series inductance increases, and increasing the series inductance gives a lower cutoff frequency, as seen in Fig. 3.18. There are attenuation poles in simulation results on the etched square head area.

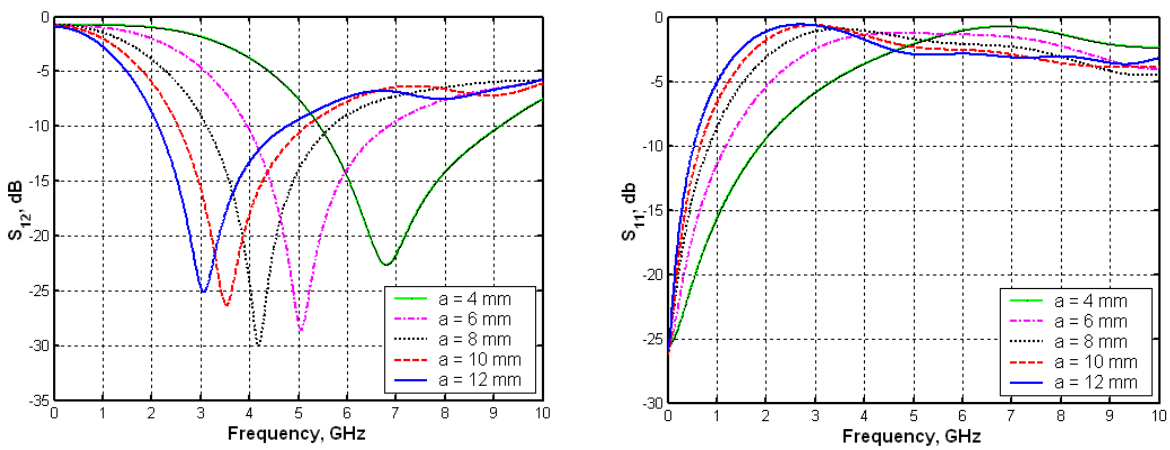

a. Transmission loss S_{12} **b. Reflection loss S_{11}**

Figure 3.18 Simulated S-parameters of square head slot for different head lengths a

Table 3.7 Square head slot characteristics for different slot head lengths a

a	f_c	f_o	C_P	L_P
0.4 cm	3.98 GHz	6.80 GHz	0.208 pf	2.629 nH
0.6 cm	2.74 GHz	5.06 GHz	0.241 pf	3.105 nH
0.8 cm	1.98 GHz	3.98 GHz	0.264 pf	6.05 nH
1 cm	1.56 GHz	3.53 GHz	0.248 pf	8.209 nh
1.2 cm	1.24 GHz	3.07 GHz	0.250 pf	10.74 nH

These attenuation poles in simulation results can be explained by parallel capacitance with the series inductance, as indicated in the previous section. This capacitance depends on the etched gap below the conductor line, which is noted as s in Fig. 3.18. The capacitance values are identical for all cases due to the identical slot width. However, the attenuation pole location, which corresponds to the resonance frequency of the parallel LC circuit, also becomes lower because as the series inductance increases, the resonance frequency of the equivalent parallel LC circuit decreases.

B. Influence of the Slot Width

An investigation on the influence of the etched slot width will be employed. The square head dimension a and slot length d were kept constant to 5.099 mm and 6 mm respectively for all the cases and the etched slot width s was varied. The simulation results are shown in Fig. 3.19. Due to the constant square head dimensions, we can expect that the effective series inductances are also constant for all cases. Unlike the influence of the head dimension, there is no change in the cutoff frequency despite the variation of the slot width. This means that the slot width does not affect the effective series inductance of a microstrip. Variation of the effective capacitance only affects the attenuation pole location. As the etched slot width increases, the effective capacitance decreases so that the attenuation pole location moves up to higher frequency. The calculated capacitances and inductances are given in Table 3.18.

Table 3.8 Square head slot characteristics for different slot widths d

S	f_c	f_o	C_P	L_P
0.6 mm	2.89 GHz	3.86 GHz	0.301 pf	3.56 nH
0.7 mm	2.89 GHz	5 GHz	0.276 pf	3.67 nH
0.8 mm	2.89 GHz	5.11 GHz	0.259 pf	3.75 nh
0.9 mm	2.89 GHz	5.22 GHz	0.243 pf	3.819 nH

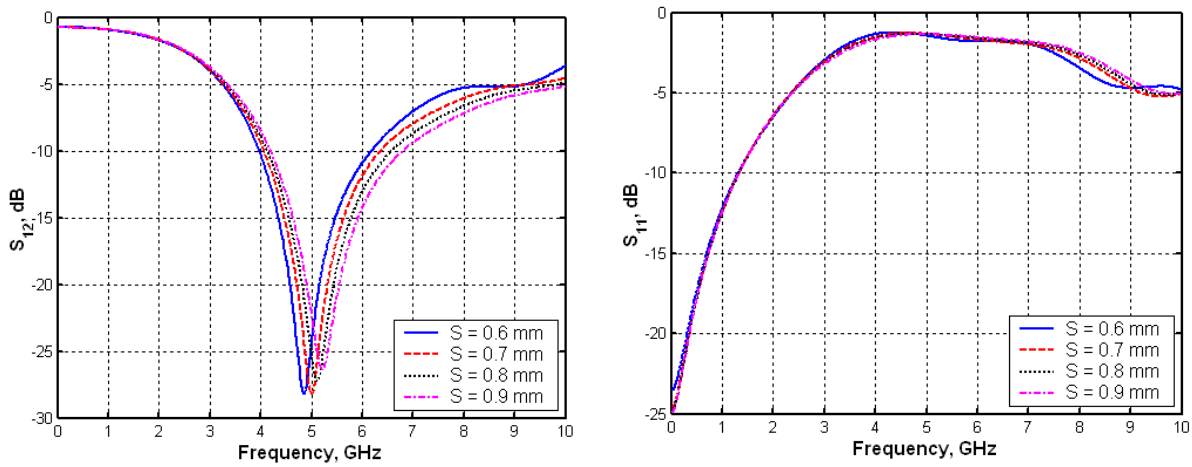

a. Transmission loss S_{12} **b. Reflection loss S_{11}**

Figure 3.19 Simulated S-parameters for square head slot for different slot widths S

C. Influence of the Slot Length

We extend our study to the influence of the slot length d. The square head dimension a and the slot width s were kept constant to 5.099 mm and 0.6 mm respectively for all the cases and the slot etched length d was varied. . The substrate with 0.813 mm thick and a dielectric constant of 3.38 was used for all simulations. The simulation results are illustrated in Fig. 3.20. The calculated capacitances and inductances are given in Table 3.9. From Fig. 3.20, the slot-head separation d has almost identical effect on the cutoff frequency and the attenuation pole frequency. Where, increasing the etched slot length increases the series inductance to the microstrip line. This effective series inductance introduces the cutoff characteristic at certain frequency.

Table 3.9 Square head slot characteristics for different slot lengths d

d	f_c	f_o	C_P	L_P
0.2 cm	3.63 GHz	7.47 GHz	0.135 pf	3.35 nH
0.4 cm	3.21 GHz	5.66 GHz	0.2351 pf	3.36 nH
0.6 cm	2.93 GHz	3.85 GHz	0.3122 pf	3.449 nH
0.8 cm	2.69 GHz	3.34 GHz	0.369 pf	3.64 nh
1 cm	2.5 GHz	3.94 GHz	0.429 pf	3.80 nH

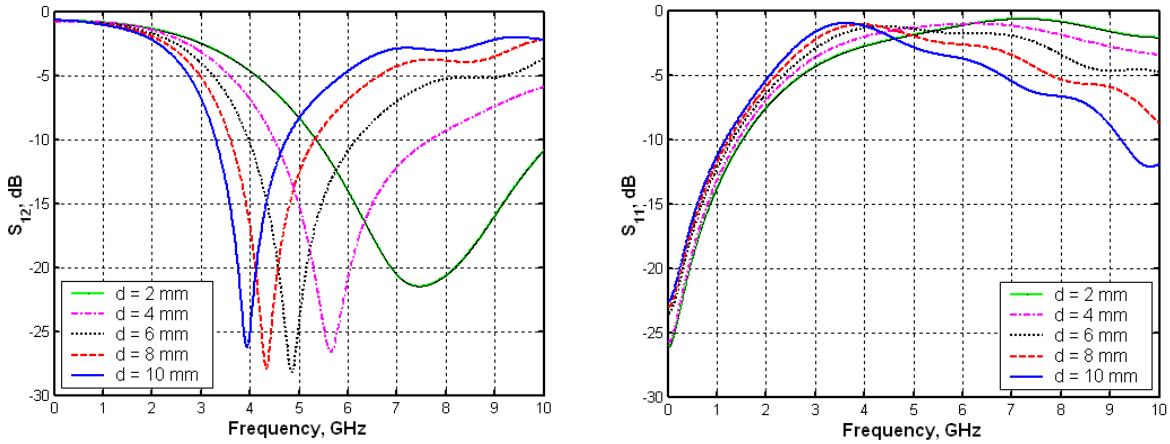

a. Transmission loss S_{12} **b. Reflection loss S_{11}**

Figure 3.20 Simulated S-parameters for square head slot for different slot lengths d

As the etched the slot-head separation d is increased, the effective series inductance increases, and increasing the series inductance gives rise to a lower cut off frequency, as seen in Fig. 3.20.

3.4.4 Arrow head slot

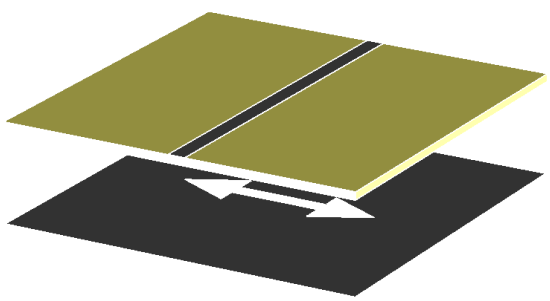

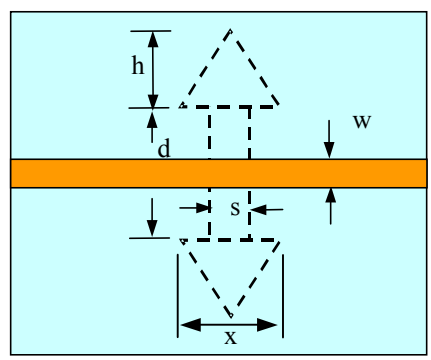

Figure 3.21.a 3-D view of the Arrow head DGS slot

Figure 3.21.b Wire frame view of the Arrow head DGS slot

A. Influence of the Arrow Head Dimension

The equilateral triangle forms an arrow head of the DGS slot. The line width was chosen to be the characteristic impedance of the 50 Ω microstrip line for simulations. Four DGS unit

circuits were simulated with different dimensions. In order to investigate the influence of the arrow head dimension x, the etched slot width and the length were kept constant to 0.6 mm and 4 mm respectively for all four cases and the etched arrow head was varied. The substrate with 0.813 mm thick and a dielectric constant of 3.38 was used for all simulations.

The simulation results are illustrated in Fig. 3.22. The calculated capacitances and inductances are given in Table 3.10. From Fig. 3.22, one clearly observes that employing the etched arrow head area increases the series inductance to the microstrip line. This effective series inductance introduces the cutoff characteristic at certain frequency. As the etched area of the square head is increased, the effective series inductance increases, and increasing the series inductance gives a lower cutoff frequency, as seen in Fig. 3.22.

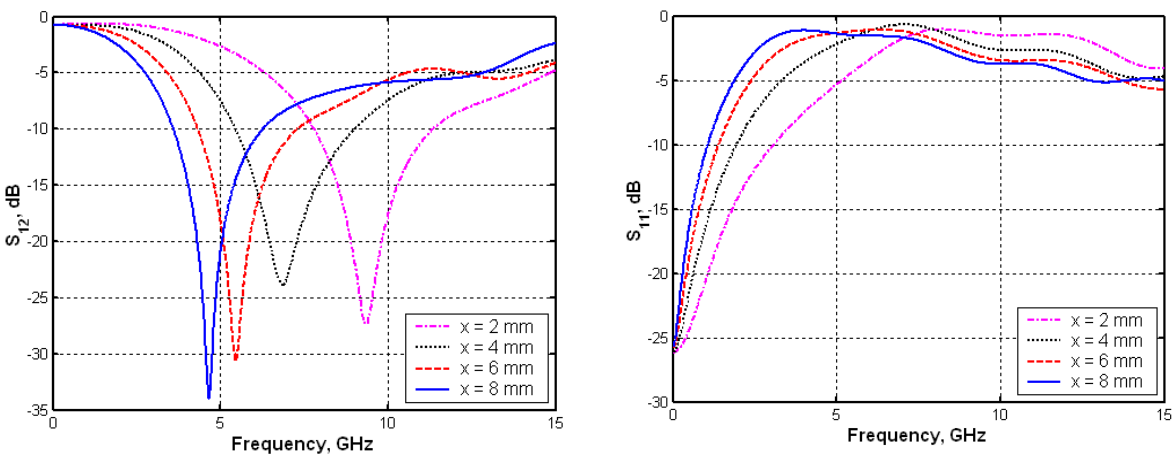

a. Transmission loss S_{12} **b. Reflection loss S_{11}**

Figure 3.22 Simulated S-parameters for different head lengths x

There are attenuation poles in simulation results on the etched arrow head area. These attenuation poles in simulation results can be explained by parallel capacitance with the series inductance, as indicated in the previous section. This capacitance depends on the etched gap below the conductor line, which is noted as s in Fig. 3.21. The capacitance values are identical for all cases due to the identical slot width. However, the attenuation

pole location, which corresponds to the resonance frequency of the parallel LC circuit, also becomes lower because as the series inductance increases, the resonance frequency of the equivalent parallel LC circuit decreases.

Table 3.10 Arrow head slot characteristics for different head lengths x

x	f_c	f_o	C_P	L_P
0.4 cm	5.66 GHz	9.34 GHz	0.1632 pf	1.779 nH
0.6 cm	3.94 GHz	6.85 GHz	0.199 pf	2.703 nH
0.8 cm	3.02 GHz	5.45 GHz	0.2335 pf	3.652 nH
1 cm	2.34 GHz	3.66 GHz	0.229 pf	5.087 nh

B. Influence of the Slot Width

An investigation on the influence of the etched slot width will be employed. The arrow head dimension x and slot length, d were kept constant to 10 mm and 6 mm respectively for all the cases and the etched slot width s was varied. The simulation results are shown in Fig. 3.23. Due to the constant arrow head dimensions, we can expect that the effective series inductances are also constant for all cases. Unlike the influence of the head dimension, there is no change in the cutoff frequency despite the variation of the slot width. This means that the slot width does not affect the effective series inductance of a microstrip. Variation of the effective capacitance only affects the attenuation pole location. As the etched slot width increases, the effective capacitance decreases so that the attenuation pole location moves up to higher frequency. The calculated capacitances and inductances are given in Table 3.11.

Table 3.11 Arrow head slot characteristics for different slot widths S

S	f_c	f_o	C_P	L_P
0.6 mm	2.1 GHz	3.09 GHz	0.271 pf	5.581 nH
0.7 mm	2.1 GHz	3.19 GHz	0.254 pf	5.675 nH
0.8 mm	2.1 GHz	3.29 GHz	0.2388 pf	5.763 nh
0.9 mm	2.1 GHz	3.37 GHz	0.228 pf	5.829 nH

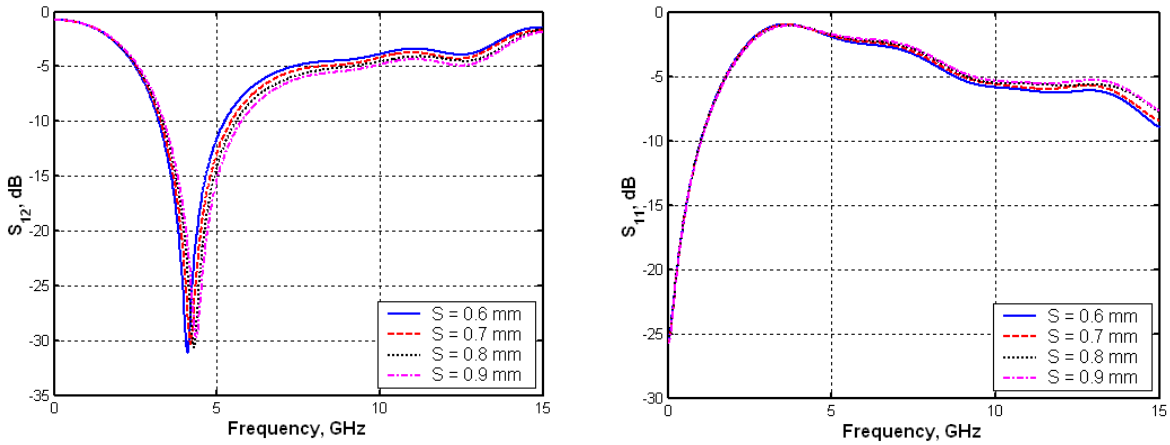

a. Transmission loss S_{12} **b. Reflection loss S_{11}**

Figure 3.23 Simulated S-parameters of arrow head slot for different slot widths S

C. Influence of the Slot Length

We extend our study to the influence of the slot length d. The arrow head dimension x and the slot width s were kept constant to 10 mm and 0.6 mm respectively for all the cases and the slot etched length d was varied. The substrate with 0.813 mm thick and a dielectric constant of 3.38 was used for all simulations. The simulation results are illustrated in Fig. 3.24. The calculated capacitances and inductances are given in Table 3.12. From Fig. 3.24, the slot-head separation d has almost identical effect on the cutoff frequency and the attenuation pole frequency.

Table 3.12 Arrow head slot characteristics for different slot lengths d

d	f_c	f_o	C_P	L_P
0.2 cm	2.77 GHz	5.67 GHz	0.180 pf	3.374 nH
0.4 cm	2.46 GHz	3.68 GHz	0.247 pf	3.682 nH
0.6 cm	2.23 GHz	3.09 GHz	0.302 pf	5.015 nH
0.8 cm	2.08 GHz	3.67 GHz	0.3621 pf	5.194 nh
1 cm	1.94 GHz	3.35 GHz	0.410 pf	5.453 nH

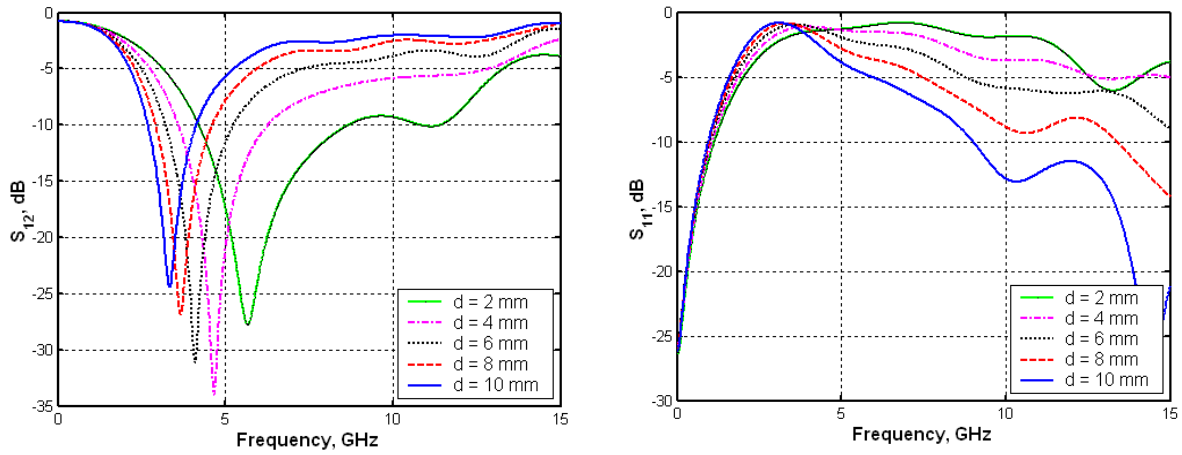

a. Transmission loss S_{12} **b. Reflection loss S_{11}**

Figure 3.24 Simulated S-parameters of arrow head slot for different slot lengths d

Where, increasing the etched slot length increases the series inductance to the microstrip line. This effective series inductance introduces the cutoff characteristic at certain frequency. As the etched slot-head separation d is increased, the effective series inductance increases, and increasing the series inductance gives a lower cutoff frequency, as seen in Fig. 3.24.

Summary of the slots investigation

We have selected the following parameters to characterize band-stop performance of the DGS slots of four simple geometrical shapes which are rectangular, dumb-bell, square head and arrow head slots:

(i) Linear dimension of the slot

(ii) Area of slot-head

(iii) Relative control of cut-off frequency f_c and attenuation pole frequency f_0 by changing dimension of slot

(iv) Sharpness factor f_0/f_c.

The slot in the ground plane for the DGS element may occupy inconveniently large linear space that can cause disturbance to other circuit elements located on the same substrate. Thus we have to look for smaller linear length of the DGS slot. It is achieved by creating the slot-head at the ends of a rectangular slot. Creation of such slot-heads provide to some

extent independent control of capacitance and inductance of the equivalent circuit. The slot-head area basically controls the inductance whereas the width (s) of connecting rectangular slot controls the capacitance [37]. However, effect of separating distance (d) of the slot is not discussed in the literature. Various dimensions involved information of a DGS slot have different degree of control on the 3 dB cut-off frequency f_c and the attenuation pole frequency f_0 of the band-reject response. Thus comparison of performance of the slots with respect to this parameter could be useful in selection of type of slots in various applications. The sharpness factor f_0/f_c determines the sharpness of transition from the band-pass region to the band-stop region. The sharpest theoretical transition is obtained for f_0/f_c =1. Lager the value of f_0/f_c -ratio poorer is its sharpness of the transition from the passband to the stopband.

To understand performance of the DGS slot we have generated a large amount of data on cut-off frequency f_c, attenuation pole frequency f_0, capacitance C and inductance L of the circuit model for four slots using the substrate with ε_r = 3.38 and h = 0.0813 cm. The general behavior of the slots is summarized in Table 3.13. The dimensions of slots are varied up to five times from their initial dimension. However, the slot width is varied 1.5 times of the initial value. The extent of variations in fc, f_0, C and L over five times dimensional change are shown in the Table 3.13. The Table 3.13 also shows average variation in the sharpness factor f_0/f_c for each slot over five times dimensional change in the slot. The study is conducted for the cut-off frequency f_c in the range 2 GHz-8 GHz and the attenuation pole frequency f_0 in the range 3 GHz – 12 GHz.

We have the following general observations:

- ***Rectangular slot:***

The change in length, as compared to change in the slot width, is more effective way to control f_c, f_0, C and L. For five times change in length or in width both C and L change almost in same magnitude. However, the change in length has a little more influence on the inductance L. Whereas, the change in width has a little more influence on the capacitance C.

- ***Dumb-bell slot:***

The change in radius (r) has stronger influence on the inductance L and the cut-off frequency f_c as compared to its influence on the capacitance C and the attenuation pole

frequency f_0. Thus the inductance can be changed without incurring much change in the attenuation pole frequency. Table 3.13 shows that the order of change in the inductance L is almost same as the order of change in L of the rectangular slot with respect to the slot length. At f_0 = 5.8 GHz the rectangular slot has length d = 2 cm and width s = 600 μm. At f_0 = 5.8 GHz the dumb-bell slot has radius r = 0.3 cm and separation d = 0.19 cm i.e. its total linear dimension is 1.39 cm. Thus for the identical attenuation pole frequency the dumb-bell shape has 30% less linear length as compared to length of the rectangular slot. Table 3.13 shows that the slot-head separation d has almost identical effect on the cut-off frequency f_c and the attenuation pole frequency f_0. It has a little more influence on inductance L than on capacitance C. The increase in separation of slot-head brings f_c and f_0 closer, thereby improving sharpness of transition.

- ***Square head slot:***

Table 3.13 shows that the square-head slot gives maximum change in inductance L for five times change in the side of square arm. It also gives maximum change in capacitance C for five times change in the separation of the slot heads. However, to get large control of the inductance we have to tolerate more variation in the frequency of attenuation pole and also in the cut-off frequency.

In summary we can say that we have to use the headed slot in the ground plane in order to reduce the linear dimension of the DGS slot. Both the inductance L and the capacitance C increase with increase in size of the slot head. However, increase in the inductance is more significant than increase in the capacitance. The sharpness factor is better for smaller size of the slot head. The separation of slot heads d increases both L and C. However, increase in C is more significant than increase in L. Finally both dimension of slot heads and their separation can be adjusted to get proper value of DGS components. They should be selected for better sharpness factor also. While selecting type of slot we should also keep in mind its influence on other circuit elements on the same substrate.

- ***Arrow head slot:***

The equilateral triangle forms the arrowhead of the DGS slot. Table 3.13 shows that its side length, as compared to radius r of the dumb-bell slot, has less influence on cut-off frequency f_c and attenuation pole frequency f_o, inductance L and capacitance C. However, the separation of heads d has more influence on C as compared to separation of heads d for

the dumb-bell slot. The sharpness factor f_0/ f_c of the arrowhead slot is better than the sharpness factor of the dumb-bell slot. To get inductance L about 3.8 nH, linear length of dumb-bell slot is 1 cm (r = 0.2cm), for the arrowhead slot it is 3.17 cm (a = 1.6 cm) and for the rectangular slot it is 3.5 cm (width = 600 μm). From point of view of linear dimension the dumb-bell slot is more compact. However from the point of view of the sharpness factor, the arrowhead is a better slot. It is noted by Ahn et al. [37] that identical area of the slot-head provides identical inductance. However, we will see in the next section that for equal area of the slot-head, the triangular slot provides better sharpness of cut-off with improved stopband response. Moreover, we will also see in the next section that the shape of the slot head has influence on the design of the filter.

Table 3.13 Comparison of characteristics of different DGS Slots

Slot	Dimensional variation (Initial: Final)	Variation in f_c	Variation in f_o	Variation in C	Variation in L	Average f_o/f_c
Rectangle	Length 1cm: 5cm	5.23	3.95	3.56	5.37	1.44
	Width 0.02cm:0.1cm	1.38	1.31	2.11	1.91	1.20
Dumb-bell	Radius 0.1cm: 0.5cm	3.24	2.59	1.26	5.46	2.40
	Separation 0.25cm:1.25cm	1.98	1.94	1.82	2.03	1.65
	Slot width 0.06cm:0.09cm	1.00	1.07	0.84	1.05	2.06
Arrow-head	Side of triangle 0.4cm:2.0cm	2.37	2.01	1.46	2.75	1.80
	Separation 0.2cm: 1.0cm	1.38	1.70	2.45	1.60	1.69
	Slot width 0.06cm:0.09cm	1.00	1.07	0.80	1.08	1.69
Square	Side of square 0.4cm: 2.0cm	5.89	3.69	1.69	7.51	2.12
	Separation 0.4cm: 1.0cm	1.45	1.90	3.15	1.15	1.78
	Slot width 0.06cm:0.09cm	1.00	1.07	0.81	1.08	1.66

(Slot width variation is 1.5 times from initial to final. Other dimensions have variation 5 times initial to final)

3.5 Stepped-Impedance Low-Pass Filter

The microwave low-pass filter (LPF) is a common circuit element in the development of mixer, oscillators etc. to suppress the harmonics, noise and other undesired signals. Usually the LPF is implemented either by all shunt stubs or by the series connected high-low (Hi-Lo) stepped-impedance microstrip line sections.

A relatively easy way to implement low-pass filters in Microstrip or stripline is to use alternating sections of very high and very low characteristic impedance lines. Such filters are usually referred to as stepped-impedance, or hi-Z, low-Z filters, and are popular because they are easier to design and take up less space than a similar low-pass filter using stubs. Because of approximations involved, however, their electrical performance is not as good, so the use of such filters is usually limited to applications where a sharp cut-off is not required.

In order to illustrate the design procedure for this type of filter, the design of a three-pole low-pass filter is described in follows.

The specifications for the filter under consideration are:

Cutoff frequency f_c =1.3 GHz

Passband ripple 0.1 dB (or return loss ≤-16.42 dB)

Source/load impedance Z_o = 50 Ω

A low-pass prototype with Chebyshev response is chosen, whose element values are

$$g_o = g_4 = 1$$

$$g_1 = g_3 = 1.0316$$

$$g_2 = 1.1474$$

for the normalized cutoff Ω_c = 1.0. Using the element transformations, we have

$$L_1 = L_3 = \left(\frac{Z_O}{g_O}\right)\left(\frac{\Omega_C}{2\pi f_C}\right)g_1 = 6.3148\times10^{-9}\,H \tag{3.7}$$

$$C_2 = \left(\frac{g_O}{Z_O}\right)\left(\frac{\Omega_C}{2\pi f_C}\right)g_2 = 2.8092\times10^{-12}\,F \tag{3.8}$$

The fabricated filter is shown in Fig. 3.25. The filter has been fabricated on a substrate with a relative dielectric constant of 3.38 and a thickness of 0.813 mm. Following the above-mentioned considerations, the characteristic impedances of the high- and low- impedance lines are chosen as Z_{oL} = 93 ohms and Z_{oC} = 24 ohms. The relevant design parameters of

Microstrip lines, which are determined using the formulas given in [78], are listed in Table 3.14, where the guided wavelengths are calculated at the cutoff frequency f_c = 1.3 GHz. The measured response of the conventional stepped-impedance low-pass filter is shown in Fig. 3.25.

Table 3.14 Physical and Normalized Dimension of 3-pole LPF Conventional

Dimensions	w_L	w_C	L_C	L_L	w
Physical	0.5mm	5.2mm	15.3mm	16.9mm	1.9mm
Normalized	0.0051 λ_g	0.0529 λ_g	0.1556 λ_g	0.1719 λ_g	0.0193 λ_g

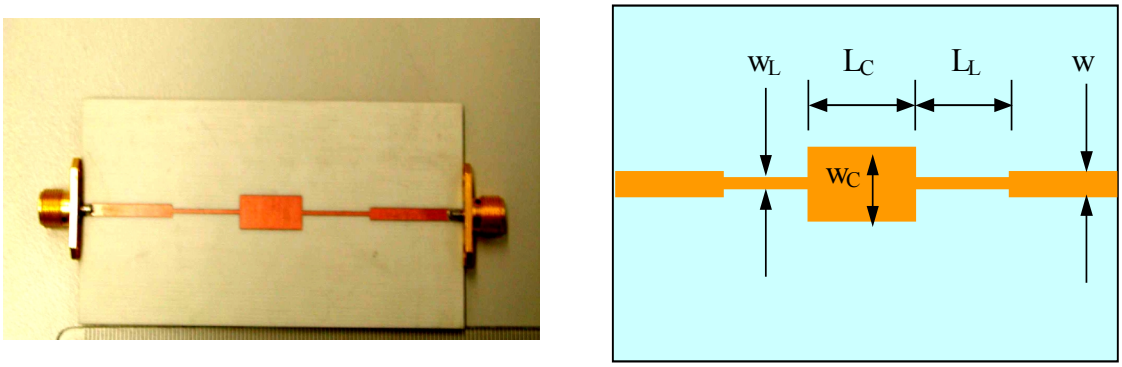

Figure 3.25 conventional microstrip stepped-impedance low-pass filter

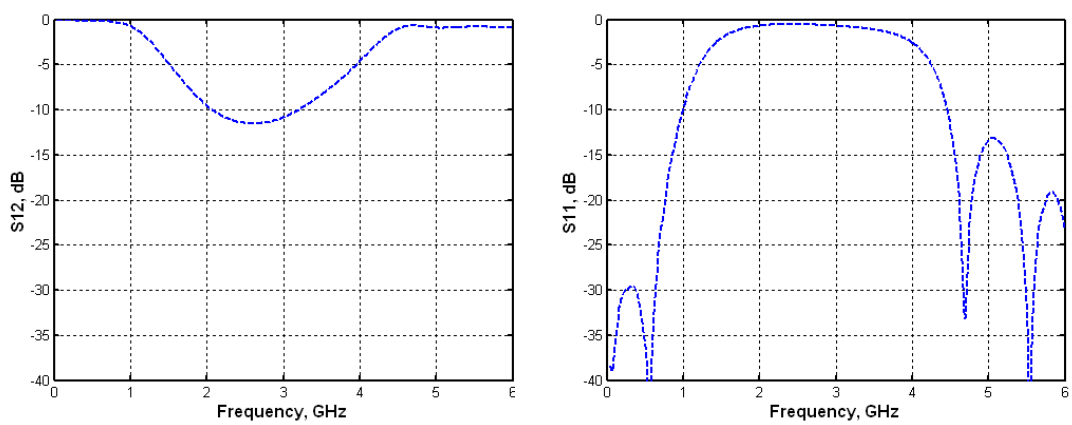

a. Transmission loss S_{12} **b. Reflection loss S_{11}**

Figure 3.26 Measured S-parameters of conventional stepped-impedance low-pass filter

3.6 Stepped impedance low-pass filter using DGS slots

The conventional stepped-impedance low-pass filter has the following disadvantages:

1- The transition and stopband response are not so good.

2- To implement the high impedance inductance with conventional Microstrip, the conductor width becomes narrow. This is a limitation to use a Microstrip low-pass filter configuration for high power applications. Also, it needs high accuracy for fabrication.

Due to these disadvantages, we intended to apply the DGS slots to implement the inductances for this type of the filter.

By employing the DGS sections, extremely small element values for implementation of a low-pass filter can be realized. Furthermore, the high impedance inductance sections were realized by using DGS sections with a conductor width corresponding to a 50 Ω Microstrip so that it can be expected that for DGS low-pass filters improve the power handling capability.

3.6.1 Study of DGS slot position on 3-pole Hi-Lo LPF

Fig. 3.27 shows realization of a 3-pole Hi-Lo LPF with the DGS slots. The slot head could be the dumb-bell, the arrowhead or the square. The DGS slots could be located either outside of the patch capacitor or inside the patch capacitor.

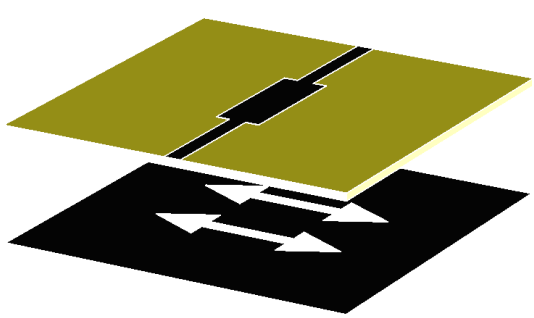

Figure 3.27.a 3-D view of the Hi-Lo LPF with arrow head DGS slots

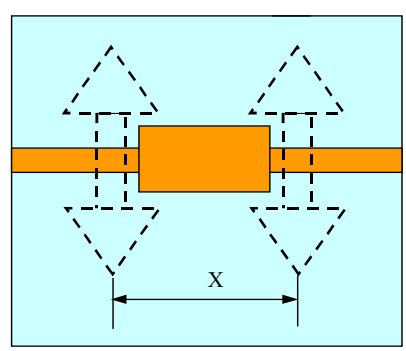

Figure 3.27.b Wire frame of the Hi- Lo LPF with arrow head DGS slots

The performance of the LPF can be examined with respect to separation X between two slot heads. The area and other dimensions of three types of slot are kept same. The LPF is designed on the substrate having $\varepsilon_r = 3.38$ and h = 0.813 mm. The 50 Ω microstrip line has width w = 1.9 mm and the patch capacitor has width w_c = 0.52 cm and length L_c=1.53 cm. Fig. 3.28, Fig. 3.30. and Fig. 3.32 show the effect of separation X on the scattering parameter, S_{12} for the arrowhead, dumb-bell, and square DGS slots respectively.

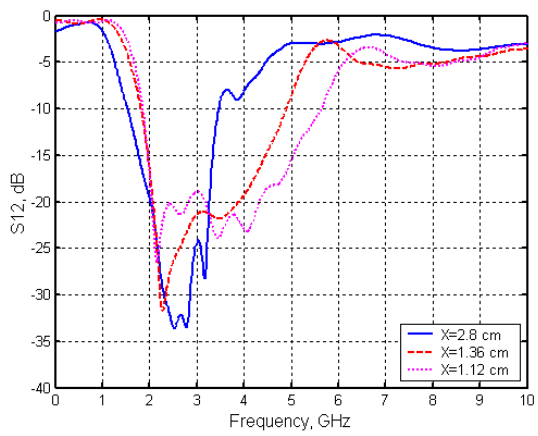

Transmission loss S_{12}

Figure 3.28 Effect of separation (X) of DGS arrow head slot on S_{12} of the LPF

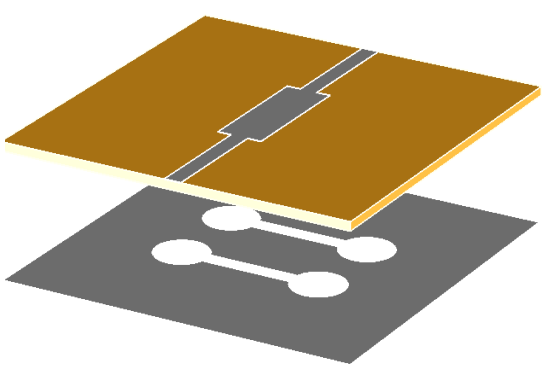

Figure 3.29.a 3-D view of the Hi-Lo LPF with dumb-bell DGS slots

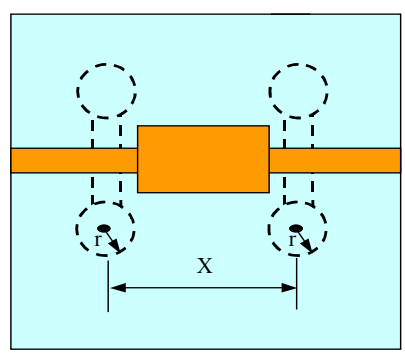

Figure 3.29.b Wire frame of the Hi- Lo LPF with dumb-bell DGS slots

It is interesting to note that the LPF is obtained with more suppressed response in the stopband when the DGS slots are located inside the patch capacitor. With decrease in the separation X inside the patch capacitor, suppression of response in the stopband improves both in magnitude and in extension of its frequency band. The cut-frequency does not change much during this process.

There is a small decrease in it with decrease in the separation X. For the slots inside the patch capacitor, performance of these slots is not much different in the passband. However, the arrowhead slot provides better sharpness and better stopband response.

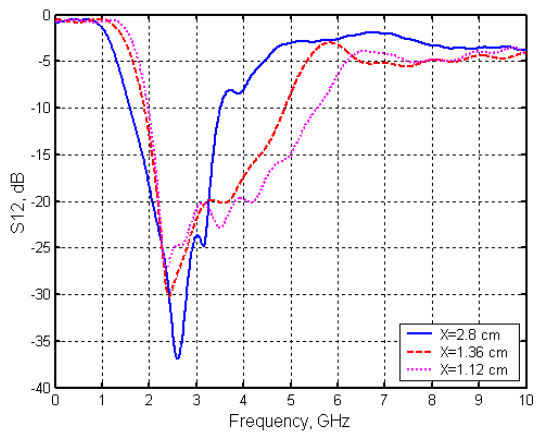

Transmission loss S_{12}

Figure 3.30 Effect of separation (X) of DGS dumb-bell slot on S_{12} of the LPF

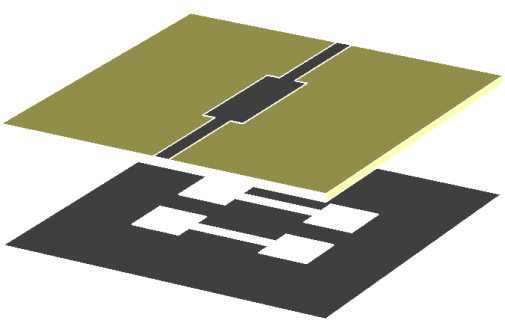

Figure 3.31.a 3-D view of the Hi-Lo LPF with square head DGS slots

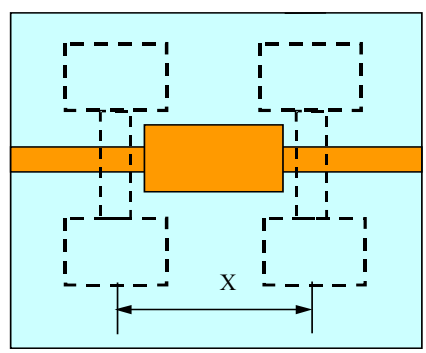

Figure 3.31.b Wire frame of the Hi- Lo LPF with square head DGS slots

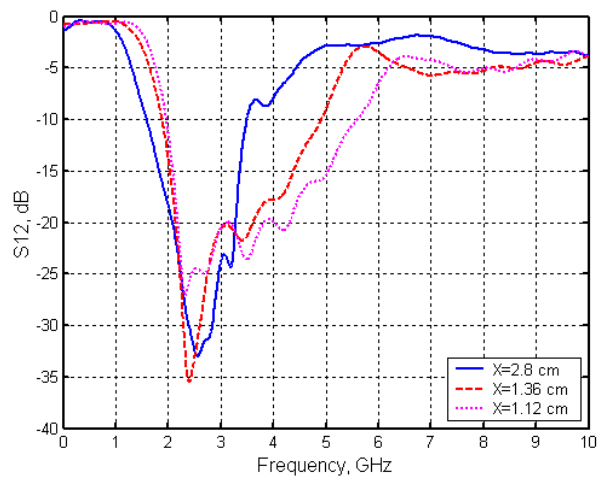

Figure 3.32 Effect of separation (X) of DGS square head slot on S_{12} of the LPF

The separation of the DGS slots outside the patch capacitor provides broadband stopband characteristics. The sharpness and bandwidth of the stopband is better for the arrowhead DGS slots. At this stage we note that even with identical area of the slot head, the band-stop responses are not identical. This section is concerned with Hi-Lo LPF; therefore we will not discuss further on the stopband filter design. This work will be examined in future and reported separately.

3.6.2 Fabrication and measurement of 3-pole Hi-Lo LPF

We have fabricated the following 3-pole microstrip LPF to compare their performance:

1) Conventional microstrip Hi-Lo LPF;
2) microstrip LPF with large dumb-bell DGS slots;
3) microstrip LPF with small dumb-bell DGS;
4) microstrip LPF with arrowhead DGS slots.

The structural details with physical dimension and normalized dimension of the fabricated 3-pole Hi-Lo LPF are shown in Table 3.15. The normalization is done with respect to the guided wavelength $\lambda_g = \frac{\lambda_c}{\sqrt{\varepsilon_r}}$. Where λ_c is the wavelength at the cut-off frequency of the LPF. The normalized dimension can be used to design the 3-pole LPF at any other cut-off frequency on other substrate. After initial design improvement in performance of the LPF

can be obtained on the EM-simulator. Fig. 3.33 shows the photograph of the four fabricated low-pass filters.

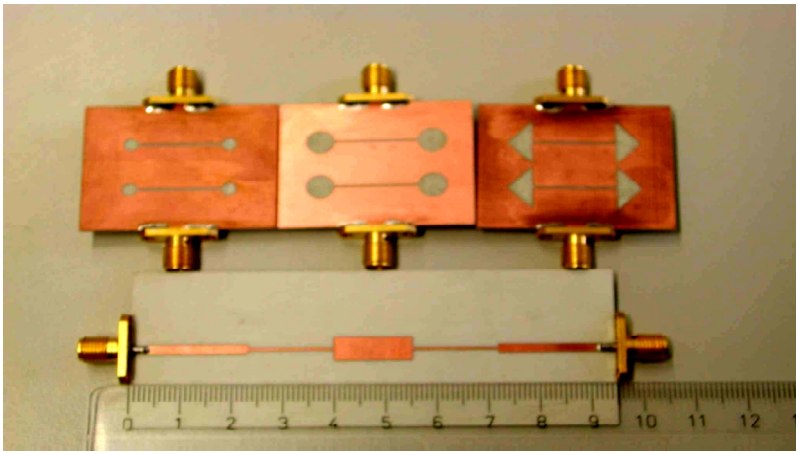

Figure 3.33 Fabricated conventional and DGS Hi-Lo LPF

These are fabricated on the milling machine. It shows DSG with arrowhead and dumb-bell shapes. Fig. 3.33 also shows the fabricated conventional 3-pole Hi-Lo microstrip LPF on the same substrate. The significant reduction in dimension of the LPF with DGS as compared to the conventional design is obvious from it.

Fig. 3.34 shows experimental study of effect of changing the slot-head size of the dumb-bell slot on the cut-off frequency of the LPF. For the large slot area the cut-off frequency is reduced due to increase of equivalent inductance. However, as discussed previously the small slot provides better sharpness factor (f_0/f_c) and also improvement in stopband rejection. Fig. 3.34 shows that cut-off frequency and the attenuation pole frequency for r = 3mm slot are 1.66 GHz and 2.86 GHz respectively. They increase to 2.31 GHz and 3.63 GHz for the r = 1.5 mm slot. Thus while keeping all dimensions of the LPF unchanged, it is possible to control the bandwidth of the LPF by changing the radius of the dumb-bell slot. The dumb-bell slot of r = 1.5 mm has sharpness factor 1.57 as compared to 1.77 for r = 3.0 mm slot. It has also 5 dB more stopband rejection.

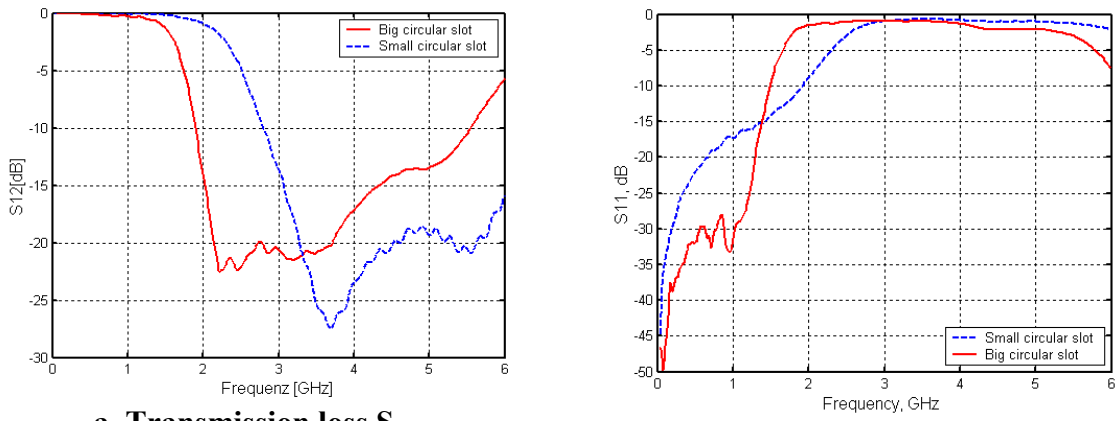

a. Transmission loss S_{12} **b. Reflection loss S_{11}**

Figure 3.34 LPF response with large and small size of dumb-bell slot head

Table 3.15 Physical and normalized dimensions of 3-pole LPF

Item	Dimensions	
Conventional	w_L = 0.5mm w_C = 5.2mm L_C = 15.3mm L_L = 16.9mm w = 1.9mm	0.0051 λ_g 0.0529 λ_g 0.1556 λ_g 0.1719 λ_g 0.0193 λ_g
DGS Arrow head	h = 5.2 mm w = 1.9 mm s = 0.6 mm d = 16.9 mm X = 11.2 mm	0.0529 λ_g 0.0193 λ_g 0.0061 λ_g 0.1719 λ_g 0.1139 λ_g
DGS dumb-bell head	r = 3 mm w = 1.9 mm s = 0.6 mm d = 16.9 mm X = 11.2 mm	0.0305 λ_g 0.0193 λ_g 0.0061 λ_g 0.1719 λ_g 0.1139 λ_g
DGS square head	a = 5.32 mm w = 1.9 mm s = 0.6 mm d = 16.9 mm X = 11.2 mm	0.0541 λ_g 0.0193 λ_g 0.0061 λ_g 0.1719 λ_g 0.1139 λ_g

The investigators [37] have noted that for equal area of the slot, the shape of slot has no influence on the performance of the LPF. However, we noted on the 3D EM-Simulator, Microwave studio that this conclusion is valid only for the cut-off frequency not for the

complete performance of the LPF. To check the performance experimentally we fabricated two LPF with the arrowhead and the dumb-bell DGS slots. The area of the slot head was kept same i.e. 28.27 sq. mm for both kind of slot heads. During fabrication equal area of the slot-heads could not be maintained. The comparison of performance is shown in Fig. 3.35. The cut-off frequency- for the dumb-bell is 1.66 GHz and for the arrowhead it is 1.55 GHz. Likewise, we get attenuation pole frequency at 2.86GHz and 2.04 GHz respectively for dumb-bell and arrowhead slots. The cut-off frequency and the pole frequency for both kinds of slot-heads could be kept constant due unequal area of slot-heads during fabrication. The fabrication is done on the milling machine. However, the sharpness factor for the arrowhead is 1.32 and for the dumb-bell it is 1.73. Thus as noted earlier the arrowhead slot provides better sharpness of transition. Likewise, it provides 3 dB more stopband rejection.

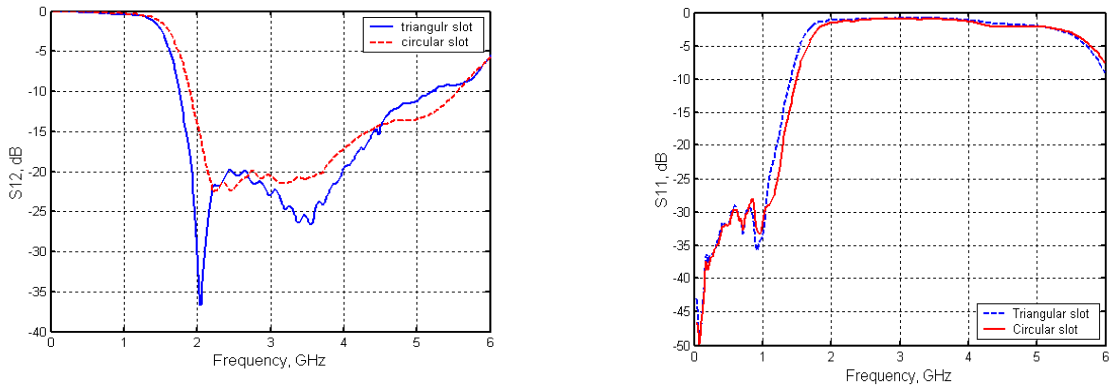

a. Transmission loss S_{12} **b. Reflection loss S_{11}**

Figure 3.35 comparison of measured performance the 3-pole Hi-Lo LPF with arrowhead and dumb-bell slots.

Finally Fig.3.36 compares the experimental performance of the 3-pole arrowhead LPF with 3-pole conventional Hi-Lo LPF. The superior performance of DGS Hi-Lo LPF is obvious- there is no spurious passband, 10 dB improved stopband rejection, sharpness of the transition looks like 5-pole LPF and 15 dB rejection up to three times of the cut-off frequency. Fig.3.36 also compares the simulated and measured performance of the DGS Hi-Lo LPF with satisfactory agreement. Fig. 3.36 also shows that we can further improve

the sharpness of transition and stopband rejection in certain frequency by using another ground plane facing the DGS slots.

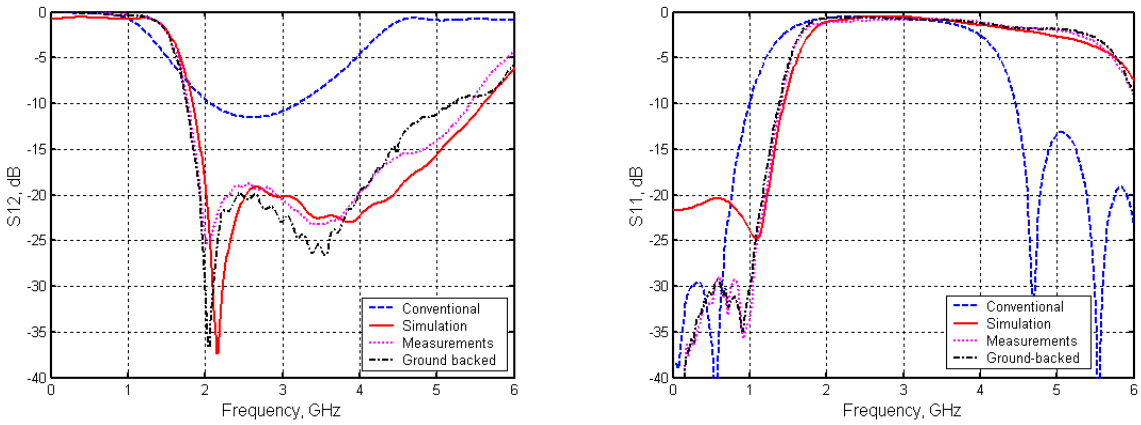

a. Transmission loss S_{12} **b. Reflection loss S_{11}**

Figure 3.36 Comparison of performance of 3-pole Hi-Lo LPF with DGS against conventional 3-pole Hi-Lo microstrip LPF

3.7 Frequency characteristics of DGS unit section with cutting gap in the 50 Ω line

Fig. 3.37 shows the etched dumb-bell slot shape of the DGS section, which is located on the backside metallic ground plane. A cut in the 50 Ω microstrip line with g mm width has been done The DGS unit section can provide not only an attenuation pole but also a transmission zero in some frequency without any periodicity of DGS. In order to investigate the frequency characteristics of the DGS section, the DGS unit section with cut in the 50 Ω Microstrip line has been simulated by the 3-D EM-Simulator Microwave Studio.

The simulation results show that two poles and one zero in the S_{12} response as shown in Fig. 3.38. Existing of a pole at the dc means the existence of a series capacitance. There is also a transmission zero which indicates the existence of a series resonance. Another attenuation pole location, which is nearly at the same place of the same structure without the cutting in the 50 Ω Microstrip line which has been modeled as a parallel resonance. due to the etched slot width of the slot. Thus, to model the frequency characteristic of the DGS

section with cut in the 50 Ω Microstrip line, the presence of two capacitances factor should be needed. The etched gap area, which is placed under the 50 Ω line as in Fig. 3.37, provides the parallel capacitance with effective line inductance and the cut in the 50 Ω line will provide the series capacitance.

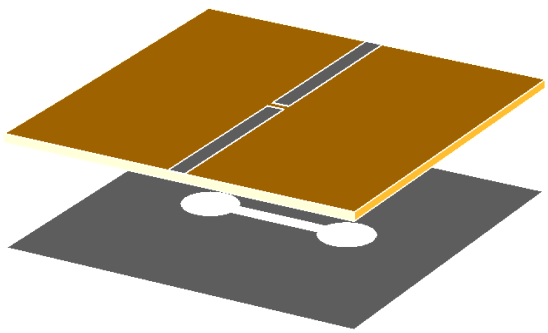

Figure 3.37 3-D view of the GDS with with gap in the 50 Ω line

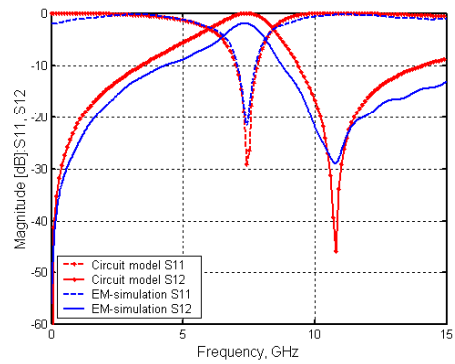

Figure 3.38 Simulated S-parameters for the GDS with gap in the 50 Ω line

3.7.1 Modeling of DGS Based Band- Reject and Band- Accept Components

The band-reject (band stop) DGS with its parallel resonance equivalent circuit is given in the previous section. It behaves as a lumped inductor at frequency below the parallel resonance frequency. The proposed band-accept (band pass) DGS configuration, shown in Fig. 3.39.a is created by a coupling gap (g) in the 50Ω microstrip line just above the neck of a dumb-bell type of defect (slot) in the ground plane. The band-accept configuration shows both the series and parallel resonance. The series- parallel combined circuit shown in Fig. 3.39.b can model such a response.

At frequency below the series resonance, the band-accept DGS configuration behaves as a capacitor. Fig. 3.38 shows the response of band-accept DGS element.

By following section 3.3.2, we can obtain the capacitance Cp in pF and the inductance Lp in nH of the equivalent circuit of a band reject (band stop) DGS shown in Fig. 3.39.b.

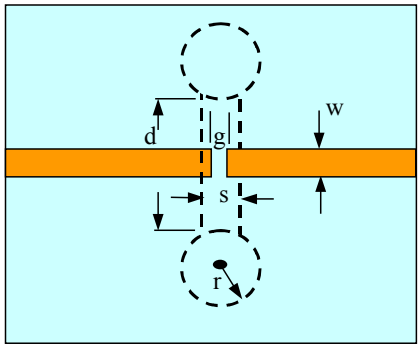

Figure 3.39.a Band-accept DGS element

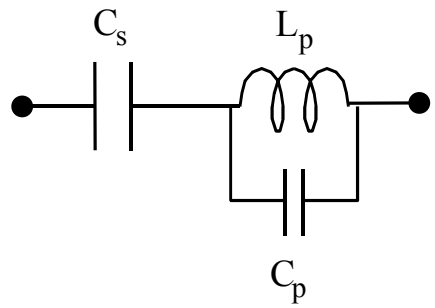

Figure 3.39.b Equivalent circuit of a band-accept DGS element

$$C_p = \frac{5 f_c}{\pi\left[f_p^2 - f_c^2\right]} \quad \text{pF} \tag{3.9}$$

$$L_p = \frac{250}{C_p (\pi f_p)^2} \quad \text{nH} \tag{3.10}$$

Where f_c is cut-off frequency in GHz of a band reject (band stop) response at 3 dB and f_p is its pole frequency in GHz. At any frequency f< f_p, the parallel resonance circuit behaves as an inductor. Its equivalent inductance in nH is obtained from

$$L_{eq} = \frac{L_p}{[1-(\frac{f}{f_p})^2]} \quad \text{nH} \tag{3.11}$$

In case of a band- accept DGS configuration, the equivalent inductance L_{eq} and coupling capacitance C_s form a series resonance circuit. However, when the dumb-bell structure is used in the band-accept mode, its pole frequency f_p is changed by a small amount. We assume that its 3dB cut-off frequency is same as in case of a band-reject DGS. The response obtained by the EM simulator provides the series resonance frequency f_s. The coupling capacitance C_s in pF is obtained from

$$C_s = \frac{25.33}{L_{eq} f_s^2} \quad \text{pF} \tag{3.12}$$

At any frequency $f < f_s < f_p$, the band-accept DGS element acts as a lumped equivalent capacitor. It is computed from

$$C_{eq} = \frac{C_s}{[1-(\frac{f}{f_s})^2]} \quad \text{pF} \tag{3.13}$$

Accuracy of the extracted parameters of a circuit model is checked by comparing the response obtained from the circuit model and also from the EM- Simulator. The simulated structures are made on RT- Duriod 6006 having $\varepsilon_r = 6.15$, $\tan\delta = 0.0019$ and h = 0.635mm. The 50 Ω microstrip line has width W = 0.97 mm. The dumb-bell slot has radius r = 1.4mm, separation d = 2 mm and slot-gap s = 600 µm. For the band-accept case, gap in the microstrip line g is 100µm. The band-reject structure has 3dB cut-off frequency f_c = 6.12 GHz and parallel resonance frequency f_p = 10.504 GHz. The circuit model of a band-reject configuration has C_p = 0.1337 pF and L_p = 1.7178 nH. The band-accept structure has series resonance f_s = 7.4433 GHz and parallel resonance f_p = 10.768 GHz. They provided C_p = 0.1241 pF, L_p = 1.7605 nH and C_s = 0.1356 pF for the circuit model. The circuit parameters are extracted as discussed above. We have assumed that the 3-dB cut-off frequency f_c for the band-accept case is also 6.12 GHz. Fig. 3.38 shows satisfactory agreement of response of circuit model with response of the EM Simulator.

3.7.2 The 3-Pole Band-Pass Filter

Our band-pass filter is based on creation of a series-resonance in the main 50Ω microstrip line and creation of attenuation pole in the shunt arm. A compact BPF based on this concept is shown in Fig. 3.40. To arrive at this structure, at first we used a dumb-bell type band accept (band pass) DGS in series with main line and on both side of it we used stub type band reject (band stop) dumb-bell shape DGS. However, in order to make the BPF compact, we combined all three numbers of dumb-bell structures located in the central region of two stubs. The centre frequency of passband is determined by the band-accept (band pass) circuit. For a fixed size of the dumb-bell slot, the passband frequency f_s is adjusted by the coupling gap g. The lower attenuation pole of a band-pass filter is determined by band-reject behaviour of the band-reject (band stop) element in the shunt arm. The dimension of shunt arm and position of a DGS dumb-bell structure decide the

lower frequency of attenuation pole. The upper frequency of attenuation pole of the BPF comes from a parallel resonance of the band-accept series circuit element. However, separation X between the stubs also influence it.

Under these broad guidelines and observations, at first we developed a BPF at 7.63 GHz by using 3 numbers of independent DGS elements. The BPF having bandwidth 35% and return-loss better than –18 dB was developed on the 3D- EM simulator, Microwave-Studio. However, when three numbers of DGS elements were combined together to get a compact BPF shown in Fig.3.40, we obtained the decreased centre frequency 4.3 GHz. In terms of wavelength, it resulted in about 77% reduction in dimension of the filter. A few more iterations were needed before arriving at final dimension of the BPF.

3.7.3 Fabrication and experimental results

A prototype 3-pole BPF at 4.3 GHz was fabricated by using a milling machining. The fabrication was done on RT-Duroid 6006 having ε_r = 6.15 and thickness 0.0635 cm. Its physical dimension and normalized dimension in term of guided wavelength are shown in Table 3.16. The guided wavelength is $\lambda_g = \lambda_s / \sqrt{\varepsilon_r}$, where λ_s is wavelength at the centre frequency f_s. ε_r is relative permittivity of the substrate.

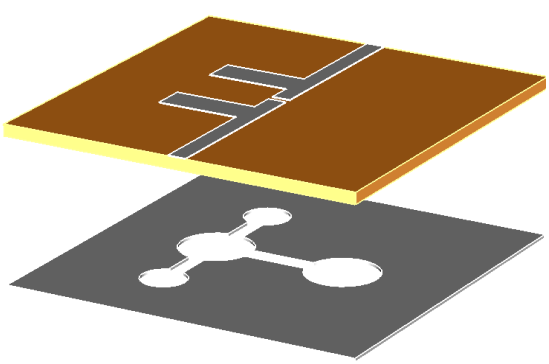

Figure 3.40.a 3-D view of of compact band-pass filter using the band-reject and band-accept DGS elements

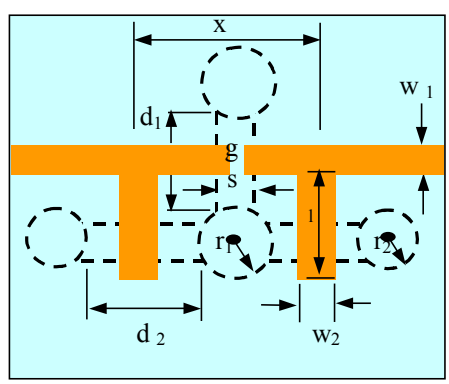

Figure 3.40.b Wire frame view of compact band-pass filter using the band-reject and band-accept DGS elements

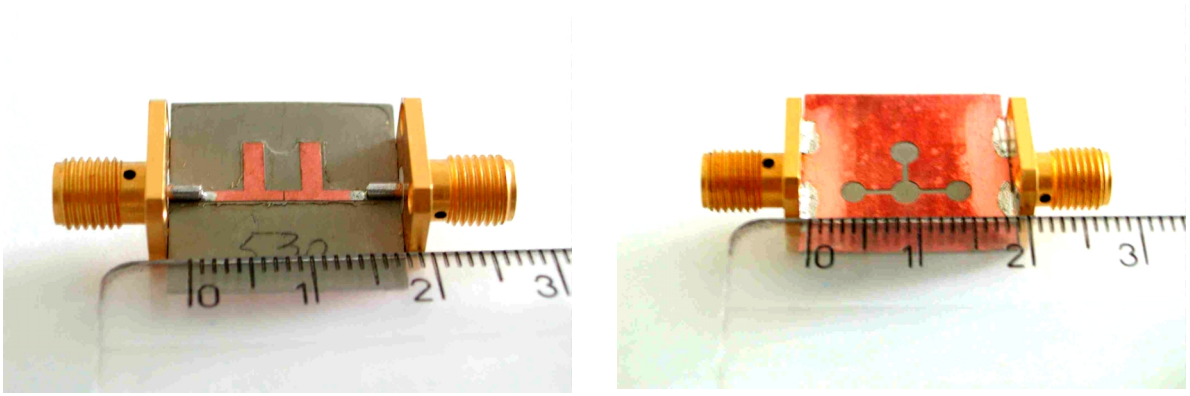

Front view of the fabricated filter

Back view of the fabricated filter showing the DGS element configuration

Figure 3.40.c Fabricated compact band-pass filter

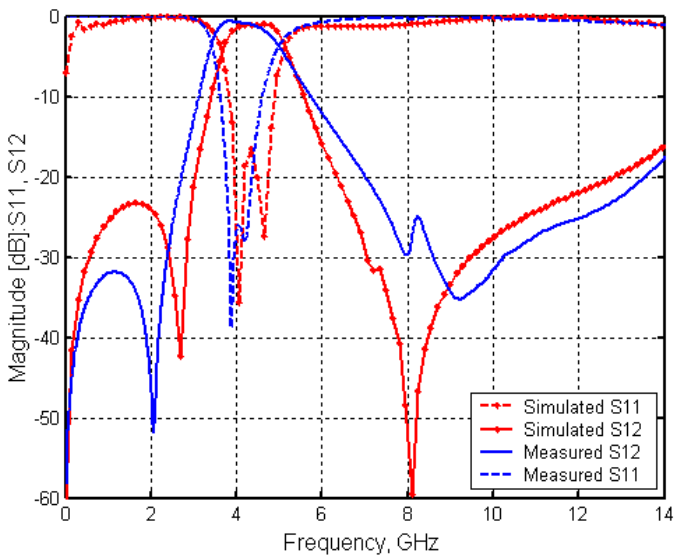

Figure 3.41 Experimental and simulation results of compact BPF

Fig.3.41 shows the simulated and measured response of the BPF. The measured centre frequency, bandwidth and insertion loss (IL) are 3.2 GHz, 38%, and 0.6 dB respectively. The rejection in the stopband, up to 12 GHz is better than 25 dB. It is about three times of centre frequency of the BPF. The rejection in the lower stopband is better than 30 dB.

Table 3.16 Structural Details of BPF

Dimension	cm	λ_g
r_1	0.140	0.0486
r_2	0.125	0.0434
g	0.010	0.0035
s	0.060	0.0200
w_1	0.097	0.0337
w_2	0.180	0.0625
l	0.450	0.1563
d_1	0.240	0.0833
d_2	0.235	0.0816
x	0.500	0.1736
c	0.240	0.0833

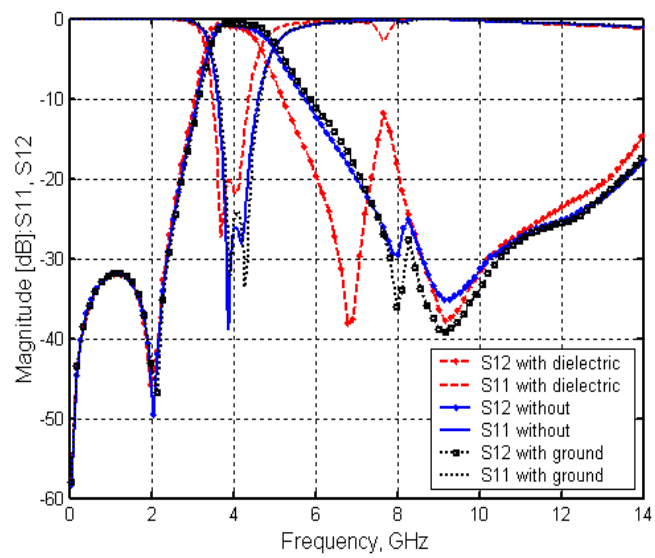

Figure 3.42 Post fabrication tuning of response of BPF

The simulated centre frequency, bandwidth and insertion loss is 3.32 GHz, 32%, and 0.3 dB respectively. Variation in the measured performance is mainly due to imprecise fabrication by a milling machine. Fig.3.42 shows an asymmetrical band-pass response.

We have experimentally examined that the asymmetry can be improved by using a dielectric cover of ε_r = 3.38 and thickness 0.0813cm on the DGS slots. The results are shown in Fig.3.42. The use of dielectric sheet on the DGS slot decreases the centre

frequency and the bandwidth to 3.0 GHz and 32.9% respectively. However, it also increases the band-stop response at 7.8 GHz to –12 dB. Finally the filter has to be put in a metallic enclosure for packaging. We have examined experimentally that nearby metal enclosure (separate ground plane) has strong adverse influence on performance of the filter. Fig.3.42 also shows that metal enclosure must be kept at least a distance more than 4mm from the DGS slot in order to avoid its influence. This information is useful for packaging the BPF.

Finally we have compared the present BPF against other microstrip type BPF. Matthaei et al. have designed an 8-pole BPF, using $\lambda_g/2$ open-circuit stub to get 30 % bandwidth [68]. This filter has spurious passband at f = 0 and f = $2f_s$. The 3-pole BPF using the DGS with coupled microstrip line has bandwidth 10 %, insertion-loss IL = 1.5 dB and return loss 20 dB [83]. Another 3-pole BPF using the PBG with coupled microstrip line has bandwidth 9 %, IL = 1.6 dB and 20 dB-25 dB rejection in the stopband [84]. Thus, the present BPF is more compact and has better performance both in the passband and stopband as compared to these filters.

CHAPTER 4

Microstrip Antenna Gain Enhancement Technique Using Quasi-Planar Surface Mounted Horn

In chapter two we presented the design of large bandwidth aperture coupled microstrip antenna using the resonant slot coupling structure in the ground plane. In this chapter we introduce the surface mounted short horn with the patch antenna in order to improve the gain by 4.5 dB without degrading the bandwidth and the return loss.

4.1 Introduction

Last three decades have seen the tremendous growth and application of the microstrip antenna, which offers several well-known features. The results of the research have contributed to the success of these antennas not only in military applications such as aircraft, missiles, and rockets but also in commercial areas such as mobile satellite communications, the direct broadcast satellite (DBS) system, global positioning system (GPS), remote sensing, wireless local area networks (WLANs), and intelligent vehicle highway system (IVHS). However the microstrip antennas also have drawbacks of limited impedance bandwidth around 1.5-2.5 %. Their gain thin substrate is also limited between 6 dBi – 8 dBi.

Several methods have been adopted to increase the bandwidth of the microstrip antenna. We have carried out the bandwidth improvement of the aperture coupled microstrip antenna by using the resonating coupling slot in the ground plane. The details have already been discussed in the previous chapter. We achieve the bandwidth of 12.4% (11.06 – 12.50 GHz) at the center frequency. By using more complex structures, a bandwidth in excess of 20 %

can be achieved. The improvement of the microstrip antenna gain is the subject of this chapter.

An experimental study of a two layer electromagnetically coupled rectangular patch antenna excited in the TM_{01} mode has been reported in [28]. By choosing the layer thickness and patch position properly, a very large gain may be realized. The gain varies proportionally to either ε or μ, depending on the configuration. However, the bandwidth is seen to vary inversely to gain so that a reasonable gain limit is actually established for practical antenna operation. To achieve directive gain of about 20 dB, impractical superstrate permitivity and or permeability values are needed.

Thus we see that both the gain and bandwidth can be improved with the help of stacked parasitic patch. However, this structure can be optimised either for the gain or for the bandwidth. Likewise, the cavity backed microstrip antenna with multiple layers of dielectric can improve the gain, however the bandwidth is very limited [34]. There is need to increase the gain of radiating patch element without sacrificing the bandwidth.

In this chapter, we introduce a new gain enhancement technique by using the surface mounted short horn. This new gain enhancement technique has been applied to aperture coupled microstrip antenna in [35] and also to probe feed microstrip antenna [117], [118]. A compact aperture coupled microstrip antenna with quasi-planar surface mounted horn of the slant-length, $l_s = \lambda_o/4$ has been investigated using the full wave 3-D Microwave Studio. The antenna It is developed in the Ku-band i.e. 11.08 GHz – 12.5 GHz. The structure has bandwidth 12.4% and has gain 10 ±0.4 dB over the full bandwidth. This method provides improvement of both the bandwidth and gain. We could introduce the surface mounted horn as a gain improvement process through experimental investigations. A probe fed microstrip antenna was initially fabricated for measurement on the power meter. As the gain of the patch antenna was not enough our measurement was not satisfactory. At this moment, we thought about collection of more power around the patch using manually fabricated small copper horn. This arrangement provided 3 dB improvements in gain. Subsequently more investigations and optimization have been carried out through numerical investigations on the 3D-EM Simulator, Microwave studio.

4.2 Aperture coupled microstrip antenna with quasi-planar Surface Mounted Horn

4.2.1 Numerical Experimentation

The cross-section of the proposed structure is shown in Fig.4.1. We have generated the design information of the surface mounted horn with help of the 3D-EM Simulator, Microwave Studio [109]. In the present arrangement, the aperture coupled rectangular patch is not the main radiating element. It is a feed to the short surface mounted horn antenna. The horn is excited mainly by the direct aperture field of the patch and also by some of the surface wave mode supported by the substrate.

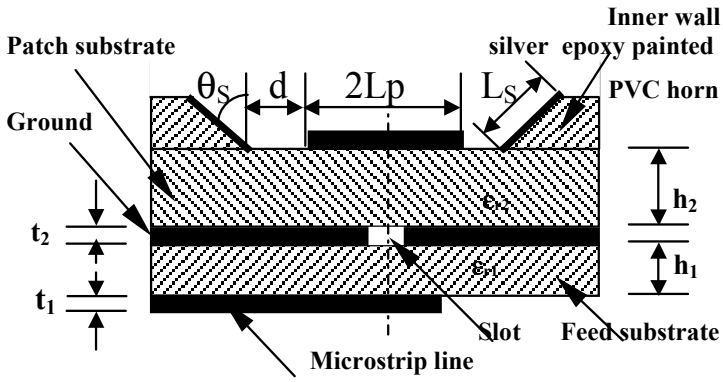

Figure 4.1 Aperture- coupled Microstrip antenna with a surface mounted horn

Fortunately the aperture coupled microstrip patch antenna and the surface mounted short horn can be designed separately. The optimised distance 'd' between edge of the patch and the horn does not have noticeable influence on the resonance frequency, return loss and input impedance of the aperture coupled microstrip antenna. However, some small adjustment in the feeding slot can improve the design. The design of the aperture coupled microstrip antenna is given in previous chapter. Thus we concentrate on the design of the surface mounted horn. Certain dimensions of slot, stub and rectangular microstrip antenna have been selected in order to get larger bandwidth by bringing the resonance frequency of the patch and that due to the coupling aperture and stub closer. This is achieved by the numerical experimentation with the help of 3D-EM Simulator.

In this study we have selected a short horn of slant length, $l_s = \lambda_0/4$ as we are interested in the quasi-planar antenna suitable to development of the high gain planar array antenna.

The maximum directive gain depends on the relative permittivity and thickness of substrate of the patch, operating frequency, separation distance, d of the horn from the edge of the patch and the slant – angle, θ_s of the horn. Using a longer horn can also increase the gain. However, the structure will not be quasi-planar. The rectangular patch feeding the horn is designed on the substrate having relative permittivity ε_{r2}=2.2, , h_2=1.575 (0.062 λ_0) at 11.78 GHz. The 50 Ω microstrip line feeding to the coupling aperture in the ground plane is designed on the substrate, ε_{r1}=6.15. We have examined the variation in the directive gain with respect to slant-angle, θ_s for d= $\lambda_o/8$, $\lambda_o/4$, and $\lambda_o/2$.

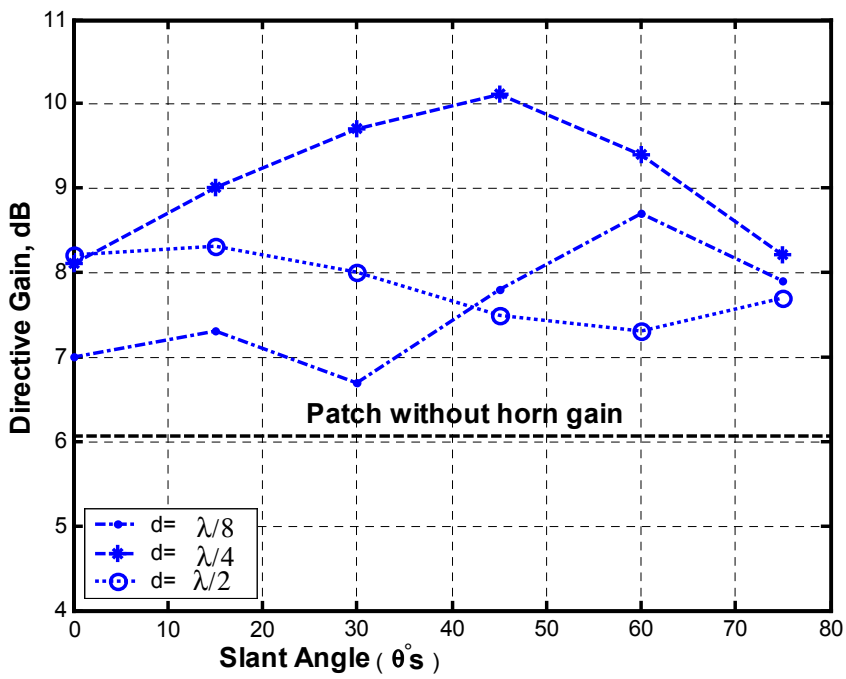

Figure 4.2 Variation in gain with respect position of horn and its slant- angle

The results of numerical experimentation conducted on the Microwave Studio are shown in Fig. 4.2.

Thus we can achieve 10.1 dBi directive gain for d= $\lambda_o/4$ and θ_s=45^0. For d= $\lambda_o/8$ and θ_s=60^0 we can achieve 8.6 dBi directive gain. The $\lambda_o/8$ separation is more suitable for the array application. The design details of the aperture coupled microstrip patch antenna are shown

in the Table 4.1. The aperture efficiency of the horn-patch combined structure is 64.3%, whereas the waveguide fed optimum pyramidal horn has 50% aperture efficiency.

The simulated radiation patterns in both the E-plane and the in the H-plane for the aperture coupled Microstrip antenna, the waveguide fed pyramidal horn and the horn- patch combination are shown in Fig.4.3 and Fig.4.4 respectively.

Table 4.1 Structural Details of Antenna

Structure	**Antenna element**	**Dimension / Parameters**
Aperture-Coupled Microstrip antenna	Patch substrate	RT/duroid 5880 ε_{r2} = 2.20, $\tan\delta_2$ = 0.0009 h_2 = 1.575 mm (0.062λ_o), t_2 = 35 μm
	Antenna dimensions	Substrate length = 53 mm Substrate width= 53 mm
	Patch dimensions	Length, $2L_p$ = 6.91 mm, Width, $2W_p$ = 5.60 mm
	Ground-Plane	Thickness, t_g = 17.5 μm
	Coupling aperture	Length L_a = 4.43 mm, width W_a = 0.43 mm
	Feed substrate	RT/duroid 6006 ε_{r1} = 6.15, $\tan\delta_1$ = 0.0019 h_1 = 0.635 mm (0.025λ_o)
	50 Ω Microstrip feed line	Length, l_f = 26.5 mm, Width, w_f = 0.96 mm, stub-length, L_s = 1.6 mm, thickness, t_1 = 17.5 μm
Horn	Horn dimension	Square base horn $2(L_P+d)$= 1.962 cm, L_S= $\lambda_o/4$, Slant angle θ_S=45° Square radiating aperture, area =2.698x2.698 cm^2
Full structure	Total height	H=7 mm

The radiation patterns of the horn –patch combined antenna structure is closer to the radiation patterns of the short pyramidal horn. However, the aperture-coupled microstrip antenna feed influences the side lobe level and radiation pattern symmetry of the proposed horn-patch combined structure in the E-plane. The E-plane radiation pattern of the simple aperture coupled microstrip antenna is itself disturbed by the coupling slot in the ground plane and the stub fringing fields. Thus for the horn-patch combined structure the E-plane has side-lobe of level –7.9 dB and the H-plane radiation pattern has no side- lobe. It has large back-lobe level –12 dB, which is in between the back-lobe level, -15.1 dB of only short horn and back-lobe level, -7.9 dB of the aperture-coupled microstrip antenna. Thus the surface mounted short horn improves not only the gain of the proposed antenna structure by 4 dB, it also improves the back- lobe level at least by 4 dB. However, the back lobe level can be improved further by using another reflecting patch behind the microstrip line [119].

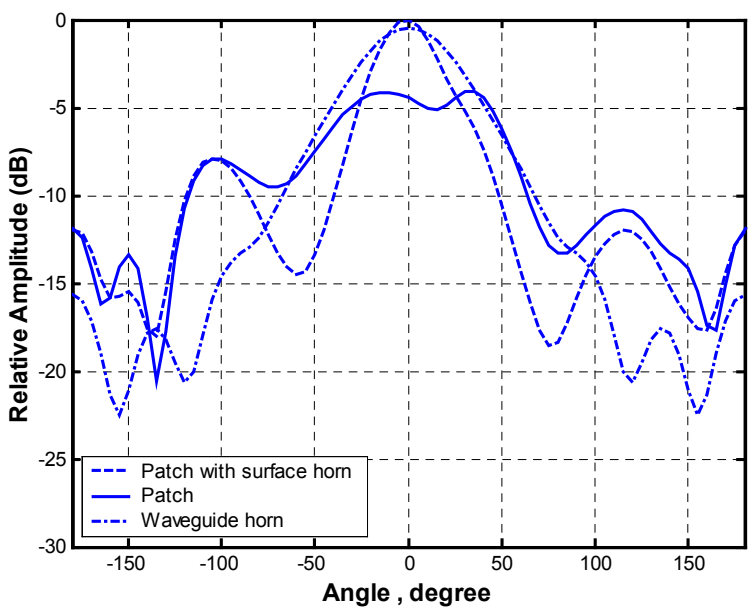

Figure 4.3 Simulated E-plane radiation patterns

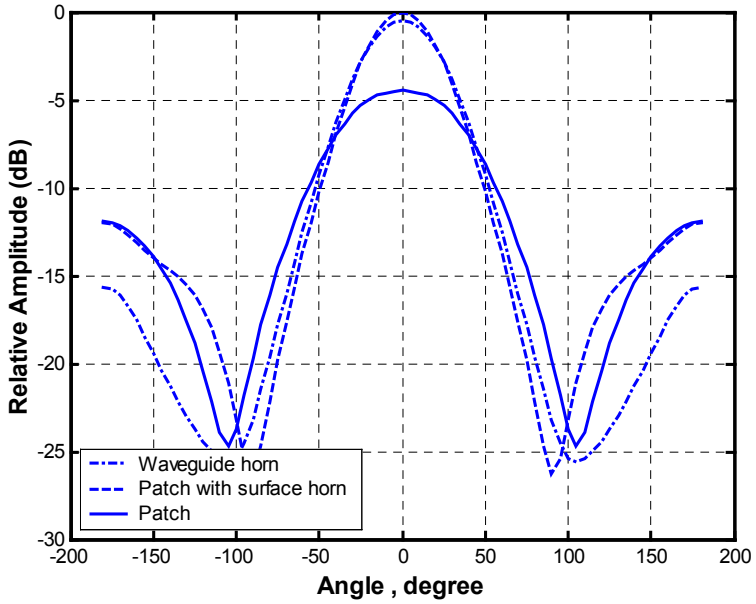

Figure 4.4 Simulated H-plane radiation patterns

4.2.2 Fabrication and Measurement

The photograph of the fabricated horn-patch structure is shown in Fig.4.5.

The horn is cut in a PVC sheet and is mounted on the surface of the substrate of the aperture coupled patch antenna feeding the horn. The inner surface of the horn is painted with the conductive silver epoxy.

The Fig. 4.6 shows the measured return loss of the aperture coupled microstrip antenna with and without horn.

It is obvious that the horn does not influence input parameters of the patch antenna. The Fig. 4.7 and Fig. 4.8 show the measured E-plane and H-plane radiation patterns respectively for the aperture coupled patch antenna, with and without horn. The horn improves the gain by 4.2 dB as shown in Fig. 4.9. The back- lobe level of the patch antenna is improved by 5.4 dB due to the horn. However, the simulator predicts only 4 dB improvement for both the gain and the back-lobe level. We have further carried out the calibrated measurement with the VNA for the gain, the back lobe level and the cross-polarization level of the aperture-couple microstrip antenna, with and without horn over

whole of the bandwidth between 11.06 GHz – 12.5 GHz. The Table 4.2 summarizes the performance of the aperture coupled microstrip antenna and the aperture coupled microstrip antenna with the quasi-planar horn.

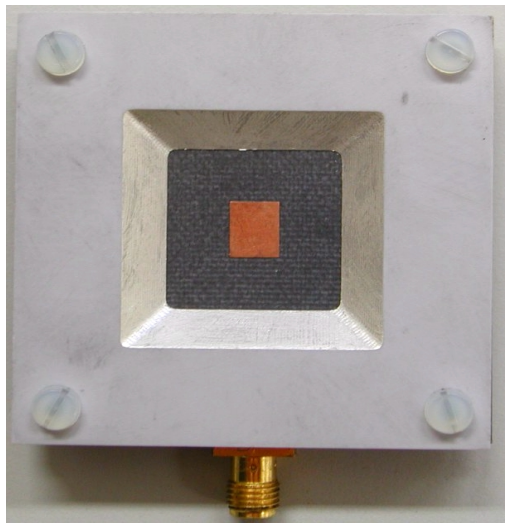

Figure 4.5 Photograph of Horn-Patch Structure

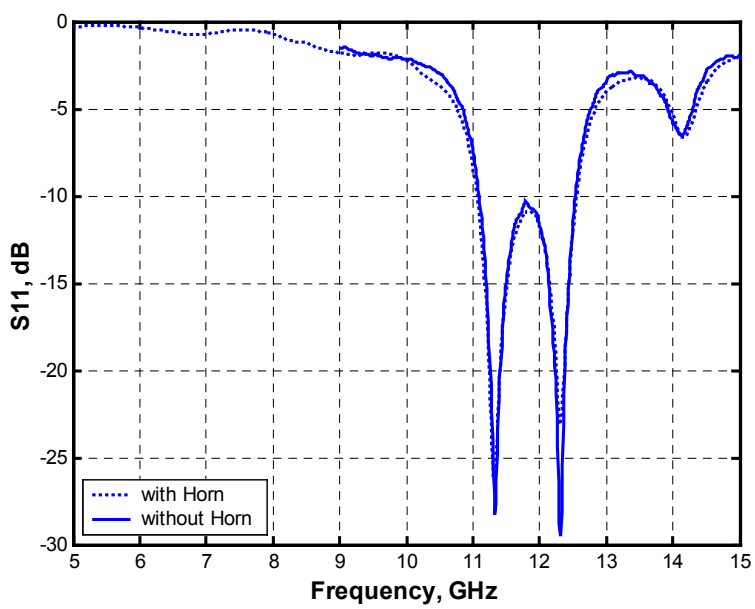

Figure 4.6 Return loss

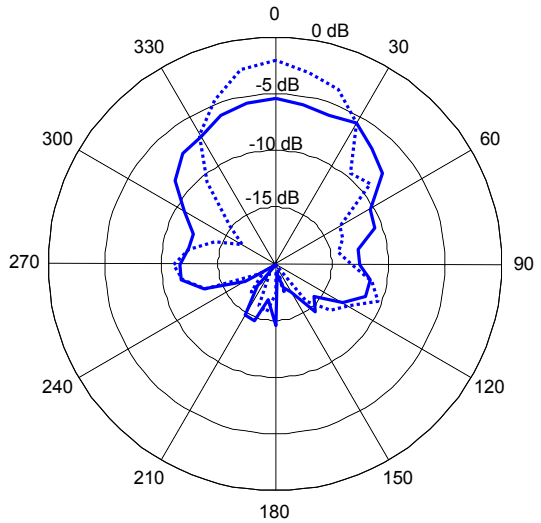

Figure 4.7 Measured E-plane radiation pattern of patch (—) and horn with patch(-----)

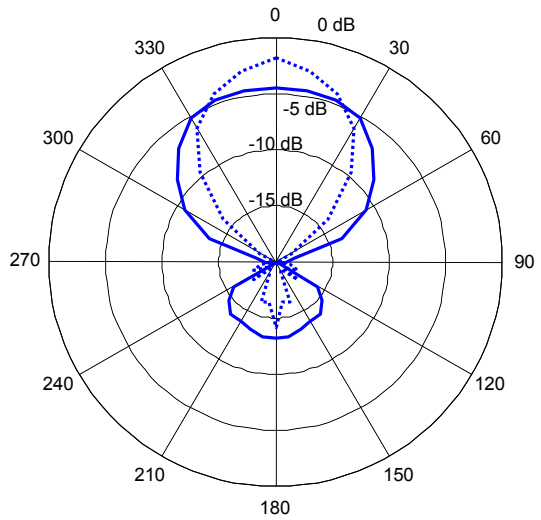

Figure 4.8 Measured H-Plane Radiation Pattern of Patch (—) and Horn with Patch(-----)

Table 4.2 Experimental and Simulated Performance of Aperture-Coupled Microstrip Antenna with and without Horn

Parameter	**With Horn**		**Without Horn**	
	Exp.	**Simu.**	**Exp.**	**Simu.**
Reso. Freq. GHz	11.82	11.8	11.815	11.78
S_{11} (dB)	-11	-10.5	-10.5	-10.7
Bandwidth %	12.4	12.2	12.4	12.2
H-plane 3dB-Beamwidth	52°	51.7°	86°	86°
E-plane 3dB-Beamwidth	41°	40°	93°	101°
Gain (dBi)	9.8	10.1	5.6	5.9
Front–to–back ratio (dB)	14.4	12	8	7.6
Cross-polarization (dB)	-30.3	—	-34.8	—

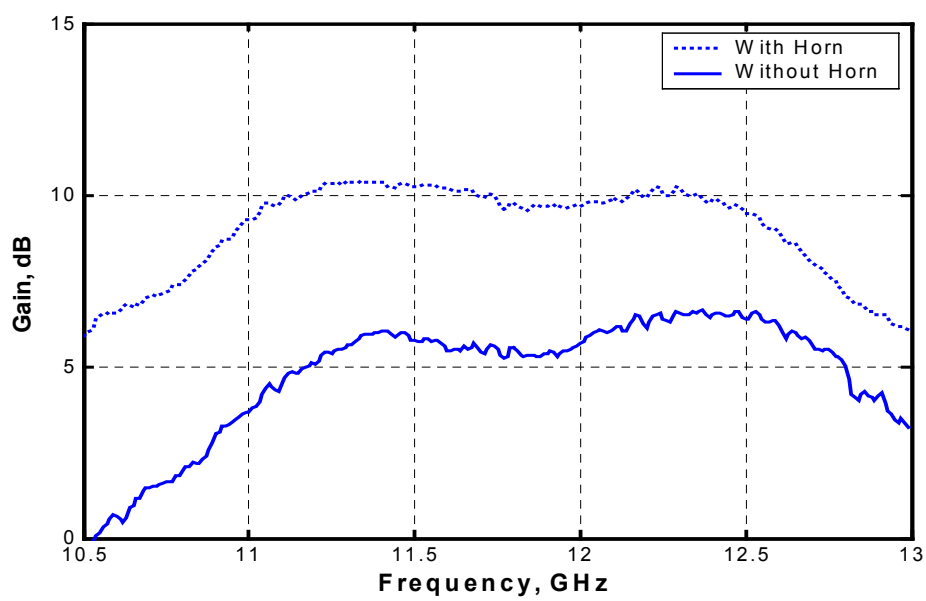

Figure 4.9 Measured Gain of Patch (—) and Horn with Patch(-----)

4.3 Aperture Coupled Microstrip Antenna with Quasi-Planar Conical Surface Mounted Horn

To test the validity of the numerical experimentation and the idea of the gain enhancement, an aperture coupled microstrip antenna with quasi-planar conical surface mounted horn has been designed and fabricated.

The photograph of the structure is shown in Fig. 4.10. The horn is cut in a PVC sheet and is mounted on the substrate surface of the aperture coupled patch antenna. The inner surface of the conical horn is painted with a conductive silver epoxy. The design details of the aperture coupled microstrip patch antenna are shown in the Table 4.3. The measured antenna input characteristics (return loss and input impedance with and without horn) are shown in Fig. 4.11 and Fig. 4.12 respectively. It is obvious that the horn has a neglected effect on the patch antenna input parameters. The measured E-plane and H-plane radiation patterns for the aperture coupled patch antenna, with and without conical horn, are depicted in Fig. 4.13 and Fig. 4.14 respectively.

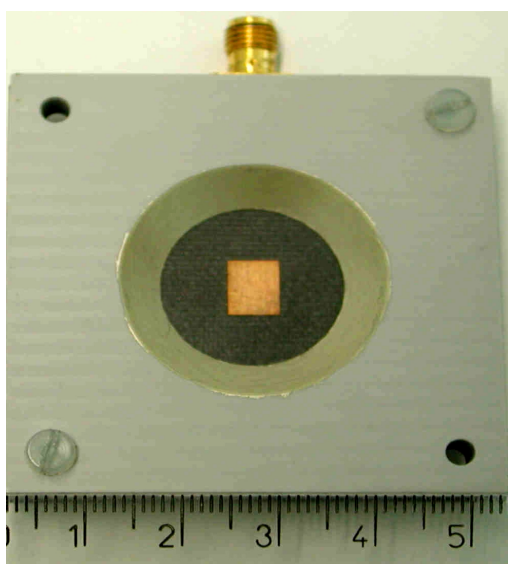

Figure 4.10 Photograph of Conical Horn-Patch Structure

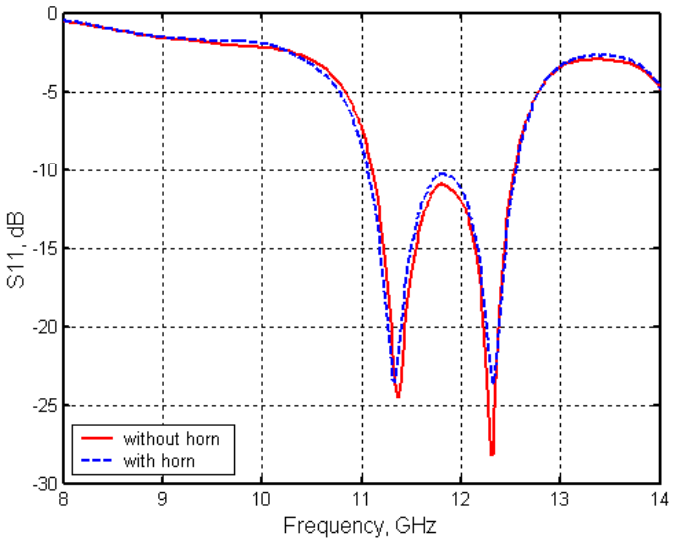

Figure 4.11 Return loss

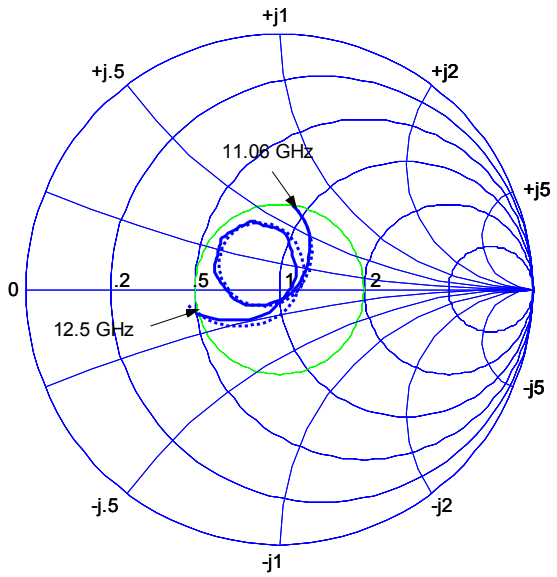

Figure 4.12 Normalized impedance of patch (—) and horn with patch(----)

Table 4.3 Structural Details of Antenna with Quasi-Surface Mounted Conical Horn

Structure	Antenna element	Dimension / Parameters
Aperture Coupled microstrip antenna	Patch substrate	ε_{r2} = 2.20, tanδ_2 = 0.0009 h_2 = 1.575 mm (0.062λ_o), t_2 = 35 μm Substrate length = 53 mm Substrate width= 53 mm
	Patch dimensions	Length, $2L_p$ = 6.91 mm, Width, $2W_p$ = 5.60 mm
	Ground-Plane	Thickness, t_g = 17.5 μm
	Coupling aperture	Length L_a = 4.43 mm, width W_a = 0.43 mm
	Feed substrate	ε_{r1} = 6.15, tanδ_1 = 0.0019, h_1 = 0.635 mm (0.025λ_o)
	50 Ω Microstrip feed line	Length, l_f = 26.5 mm, Width, w_f = 0.96 mm, stub-length, L_s = 1.6 mm, thickness, t_1 = 17.5 μm
Horn	Conical horn dimension	Bottom diameter 2(L_P+d)= 1.962 cm, L_S= λ_o/4, Slant angle θ_S=45° Top diameter=3 cm , area = 7.0686 cm^2
Full structure	Total height	H= 6.6750 mm

The conical horn improves the gain of the aperture coupled microstrip antenna by only 4 dB. The gain of the antenna with the surface mounted pyramidal horn is greater than that with the surface mounted conical horn by 0.5 dB. The aperture area of the pyramidal horn is more than that of the conical horn. As a result, a reasonable gain enhancement can be obtained using horn with slant length of λ_0 /4, slant angle of 45°, and base horn diameter of ($2L_P$ +d). Where, $2L_P$ is the patch length and 2d is equal to λ_0 /2.

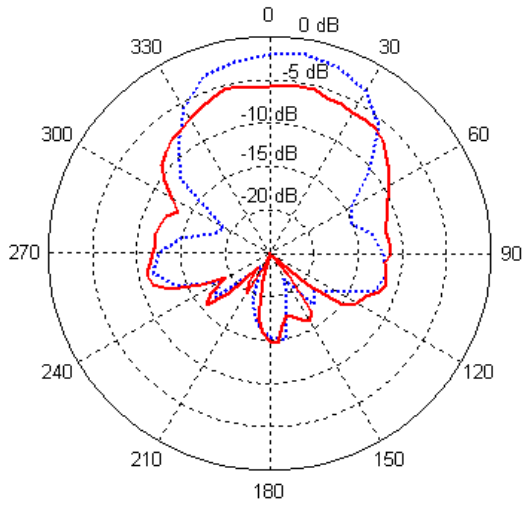

Figure 4.13 Measured E-plane radiation pattern of patch (—) and horn with patch(-----)

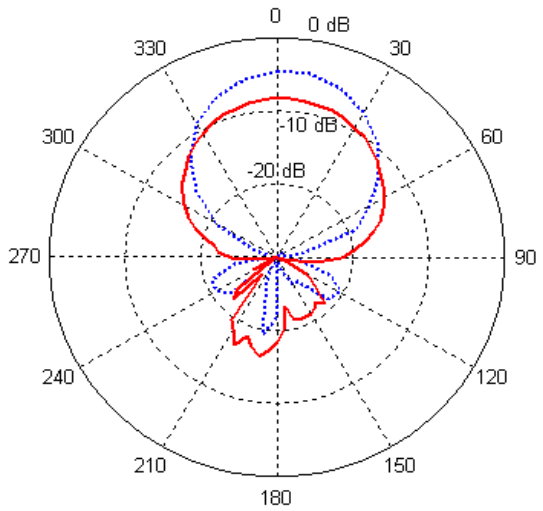

Figure 4.14 Measured H-plane radiation pattern of patch (—) and horn with patch(-----)

4.4 High Gain Wideband Probe Feed Compact Microstrip Antenna With Quasi-Planar Surface Mounted Horn

Another frequency, feed and substrate are used to examine the validity of the new gain enhancement technique.

This section introduces a new probe fed microstrip antenna element with the quasi-planar surface mount short horn. The slant length of the horn is only $\lambda_o/4$ to achieve high gain i.e. 11 dBi. Bandwidth of 9.0 % has been obtained for the structure which can be further increased by use of thicker substrate [120]. A systematic numerical experimentation on a 3-D EM simulator [109] is presented to achieve high directivity. The microstrip antenna with a surface mounted horn is fabricated with plastic sheet. The horn surface is silver epoxy painted. Two element array has been fabricated and tested. An improvement of 10 dB isolation between the elements; as compared to the array without horn, is achieved by use of the surface mounted quasi-planar horn.

4.4.1 Numerical Experimentation

The proposed new structure is shown in Fig. 4.15. At first, we have attempted to optimize size of a quasi-planar short horn and its placement with respect to the patch in order to obtain the maximum possible gain for the compact structure. A probe-fed square microstrip antenna, with dimension, 0.857cmx0.857cm is designed on a square dielectric substrate of size, 8.0 cm x 8.0 cm x 0.081cm and relative dielectric constant ε_r =4.38. The patch antenna resonates at 8.77 GHz. A short horn of slant length, $L_s = \lambda_o/4 = 0.875$ cm is selected in this work. λ_o is the wavelength at the resonance frequency.

The total distance between center of the patch and inner edge of the horn is, $D=L_p+d$. Where $2L_p$ is the dimension of square patch and d is the distance between edge of the patch and inner edge of the horn. The patch has 6.27 dBi directivity without horn. The slant length of horn makes θ ° angle with respect to the vertical axis to the patch. Through numerical experimentation we optimize horn position, d and slant angle θ ° to achieve the maximum gain. For several horn position, d between $\lambda_o/16$ to λ_o, we compute broadside directivity of the patch radiator at slant angles between θ ° =0 ° and 90 ° with help the 3D-EM simulator [109].

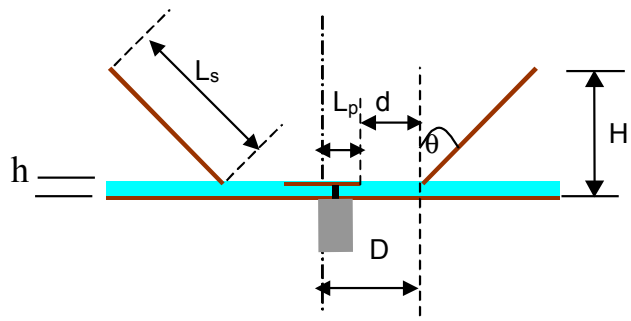

Figure 4.15 Microstrip patch antenna with quasi-planar surface mounted horn

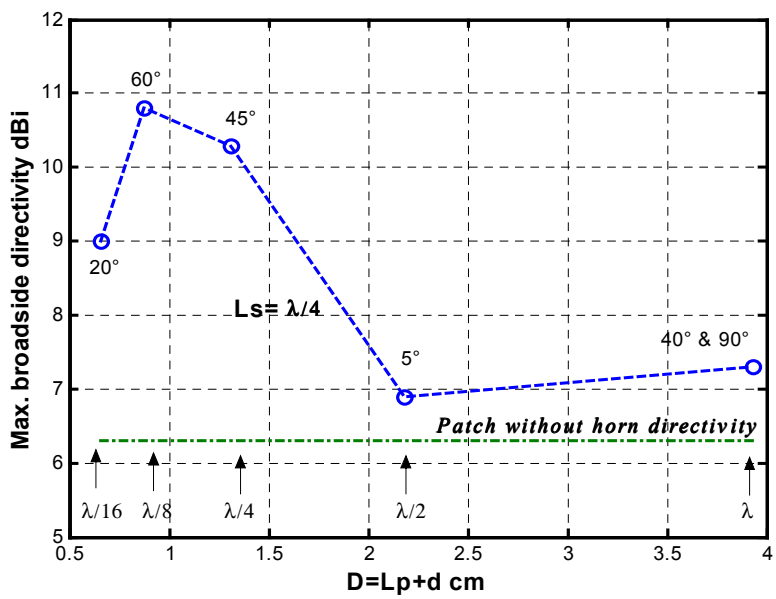

Figure 4.16 Position of Horn for Maximum Directivity at Different Slant Angle (θ) of Horn.

The final results for horn of the slant length $L_s = \lambda_o/4$ is presented in the Fig. 4.16. The θ for maximum directivity is shown in the figure and the corresponding position, d in wavelength is also shown. Thus we can achieve the high directivity at the horn position, $d = \lambda_o/8$ and $\lambda_o/4$ for the horn slant angle, θ= 60 ° and 45°. While maintaining nearly high gain, distance, d and slant angle, θ can be adjusted to meet requirement of an array arrangement.

A microstrip antenna on the thin substrate provides narrow bandwidth, typically about 2%. Therefore, we examined the microstrip antenna with and without horn on the thick substrates also.

The numerical investigation is carried out for the qusi-planar horn of slant length, $L_s = \lambda_o/4$, slant angle, θ = 60 ° and horn position, $d = \lambda_o/8$ and $\lambda_o/4$. The thickness of substrate, h is 0.081 cm and thick substrates are taken in multiple of this basic thickness. The results of numerical investigation is shown in Table 4.4. The table shows that for the horn position, $d = \lambda_o/8$, directivity of the antenna with horn decreases from 10.7 dBi to 7.8 dBi with the increase in the substrate thickness from h to 4h. There is only a marginal increase in directivity of the simple patch from 6.23 dBi to 6.9 dBi for 4h thick substrate. The degradation in directivity of the patch antenna with horn is due to leakage of power from the thick radiating aperture of the patch. The leaked power does not reach to the horn for sufficient radiation. Table 4.4 further shows that for the horn position, $d = \lambda_o/4$ the directivity is increased to 11 dBi. The enlarged dimension, d of base of the horn helps to collect more power to the horn. This makes size of the radiating element large and may not be suitable for an array application. Therefore, for an array application we can restrict ourselves for 3h thick substrate and accept 9.7 dBi directivity with some reduced bandwidth around 7.82 %.

Table 4.4 further shows that with increase in thickness of the substrate from h to 4h, the bandwidth of the patch radiator increases from 2.67 % to 11.8%. For the horn placed at $d = \lambda_o/8$, the bandwidth is reduced a little. However, it increases from 2.30 % to 11.6 % with increase in substrate thickness from h to 4h.The bandwidth shows improvement for the horn position, $d = \lambda_o/4$. Table 4.4 shows that the feed position for the proper matching

changes with thickness of the substrate and also by presence of the horn. This should be taken care of to design the microstrip antenna with surface mounted qausi-planar horn.

Table 4.4 Simulated results for slant angle θ = 60° and $L_s = \lambda_o/4$

Substrate thickness (h=0.081 cm)	Directivity without horn (dB_i)	Directivity with horn $d=\lambda_o/8$ (dB_i)	Directivity with horn $d=\lambda_o/4$ (dB_i)	Band-Width No horn	Band-Width with horn $d=\lambda_o/8$	Band-Width with horn $d=\lambda_o/4$	Feed position without horn	Feed position with horn $d=\lambda_o/8$	Feed position with horn $d=\lambda_o/4$
1	6.27	10.7	10.1	2.67%	2.3%	2.63%	0.12	0.105	0.115
2	6.47	10.5	11.0	6.58%	4.48%	5.58%	0.17	0.14	0.150
3	6.70	9.70	11.0	10.5%	7.82%	9.2%	0.27	0.23	0.250
4	6.90	7.80	10.7	11.8%	11.6%	10.93%	0.40	0.39	0. 400

4.4.2 Fabrication and Experimental Results

The patch antenna and patch antenna with qausi-planar short horn is fabricated for the experimental investigation. One set of patch antenna is fabricated on the thin substrate, h = 0.081 cm, ε_r = 3.38 and the square patch length $2L_p$ = 0.857 cm to resonate at f_r = 8.77 GHz. The horn has a slant angle θ = 30 ° and slant length, L_s =0.875 cm. Length of square base of the horn is 2.2 cm. Another set of square patch antenna is fabricated on the thick substrate, 3h = 0.243 cm, ε_r = 4.38 and the square patch length L_p = 8.44 cm to resonate at f_r = 9.2 GHz. The horn has slant angle θ = 60 ° and slant length, $L_s = \lambda_0/4$. The slant angle is changed to confirm high gain obtained through simulation for θ between 30 ° and 60 °. The horn is placed at $d=\lambda_0/4$. For light weight antenna structure, the short quasi-planar horn structure is fabricated from a thick sheet of PVC. The total thickness of the antenna structure with horn (H) is only 6.94mm. The conducting surface of the horn is painted with silver

epoxy paint. An array of two elements on the thin substrate is also fabricated to test the radiation property, bandwidth and isolation between the radiating elements for large array application. The fabricated patch element and two element array with the surface mounted plastic horn is shown in Fig.4.17. We note that for the array both horns are made in one plastic block. For a large array also the horns could be cut in one plastic sheet and inner surfaces could be properly metalized to achieve high gain.

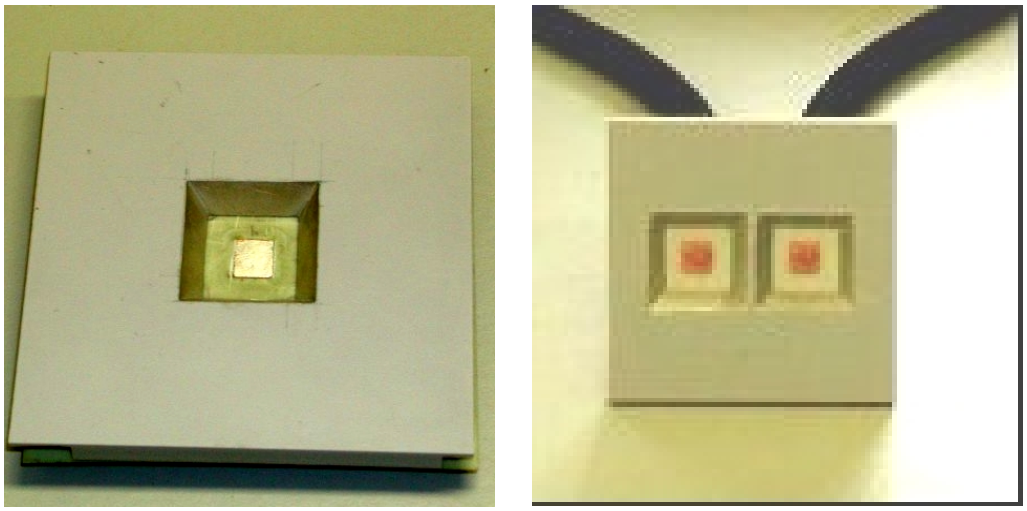

Figure 4.17 Fabricated Patch with Surface Mount Quasi-Planar

Fig. 4.18 and Fig. 4.19 show radiation patterns of the patch antenna in the E-plane and H-plane respectively for the patch with horn on the thin substrate, h= 0.081 cm. The experimental results validates the simulation. The deviation in the back-lobe is due to measurement condition, and point to point manual measurement.

We make a detail comparison between the measured performance and the simulation of the patch antenna, with and without horn in the Table 4.5. We obtain 9.0 dBi gain as compared to the standard horn. We get 9.2 dBi directivity from the measured beam-widths. The Table 4.5 also shows an improvement of 3.5 dB gain by use of the quasi-planar horn. As shown in Fig. 4.20, the horn reduces the bandwidth slightly, from 2.4% to 2.3%.However, it has improved the return loss from –22 dB to –35 dB. Similar results are obtained for the

patch on thicker substrate, h=0.243 cm. For this case we obtained 11.0 dBi gain with 9.0% bandwidth.

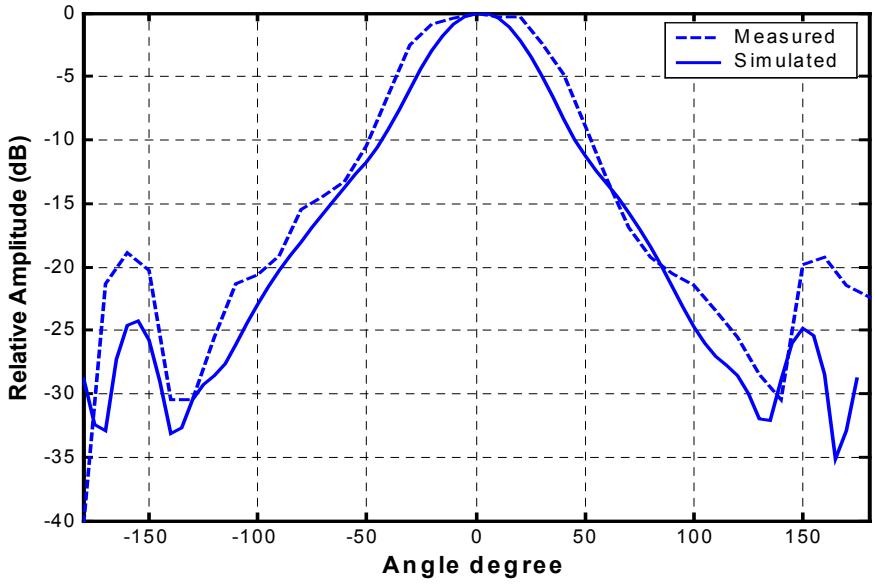

Figure 4.18 Measured and simulated E-plane field with horn

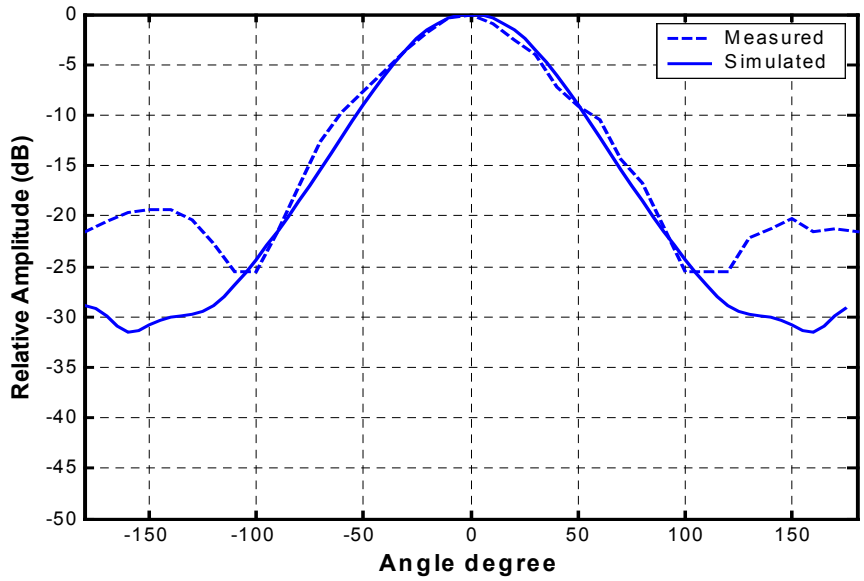

Figure 4.19 Measured and simulated H-plane field with horn

Table 4.5 Experimental and Simulated Performance of Probe-fed Microstrip Antenna with and without Horn

Parameter	With horn		Without horn	
	Experiment	Simulation	Experiment	Simulation
S_{11} (dB)	-35	-40	-22	-25
Bandwidth	2.3%	2.3%	2.4%	2.67%
Resonance frequency	8.85 GHz	8.77 GHz	8.832 GHz	8.75 GHz
Beamwidth E-plane	55°	44.5°	135°	120°
Beamwidth H-plane	57°	55.3°	74°	71°
Gain	9 dB	10 dB	5.5 dB	6 dB

Fig. 4.21 shows the measured radiation patterns in the E-plane for a two element array with and without horn. The horn improves the gain of two element array by 3 dB. There is also a significant improvement in the side lobe level due to presence of the horn. We obtained 11.5 dBi gain of the two element array with horn and 8.5 dBi gain of the array without horn with the help of a standard horn. Fig.4.22 shows the measured isolation between the patches of two element array. The center to center distance between two patches is $0.82\lambda_o$. The horn improves the isolation nearly by 10 dB.

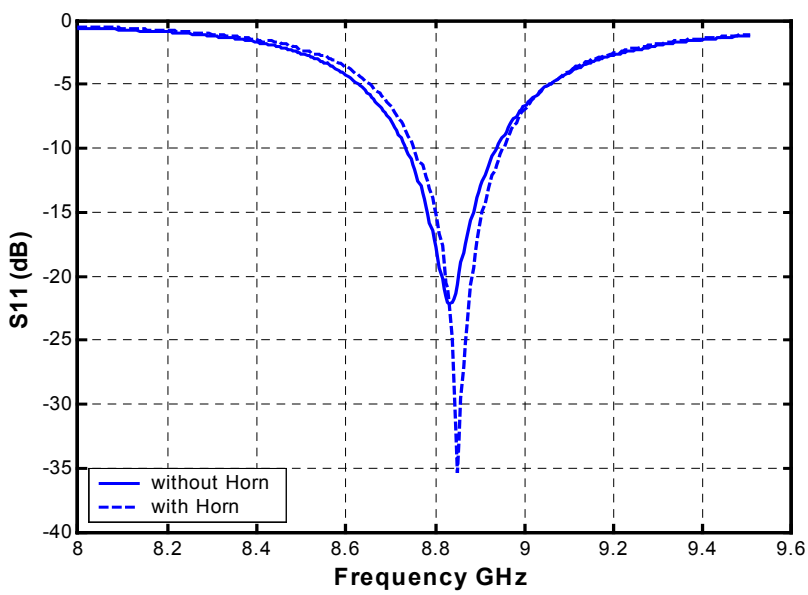

Figure 4.20 Measurement of return-loss with and without horn

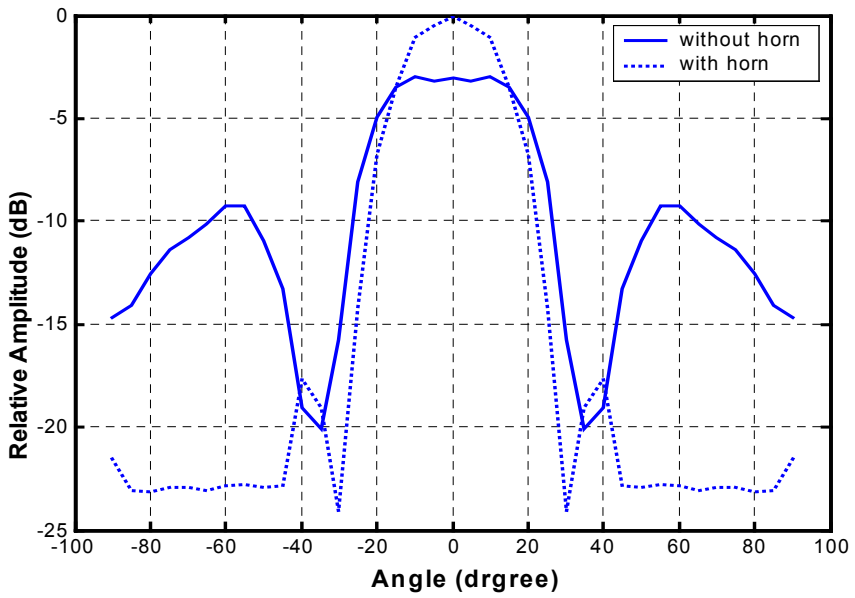

Figure 4.21 Two-Element measured E-plane field with and without horn

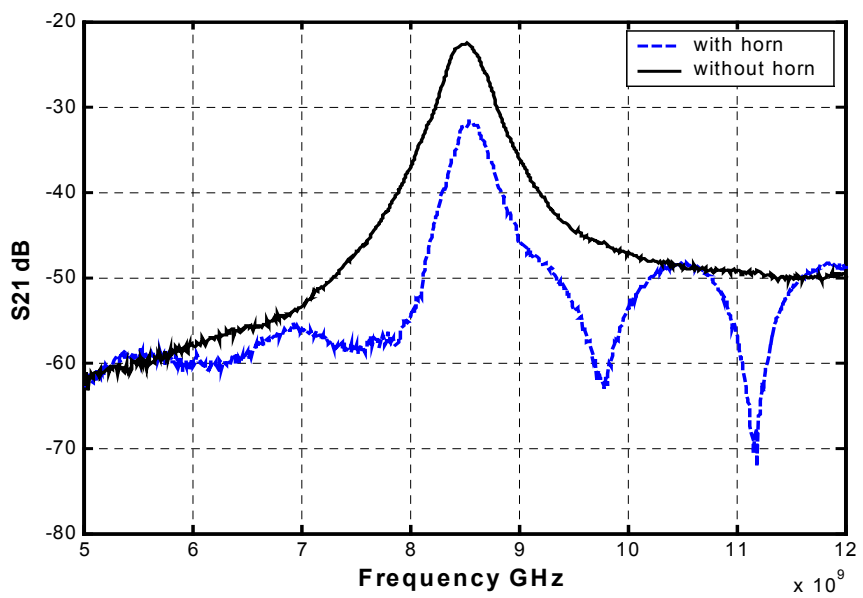

Figure 4.22 Measured coupling between two radiating elements with and without horn

4.4.3 Gain Behavior of Inserted Horn

At certain substrate thickness, the surface mounted horn can not improve the gain much more as discussed in section 4.4.1 and Table 4.4.

By increasing the substrate thickness, the surface mounted horn is not able to trap the total power. Some of the power leaks through the substrate as a surface waves. To trap and guide this leaked power to the broadside direction, the horn has to be inserted into the substrate thickness till the ground plane. By inserting the horn into the substrate, the gain will increase by more than 1.5 dB as indicated in Table 4.6.

Two different substrates have been used to investigate the effect of the relative permittivity and the thickness on the behavior of the surface mounted and inserted horn. Less gain has been obtained in case of high relative permittivity materials due to the small dimension of the microstrip antenna as shown in Table 4.6.

Table 4.6 Performance of Probe-fed Microstrip Antenna with Inserted and Surface Mounted Horn for Practical Substrates having Different Thickness and Relative Permittivity

Substrate RT/duroid 6006						
h_f	ε_{rf}	$\tan\delta_f$	t_f (μm)	Broadside Gain (dB)		
				Patch without horn	Patch with surface mounted horn	Patch with inside mounted horn
0.0157 λ_0	6.15	0.0019	17.5	5.1	10.1	10.49
0.0313 λ_0	6.15	0.0019	17.5	5.3	10.3	10.89
0.0627 λ_0	6.15	0.0019	17.5	5.9	9.7	11.18
Substrate RT/duroid 5880						
h_f	ε_{rf}	$\tan\delta_f$	t_f (μm)	Broadside gain (dB)		
				Patch without horn	Patch with surface mounted horn	Patch with inside mounted horn
0.0203 λ_0	2.2	0.0009	35	6.7	10.9	11.4
0.0407 λ_0	2.2	0.0009	35	6.57	10.6	11.7
0.082 λ_0	2.2	0.0009	35	6.57	10.16	12.00

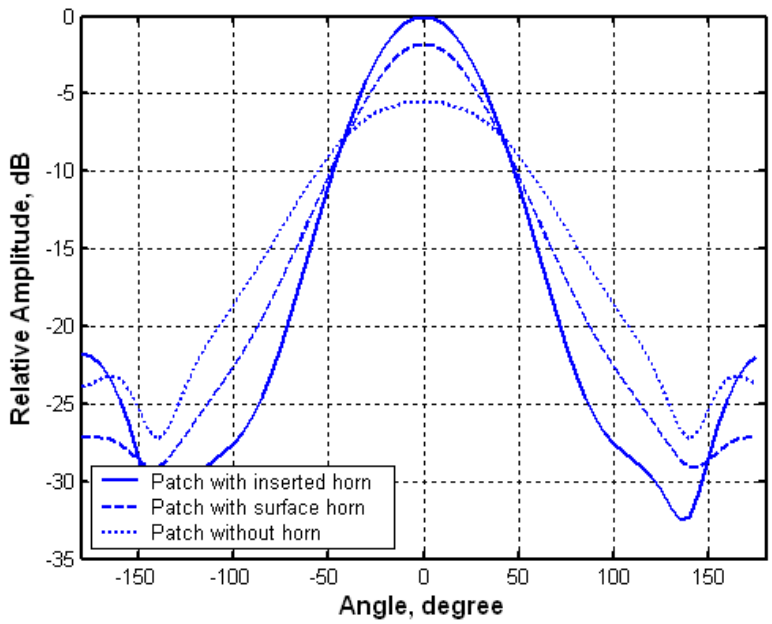

Figure 4.23 Simulated H-plane radiation patterns

CHAPTER 5

Gain Enhancement of Microstrip Antenna Array Using Surface Mounted Horn

In the previous chapter we presented the gain enhancement of the aperture coupled microstrip antenna and the probe feed microstrip antenna. In this chapter we introduce the surface mounted horn with the patch antenna array in order to improve the gain of the array by 3.5 dB and the side lobe level by 8 dB.

5.1 Patch Antenna Array

Some particular applications, such as indoor communications, require wide beams, which single patch antenna provide. However, on the other hand radar and communication systems operate with very narrow beams, which can be obtained by assembling several patches to form an array. Patches are grouped in a more or less regular pattern in such a way that the radiated fields combine along the desired direction and cancel out elsewhere. The radiating elements are combined to form rectangular, circular, linear or more complex assemblies of sub-arrays.

To determine the fields radiated by an array, one sums the contributions of every patch. In the first approximation, it is assumed that the radiation pattern of a patch remains the same as when the patch is alone. The array pattern is the original pattern of a patch multiplied by an array factor that accounts for the amplitudes and phases of the currents fed to them [94].

In reality, however, patches interact with each other due to proximity and vicinity with adjacent elements. The currents are induced in surrounding patches and, hence, provide coupling among the radiators [121]. The radiation pattern and the input impedance are affected by surrounding elements in a manner that depends upon the location of the patch within the array. Thus, the radiation pattern of an array or any complex structure can be

found more realistically by using the full wave based electromagnetic simulator, Microwave Studio [109]. An array can provide a fixed radiation pattern, either perpendicular to the plane of the array (broadside) or with some tilt angle, obtained by feeding signals with different phase shifts to the different elements.

5.1.1 Array Feeds

The array can be fed in several different manners, as shown in Fig. 5.1 [122]. In a series feed arrangement, a single transmission line is directly coupled to the radiating elements, with part of the power fed to each one of them in sequence. The line can be terminated into a resistive load, in which case only a forward wave travels along the line.

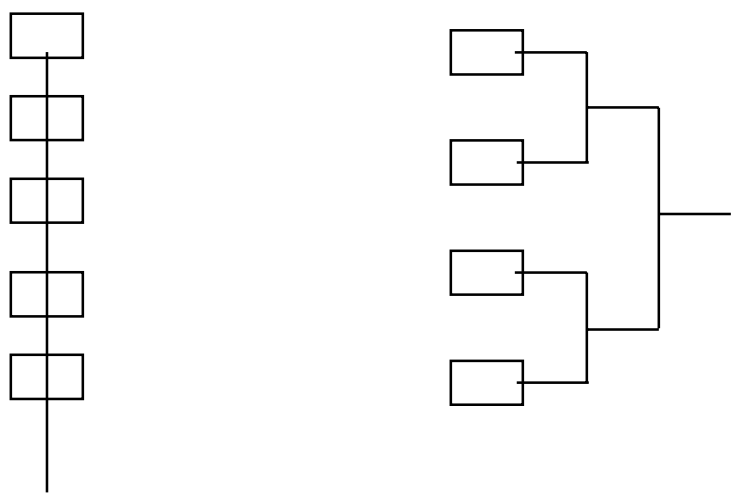

a. Series feed b. Corporate feed

Figure 5.1 Series and corporate feeds for a linear array

Since the series feed is made by a single transmission line, without any junction or power divider, this approach is particularly simple to implement and provides a compact design. However, the transmission line sections between successive patches provide frequency dependent phase shifts, which cause the direction of the beam to depend on frequency. However, this feature is a major disadvantage in usual applications where the antenna beam should point toward a fixed direction at all operating frequencies.

The parallel feed, also called corporate feed, divides the input power into several channels, which individually feed each of the radiating elements. This arrangement provides an inherently wider bandwidth capability with a stable phase distribution.

5.1.2 T-junction

The T-junction is usually used as a power divider in the antenna array. A nonsymmetrical T-junction and its equivalent circuit are shown in Fig. 5.2. Possible reference planes are shown as dashed lines at the junction in the figure. The transformers represent the changes in impedance levels caused by the width changes, and the susceptance B_T represents energy stored in the junction due to parasitic elements [93]. The reference plane excitations, turns ratio, and shunt susceptance at the symmetric T-junction ($Z_{1a} = Z_{1b} = Z_1$, $d_{1a} = d_{1b} = d_1$) is defined by the closed-form expressions proposed in [123] or by the program MICTEE [93]

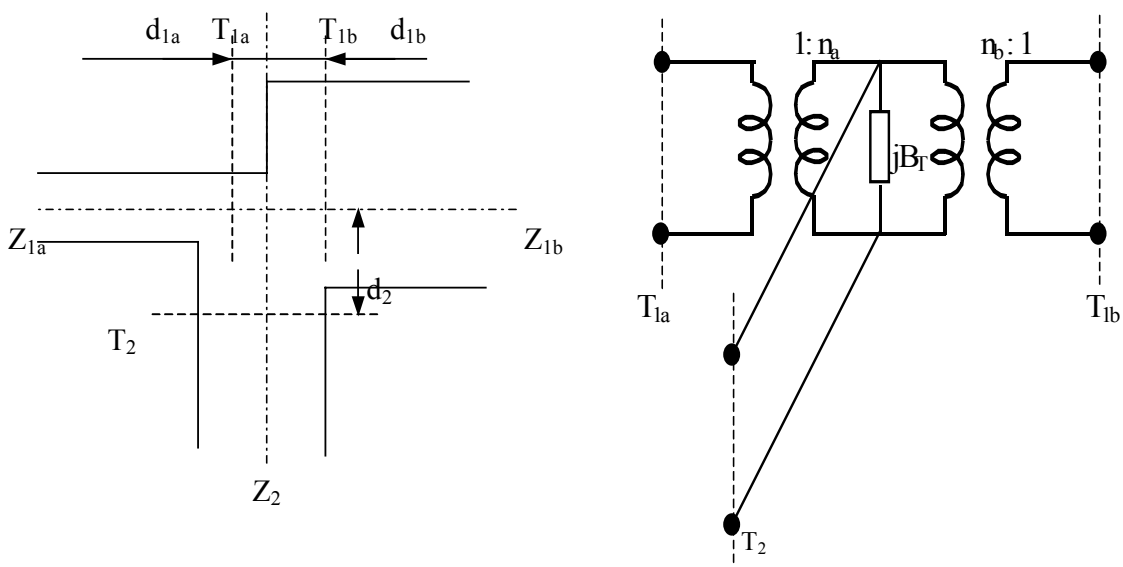

Figure 5.2 Microstrip T-junction and its Equivalent Circuit

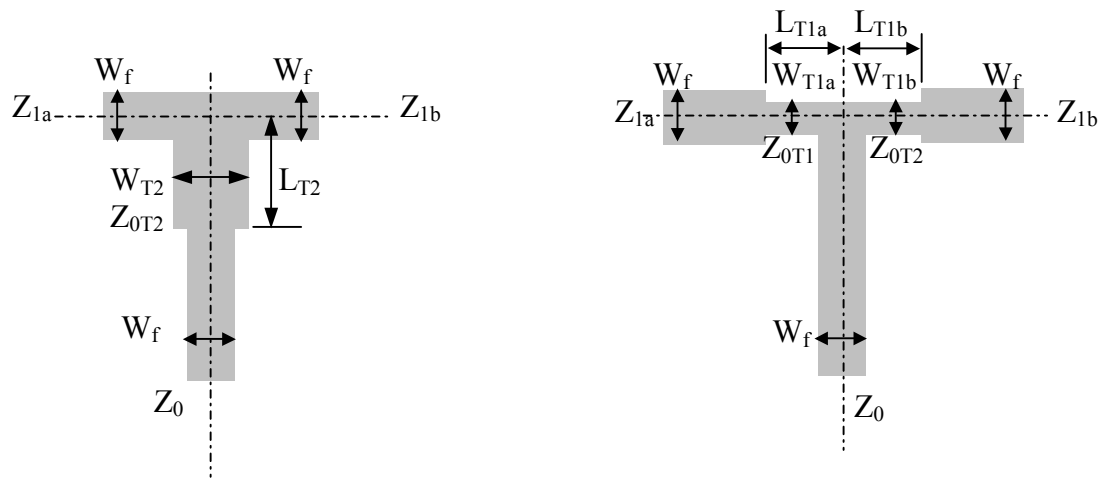

a. 35.355/(2x50) Ω b. 50/(2x70.711) Ω

Figure 5.3 Two Types Microstrip T-junctions Used as Dividers

$$\frac{d_1}{D_2} = 0.055\left[1 - 2\frac{Z_1}{Z_2}\left(\frac{f}{f_{p1}}\right)^2\right]\frac{Z_1}{Z_2} \tag{5.1}$$

$$D_2 = \frac{120\pi h_f}{Z_2\sqrt{\varepsilon_{rf2eff}(f)}} \tag{5.2}$$

$$f_{p1}[GHz] = 0.4Z_1/h_f[mm] \tag{5.3}$$

$$\frac{d_2}{D_1} = 0.5 - \left[0.05 + 0.7\exp\left(-1.6\frac{Z_1}{Z_2}\right) + 0.25\frac{Z_1}{Z_1}\left(\frac{f}{f_{p1}}\right)^2 - 0.17\ln\frac{Z_1}{Z_2}\right]\frac{Z_1}{Z_2} \tag{5.4}$$

$$D_1 = \frac{120\pi h_f}{Z_1\sqrt{\varepsilon_{rf1eff}(f)}} \tag{5.5}$$

$$n^2 = 1 - \pi\left(\frac{f}{f_{p1}}\right)^2\left[\frac{1}{12}\left(\frac{Z_1}{Z_2}\right)^2 + \left(0.5 - \frac{d_2}{D_1}\right)^2\right] \tag{5.6}$$

$$B_T = \frac{5.5}{Z_2}\frac{D_1}{\lambda_1}\frac{\varepsilon_{rf}+2}{\varepsilon_{rf}}\left[1+0.9\ln\frac{Z_1}{Z_2}+4.5\frac{Z_1}{Z_2}\left(\frac{f}{f_{p1}}\right)^2-4.4\exp\left(-1.3\frac{Z_1}{Z_2}\right)-20\left(\frac{Z_2}{120\pi}\right)^2\right]n^{-2}\frac{d_1}{D_2} \tag{5.7}$$

$$\lambda_1 = \frac{\lambda_0}{\sqrt{\varepsilon_{rf1eff}(f)}} \tag{5.8}$$

where Z_1 and Z_2 are the characteristic impedances of corresponding Microstrip feed lines.

5.1.3 Power Divider

The best result is obtained by the use of matched dividers (splitters) such as Wilkinson power divider. In this chapter, simple reactive power dividers are chosen. Because the divider outputs are not isolated, some care must be exercised when they are used. The feed line design must be as accurate as possible to minimize mismatch reflections that will disrupt the excitations. Two types of dividers based on microstrip T-junction are shown in Fig. 5.3. If $Z_{1a} = Z_{1b} = Z_0$, the corresponding characteristic impedances are

Table 5.1 Basic Characteristics of Two Types of Dividers

Input data						
f_0 (GHz)	Z_0 (Ω)	ε_{rf}	h_f (mm)	$\tan\delta_f$	t_f (μm)	Conductor
11.6	50	6.15	0.635	0.0019	17.5	copper
Output data						
Divider type	W_{1T} (mm)	W_{2T} (mm)	d_1 (mm)	d_2 (mm)	n	B_T mhos
35.355/(2x50)Ω	0.972	1.737	0.140	0.800	0.96	0.002653
50/(2x70.711)Ω	0.463	0.972	0.140	0.600	0.98	0.000894

$$Z_{0T2} = Z_0/\sqrt{2} \tag{5.7}$$

$$Z_{0T1} = Z_0\sqrt{2} \tag{5.8}$$

Using the programs MICRO and MICTEE [93], the basic characteristics of dividers are defined at frequency f =11.6 GHz and shown in Table 5.1.

According to the above results, the divider 50/(2x70.711)Ω shown in Fig. 5.3.b is chosen because of minimum value of its susceptance B_T.

5.1.4 Aperture Coupled Microstrip Antenna Linear Array with Surface Mounted Horn

The vehicular satellite communication and automotive radar applications require light-weighted and low cost antennas with possibility of conformal integration. The microstrip antenna is a good choice. However, they have typical gain of about 6-7 dBi only. Thus high gain array requires more number of elements. The typical millimeter-wave systems could accommodate more number of elements, however, physical size of the array may become unmanageable in the Ku and X-bands. This section introduces a new microstrip 4 elements linear array with surface mounted PVC horn, which achieves high gain with less number of elements. The inner surface of horn is painted with silver epoxy for metalization. The array has half power beamwidth 15° in the elevation and 32° in the azimuth. The automotive applications require a half power beamwidth less than 10°x20° [124] in the elevation and the azimuth planes respectively.

5.1.5 Fabrication and Experimental Results

As seen in the previous chapter, the gain of the single microstrip antenna element can be improved using the surface mounted PVC horn. It is also possible to use the surface mounted PVC horn to improve the gain of the array without affecting other parameters of the array . As we know, the losses associated with the feed network will increase by increasing the array elements. The measured gain of single element aperture coupled microstrip antenna is around 6 dB. If we use an array of four elements, the theoretical gain is 12dB. However, we got only 10.5 dB gain from our practical measurements. This means 1.5 db has been lost in the feed structure. We have used the surface mounted PVC horn to improve the gain of the linear array.

Four element aperture coupled linearly polarized microstrip array with quasi-planar surface mounted horn has been designed, fabricated and measured.

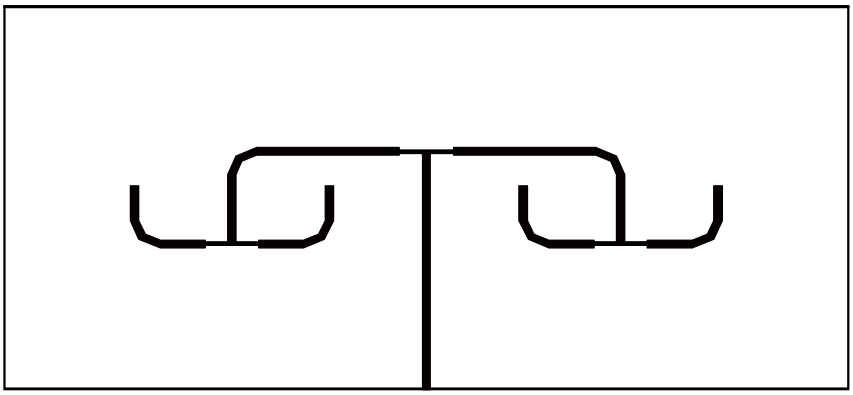

Figure 5.4.a Four element linear array feed circuit

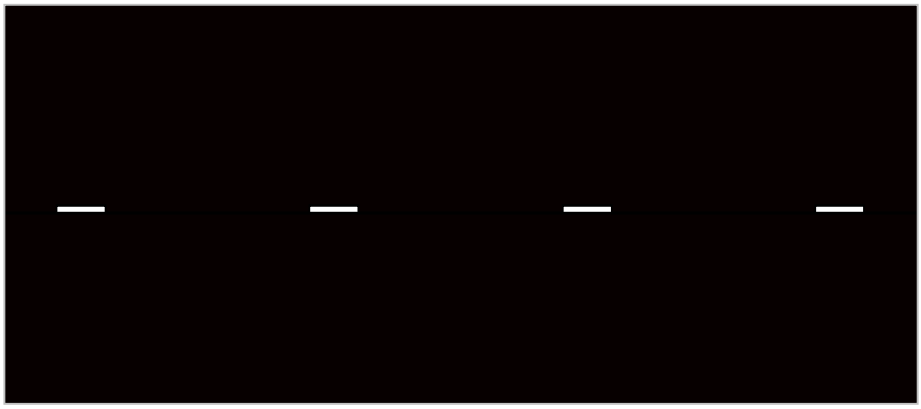

Figure 5.4.b Four element linear array ground plane

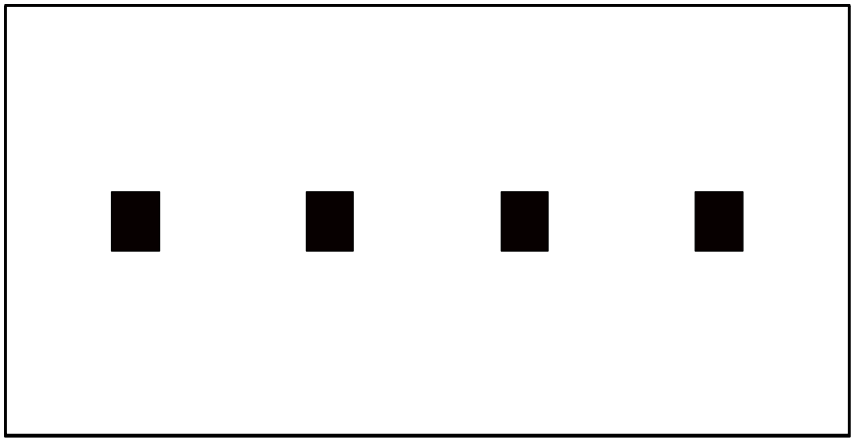

Figure 5.4.c Four element linear array patch radiators

The structure details of the array are given in Table 5.2. Fig. 5.4 shows the masks of the feed network, the slots in the ground plane, and the patches. Fig. 5.5 shows a picture of the fabricated 4-element aperture coupled microstrip antenna array with the horn. Fig. 5.6 and Fig. 5.7 show the measured E and H-planes radiation pattern respectively. 3.5 dB improvement of gain has been obtained due to the surface mounted horn frame.

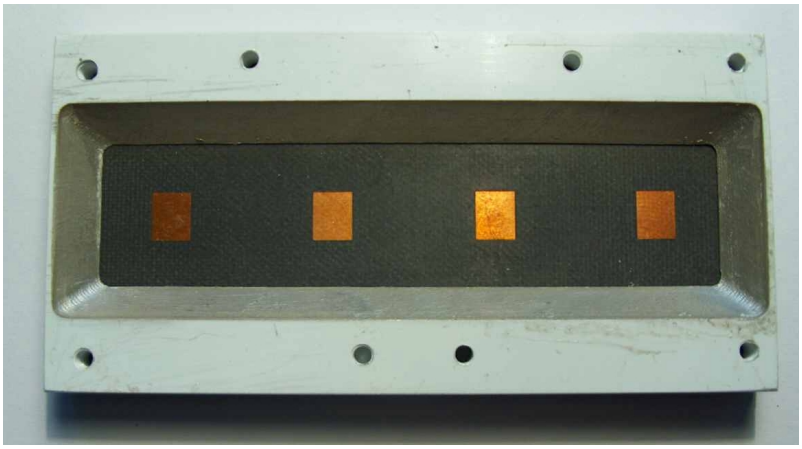

Figure 5.5 Photograph of Horn-4 Element Linear Array Structure

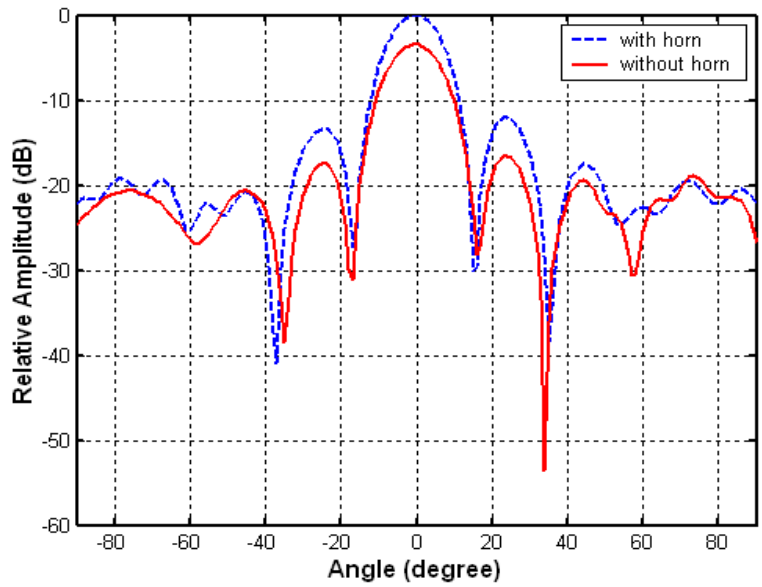

Figure 5.6 Measured E-plane radiation pattern of 4-Element linear array (—) and horn with 4-Element linear array (-----)

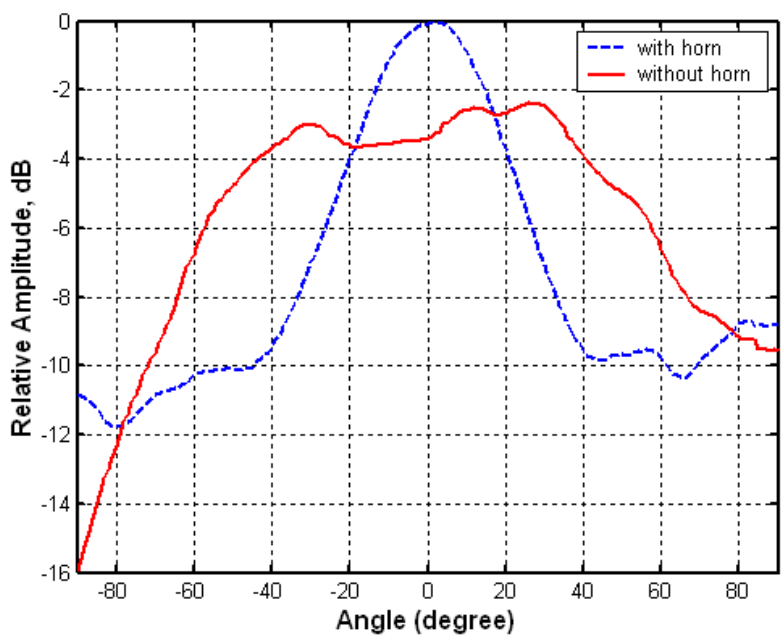

Figure 5.7 Measured H-plane radiation pattern of 4-Element linear array (—) and horn with 4-Element linear array (-----)

Table 5.2 Dimensions and Properties of the Designed Linearly Polarized Aperture Coupled 4-Element Linear Array

Array substrates	
Patch Substrate	RT/duroid 5880 $\varepsilon_r = 2.2$, $\tan\delta_2 = 0.0009$ h = 0.1575 mm t = 35 μm Rectangular substrate =5x10 cm^2
Feed Substrate	RT/duroid 6006 $\varepsilon_r = 6.15$, $\tan\delta_2 = 0.0019$ h = 0.635 mm t = 17.5 μm
Patch dimensions	Length, $2L_p$ = 6.91 mm, Width, $2W_p$ = 5.6 mm Thickness, t = 35 μm
Elements separation (S)	2.3 cm (0.88 λ_o)
Horn dimensions	
Bottom aperture	8.8 cm x 2 cm
Top aperture	9.8 cm x 3 cm
Height	0.5 cm

5.2 Gain Enhancement of Microstrip Antenna Array Using Surface Mounted Horn

This section introduces the possibility of application of the surface mounted horn to the 4 and 8 elements patch planar array for enhancement of the array gain. The height of the horn is a fraction the wavelength. For the 4 element square array we have measured 4 dB gain improvement for the 2×4 element array we have achieved 3.5 dB gain improvement. We have also observed about 9 dB improvement in the side lobe level due presence of the surface mounted horn. We present a systematic numerical experimentation on the 3D- EM simulator [109], to achieve high directivity for the patch array.

5.2.1 Numerical Experimentation

Fig. 5.8 shows the cross -section of the array of 4 element square patch antenna with surface mounted horn. The 4 element patch antenna array with corporate feed is designed on a square dielectric substrate of size, 6.0 cm x 6.0 cm x 0.081cm having dielectric constant ε_r =3.38. The square patch of size 0.66cmx0.66cm resonates at 11.45 GHz. A short horn of slant length, $L_s = \lambda_o/4$ = 0.65 cm is selected in this experimentation. λ_o is the wavelength at the resonance frequency. The dimensions of structure are shown in Table 5.3.

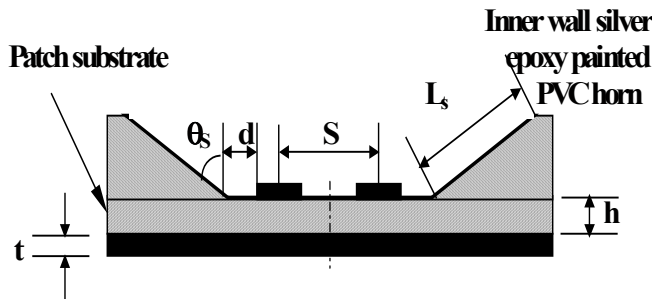

Figure 5.8 Horn-with 4 element array structure

Using the numerical experimentation conducted on MICROWAVE STUDIO^{TM}, we have attempted to optimize size of the $\lambda_o/4$ slant length horn frame for the 4 elements array to obtain the maximum gain. The numerical experimentation was carried out for the slant-angle (θ_S) =30°,45°,60° and horn position (d) =$\lambda_o/8$, $\lambda_o/4$,$3\lambda_o/8$ to determine separation (s) between the patch to achieve the optimum directivity. The results are shown in Fig.5.9.a – Fig. 5.9.c.

We can achieve maximum directivity16.2 dBi at patch separation (S) 0.8 λ_o for the slant – angle 45° when horn is placed at d=$3\lambda_0$ /8. Fig. 5.9.a – Fig. 5.9.c can be used as guide to design. During the experiment we noted that the array without horn gives very large side-lobe level for such separations. However, the horn improves the side level about 9 dB. In the present structure the array is primarily a feed to the horn aperture. The optimum separation between the patches creates an almost uniform electric field distribution in the

E-plane of the aperture and a tapered field distribution the H-plane of the aperture. This was confirmed during numerical experimentation as we obtained higher SLL in the E-plane and low SLL in the H-plane of the radiation pattern. This was further confirmed by the measurement. Similar study was also conducted for 2×4 array with short planar horn. However, to achieve 4 dB gain enhancement, we have to increase the slant length from $\lambda_o/4$ to $3\lambda_o/2$. The distance of the horn base from the edge of the patch (d) was maintained at $\lambda_o/4$ and separation between patches was taken as $0.85\lambda_o$.

Table 5.3 Dimension of the 4 and 8 Elements Array Structures

Array substrate	RO4003C $\varepsilon_r = 3.38$, $\tan\delta_2 = 0.0027$ h = 0.813 mm t = 35 μm Square substrate =6x6 cm^2
Patch dimensions	Length, $2L_p$ = 6.6 mm, Width, $2W_p$ = 6.6 mm Thickness, t = 35 μm
Horn with 4 elements	
Elements separation (S)	2.2 cm (0.85 λ_o)
Bottom aperture	4.2cmx4.2cm
Top aperture	5.1cmx5.1cm
Height	0.5 cm
Horn with 8 elements	
Elements separation (S)	2.2 cm (0.85 λ_o)
Bottom aperture	4.2cmx8.6cm
Top aperture	7cmx11.4cm
Height	1.4 cm

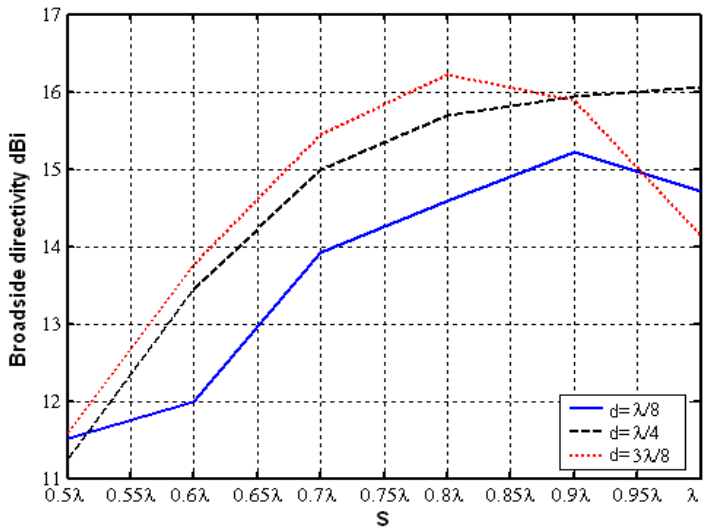

Figure 5.9.a Directivity at slant angle (θ_S=30°) for elements separation (S)

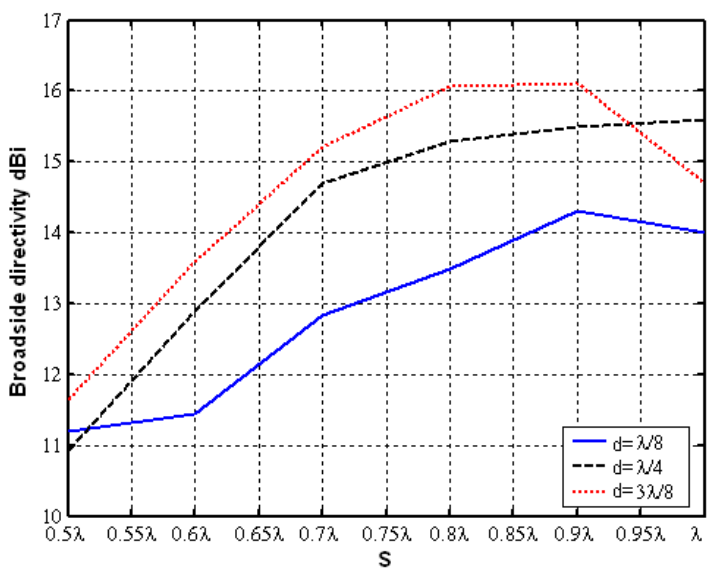

Figure 5.9.b Directivity at slant angle (θ_S=45°) for elements separation (S)

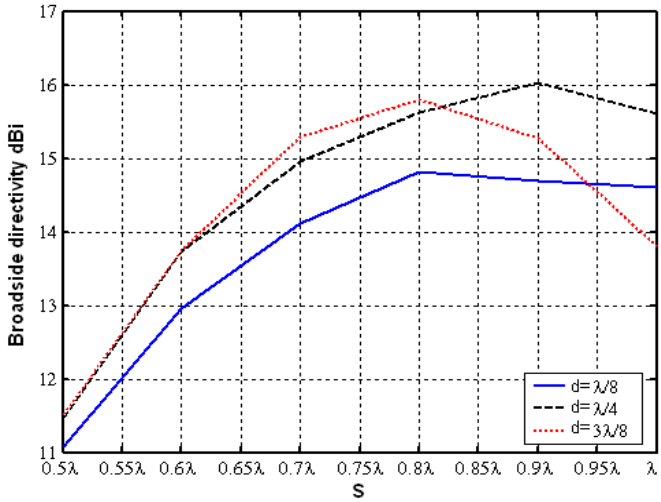

Figure 5.9.c Directivity at slant angle (θ_S=60°) for elements separation (S)

5.2.2 Fabrication and Experimental Results

The horn was fabricated from a thick sheet of PVC and painted with conductive silver epoxy paint. Fig. 5.10 shows photograph of the 4 elements. The return loss and radiation patterns are shown in Fig. 5.11 and Fig. 5.12 for the 4 elements. Fig. 5.13 shows photograph of the 8 elements. The return loss and radiation patterns are shown in Fig. 5.14 and Fig. 5.15 for the 8 elements. The horn also suppresses the side lobe by 9 dB. The horn does not degrade the return loss.

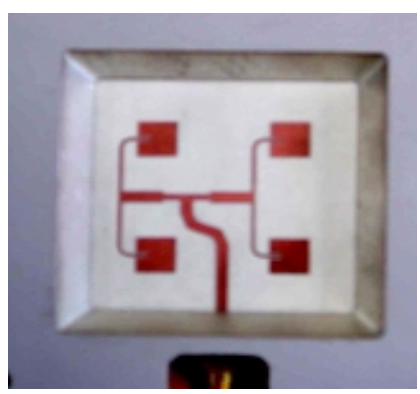

Figure 5.10 Photograph of horn-with 4 element array

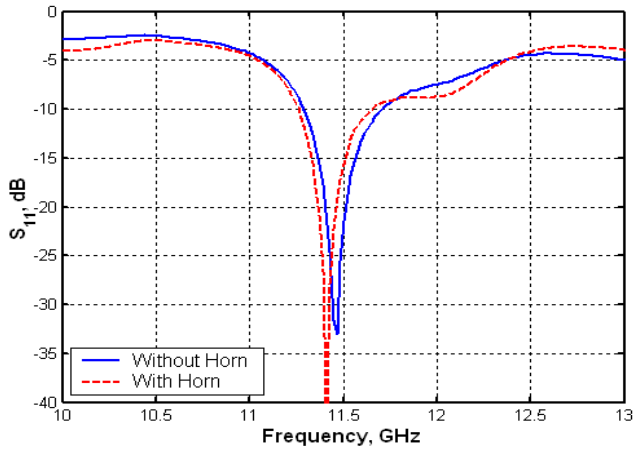

Figure 5.11 Return-loss for 4-elements array without horn (—) and with horn (-----)

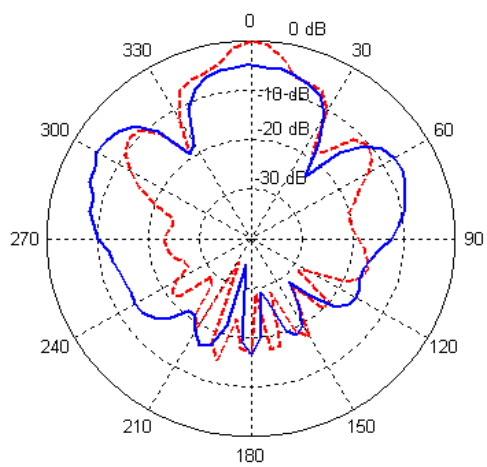

Figure 5.12.a E-plane radiation pattern of 4-element array without horn(—) and with horn (-----)

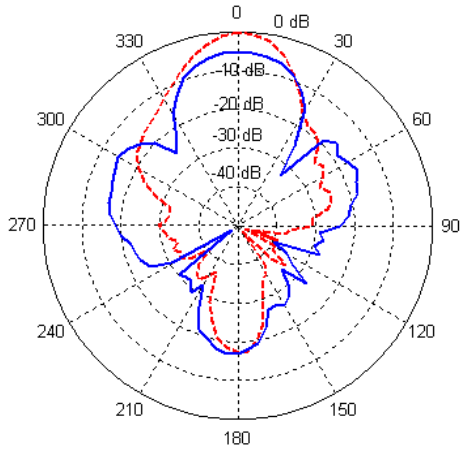

Figure 5.12.b H-plane radiation pattern of 4-element array without horn(—) and with horn (-----)

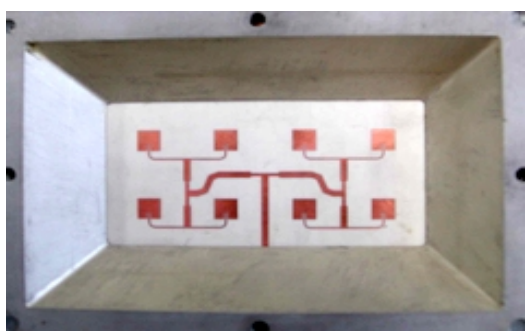

Figure 5.13 Photograph of horn-with 8 element array

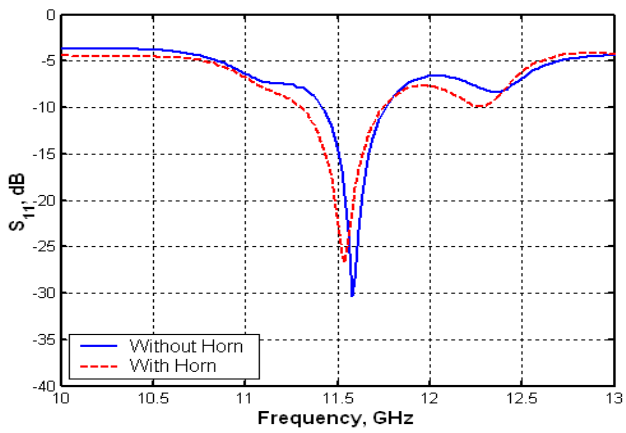

Figure 5.14 Return-loss for 8-elements array without horn (—) and with horn (-----)

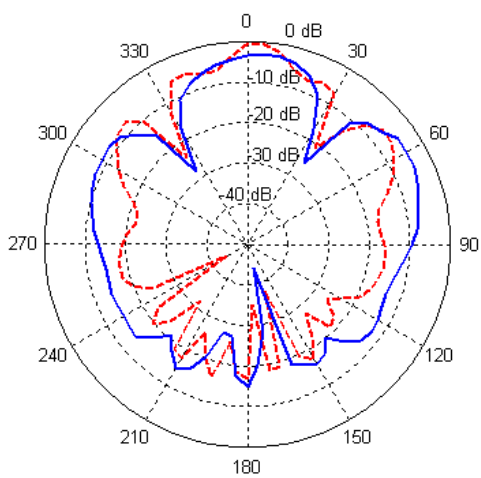

Figure 5.15.a E-plane radiation pattern of 8-element array without horn(—) and with horn (-----)

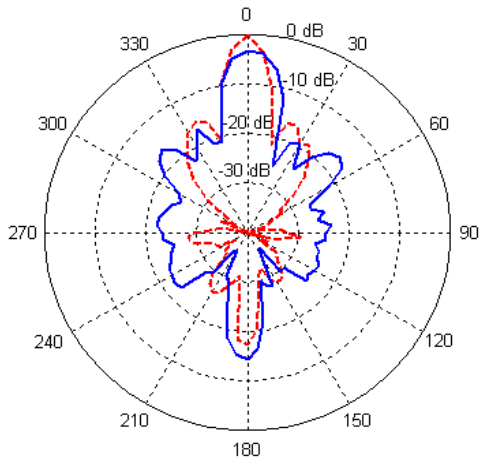

Figure 5.15.b H-plane radiation pattern of 8-element array without horn (—) and with horn (-----)

Thus the surface mounted can be effectively used to improve the gain of the array and its side –lobe level in meaningful way. This arrangement does not occupy much space and can be easily implemented for most of the communication systems

CHAPTER 6

Summary and Suggestions for Future Work

Two aspects of microwave communication technology have been covered in this thesis. The first aspect is the design of new wideband high gain microstrip antennas and the second is the design of compact high performance low pass and band pass filters.

6.1 Antennas

An antenna serves as the "transition" between the RF front-end circuitry and the radiation and propagation of electromagnetic waves in free space. Antennas play a critical role in microwave and other wireless applications systems. Planar oriented antenna, such as microstrip patch has attracted significant attention among antenna engineers due to the tremendous benefits they bring to modern wireless systems in comparison to more conventional designs.

We have introduced in this thesis the resonating coupling slot in the aperture coupled microstrip antenna to increase its bandwidth. By choosing the suitable substrates relative permittivity and thickness, a bandwidth of 12.4 % has been obtained from a simple, low profile, and light weight aperture coupled Microstrip antenna. This bandwidth is the maximum that one can get from the non multilayer structures.

A simple and efficient technique for an impedance matching improvement of a class of wideband antennas has been introduced. These antennas have an impedance characteristic which exhibits dual (or multiple) resonance.

For many applications such as satellite communications and mobile radio, for which printed antennas are otherwise well suited, low gain may be a serious disadvantage. The electromagnetically coupled stacked patch antenna has been investigated to improve the gain and bandwidth of the microstrip antenna. An experimental study of a two layer

electromagnetically coupled rectangular patch antenna excited in the TM_{01} mode has been reported. More efforts have been made to increase both the gain and bandwidth with the help of stacked parasitic patch. However, this structure can be optimised either for the gain or for the bandwidth. Likewise, the cavity backed microstrip antenna with multiple layers of dielectric can improve the gain, however the bandwidth is very limited. There is need to increase the gain of radiating patch element without sacrificing the bandwidth.

We have introduced in this thesis a new combination of the aperture coupled microstrip antenna and a quasi-planner surface mounted short horn to increase the gain of the patch antenna by 4.5 dB. Horn has no significant effect on the resonance frequency, bandwidth and return loss. The combined structure has 12.4 % bandwidth. The presence of the quasi-planner horn has improved the back-lobe level by 5.4 dB.

At certain substrate thickness, the surface mounted horn can not improve the gain much more. By increasing the substrate thickness, the surface mounted horn is not able to trap the total power. Some of the power leaks through the substrate as a surface waves. To trap and guide this leaked power to the broadside direction.

By inserting the horn into the substrate, the gain of the patch antenna has been increased by more than 6 dB.

The vehicular satellite communication and automotive radar applications require lightweight, compact, and low cost antennas with possibility of conformal integration. As we know, the microstrip antenna is a good choice. However, they have typical gain of a bout 6dB only. Thus high gain array requires more number of elements. The losses associated with the feed network will increase by increasing the array elements. The measured gain of single element aperture coupled microstrip antenna is around 6 dB. In case of four element, the theoretical gain will be 6 dB + 6 dB = 12 dB. The measured gain of the four elements is only 10.5 dB. I.e. 1.5 dB has been lost.

The surface mounted horn has been applied around the four and eight element arrays. 3.5 dB more gain has been obtained with the horn frame around the array elements

6.2 Filters

Filters play important roles in many RF/microwave applications. They are used to separate or combine different frequencies. The electromagnetic spectrum is limited and has to be shared; filters are used to select or confine the RF/microwave signals within assigned

spectral limits. Emerging applications such as wireless communications continue to challenge RF/microwave filters with ever more stringent requirements higher performance, smaller size, lighter weight, and lower cost. Depending on the requirements and specifications, RF/microwave filters may be designed as lumped element or distributed element circuits; they may be realized in various transmission line structures, such as waveguide, coaxial line, and microstrip.

We have introduced in this thesis the limitations of classical microstrip line based low pass and band pass filters and way to improve the design and response by using the defected ground plane structures. New investigations are presented on the choice of geometrical shapes for the DGS structure as an element for the LPF. We have also introduced the band accept (band pass) structure in DGS and used it for the development of a new compact BPF. This band pass filter is based on creation of a series-resonance in the main 50Ω microstrip line and creation of attenuation pole in the shunt arm.

6.3 Suggestions for future work

Based on observations gathered while completing this thesis, topics were identified which would benefit for further investigation.

1. It was found that the geometrical shapes of the DGS slot like rectangular, dumb-bell, square head slot and arrow head slot has an influence on the sharpness of the transition and stop band rejection. It will be an interesting to investigate the effect of these four slots (apertures) on the following aperture coupled microstrip antenna characteristics:

- The impedance bandwidth
- The cross-polarization levels in both E and H planes
- The front-to-back ratio of the antenna
- The antenna gain

2. We introduced the surface mounted short PVC horn with the linearly polarized aperture coupled microstrip antenna to improve the gain by 4.5 dB without degrading the bandwidth and the return loss. A dual-polarized aperture coupled microstrip antenna with the surface mounted PVC horn can be used to increase the gain. A new antenna concept for Direct to home (DTH) reception contains a parabolic reflector and a low noise block converter. The parabolic reflector can be fed using the high gain wide bandwidth dual-

polarized aperture coupled microstrip antenna with surface mounted PVC horn to increase the antenna efficiency.

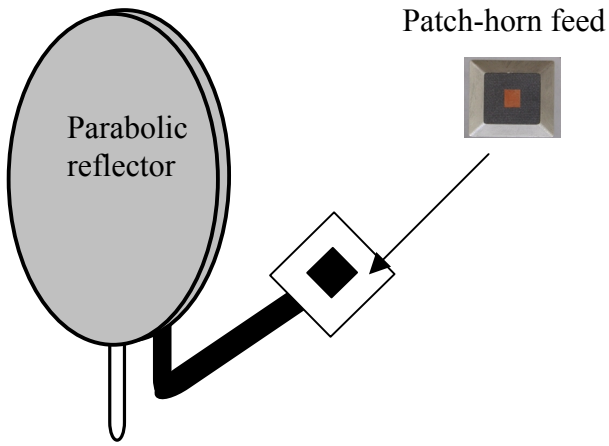

Figure 6.1 Proposed broadband aperture coupled and dual polarized microstrip antenna for DTH reception

3. We introduced the surface mounted short PVC horn with the linearly polarized aperture coupled microstrip antenna to improve the gain by 4.5 dB without degrading the bandwidth and the return loss. In many instances a circularly polarized antenna is desirable. For example, it may be difficult to know beforehand the required orientation of the antenna when linear polarization is used. As a future work, the surface mounted PVC horn can be used with the circularly polarized aperture coupled microstrip antenna to improve the gain without degrading the bandwidth and the return loss.

4. As found in chapter 5, the side lobes have been used to feed the horn aperture with the array. As it is well known, the grating lobes will appear by increasing the separation between the array elements more than λ_0. An interesting future work is to investigate the possibility of feeding the surface mounted PVC horn with an array having grating lobes.

5. The stringent requirements of modern microwave communication systems are often met only by high performance and compact filtering structures. Several compact and high performance filters have been presented in chapter 3 using generic structures called the

defected ground structures (DGS). Since DGS cells have inherently resonant properties, many of them have been used in filtering circuits to improve the stop and pass band characteristics. The DGS have been proposed for improving the spurious response of microstrip low pass filters and coupled microstrip line band pass filters. The DGS are not viewed as the central building blocks, they are rather used to enhance the response of already designed devices such as filters and couplers.

As a promising future work, we propose an alternative approach in which the DGS themselves are considered the building blocks of the device. new compact DGS resonators and ways to implement intra-resonator and external coupling can be achieved. Different coupling configurations can be considered.

These new resonators can be used to

- design bandpass filters with Chebyshev or pseudo-elliptic responses by applying the general theory of coupling to the DGS resonators,
- design higher order filters using DGS resonators,
- design dual-mode filters using DGS resonators,
- design parallelized filters by using both sides of the substrate at the same time,
- combine the patch antenna with the DGS resonator to improve its bandwidth.

Zusammenfassung

Diese Arbeit umfasst zwei wesentliche Aspekte der Mikrowellen-Kommunikationstechnik, das Design von breitbandigen Mikrostreifenantennen mit hohem Gewinn und die Entwicklung von kompakten, hochleistungsfähigen Tiefpass- und Bandpassfiltern.

Antennen

Eine Antenne dient als "Übergang" zwischen dem RF-Endgerät und der Strahlung und Ausbreitung der elektromagnetischen Wellen im Freiraum. Die Antenne spielt eine entscheidende Rolle in Mikrowellensystemen und in anderen drahtlosen Anwendungen. Planare Antennen, wie die Mikrostreifen-Patch-Antenne haben wegen des enormen Nutzengewinns, den sie im Vergleich zu herkömmlicheren Strukturen in modernen drahtlosen Systemen ermöglichen, unter Antenneningenieuren viel Aufmerksamkeit erregt. In dieser Arbeit wird ein mitschwingender Koppelungsschlitz in der mit der Mikrobandleiterantenne verbundenen Blendenöffnung eingeführt, um so die Bandbreite zu erhöhen. Das Konzept des angebrachten kurzen Oberflächenhorns wird verwendet, um den Gewinn zu erhöhen, ohne die Bandbreite nachteilig zu beeinflussen. Indem man die Stärke und relative Permittivität des verwendeten Substrates wählt, ist eine Bandbreite von 12.4 % bei Verwendung einer einfachen Blendenöffnung vor der Mikrobandleiterantenne realisiert worden. Diese Bandbreite ist das Maximum, das man mit Hilfe der nicht mehrschichtigen Strukturen erhalten kann.

Mobile Satellitenverbindungen und Automobilradaranwendungen erfordern leichte, kompakte Antennen, die zu niedrigen Kosten produziert werden können und mit der Möglichkeit einer konformen Integration ausgestattet sind. Wie wir wissen, ist die Mikrobandleiterantenne dafür eine gute Wahl. Jedoch hat sie typischerweise einen Gewinn von nur 6 dB. Der gemessene Gewinn bei Verwendung von vier Elemente beträgt 10.5 dB. Wir haben das Oberflächenhorn angebracht und somit für die Strukturen mit vier bzw. acht Elementen den Gewinn um 3.5 dB verbessert.

Filter

Anwendungen wie drahtlose Kommunikationen erfordern RF/Microwave Filter mit immer höherer Leistung, kleinerer Größe, geringerem Gewicht und niedrigeren Produktionskosten. Abhängig von den Anforderungen und Spezifikationen können RF/Microwave Filter wie konzentrierte Elemente oder wie verteilten Elementstromkreise entworfen werden. Dabei können verschiedene Leitungsstrukturen, wie Wellenleiter, Koaxialleiter oder Mikrostreifenleiter verwendet werden. Wir haben in dieser Arbeit die

Auswahl auf Tiefpass- und Bandpassfilter in klassischer Mikrostreifenleiterarchitektur beschränkt, deren Design und Verhalten durch die Verwendung von defected Grundsubstratstrukturen verbessern werden soll. Für die Wahl der geometrischen Formen für die DGS-Struktur als Element für den LPF werden neue Untersuchungsergebnisse vorgestellt. Wir haben auch Bandpassstrukturen in die DGS Umgebung eingeführt und diese für die Entwicklung eines neuen Bandpassfilters genutzt. Dieser Bandpassfilter basiert auf einer Reihen-Resonanz in der 50-Ohm Mikrostreifenleitung und auf der Existenz von Dämpfungspolen im Shuntarm.

Gliederung dieser Arbeit

Kapitel 1 dient als Einleitung und beschreibt die mit der Mikrostreifenantenne und den Mikrostreifenfiltern verbundenen Probleme. Es gibt eine allgemeine Übersicht über die vorhergehende Arbeiten und neue Methoden die dargestellten Probleme zu überwinden.

Kapitel 2 gibt einen Überblick über die Speisestruktur einer Mikrostreifenantenne und eine Zusammenfassung der Design-Gleichungen. Eine breitbandige, aperturgekoppelte Mikrostreifenantenne wird im Ku-Band entworfen, simuliert und gemessen. Wir erzielten eine große Bandbreite durch einen mitschwingenden Schlitz in der gemeinsamen Grundfläche. Eine neue Methode zur Anpassung der Antenne Struktur an die 50-Ohm Mikrostreifen-Speisestruktur wird vorgestellt. Das Design wird durch systematische Anwendung des 3D EM-Simulators Microwave Studio erzielt.

Kapitels 3 erläutert die grundlegenden Beschränkungen der klassischen, auf Mikrostreifenstrukturen begründeten Tiefpass- und Bandpassfilter und stellt Methoden vor, die das Design verbessern, indem sie die defected Grundsubstratstrukturen verwenden. Neue Untersuchungen bezüglich der Wahl der geometrischen Formen für die DGS-Struktur als Element für das LPF werden vorgestellt.

Kapitel 4 führt das an der Oberfläche der Mikrostreifenantenne angebrachte, breitbandig aperturgekoppelte kurze Horn ein, durch das der Gewinn um 4.5 dB verbessert wird, ohne die Bandbreite und die Rückflussdämpfung zu vermindern. Es stellt auch das eingefügte Horn dar, das den Gewinn im Fall dicker Substrate um 5.5 dB verbessert.

Kapitel 5 stellt als Erweiterung eine Anwendung des angebrachten Oberflächenhorns für eine lineare Reihe von 4X1 Elementen und eine planare Reihe von 2X2 Elementen bzw. 4X2 Elementen vor, durch die der Gewinn der Struktur um 3.5 dB verbessert wird.

In Kapitel 6, werden eine Zusammenfassung und Vorschläge für die zukünftige Arbeit präsentiert.

Bibliography

[1] R. Garg, P. Bhartia, I. Bahl, and A. Ittipibon, Microstrip Antenna Design Handbook, Artech House, Boston. London, 2001.

[2] D. M. Pozar, " A review of bandwidth enhancement techniques for Microstrip antennas, In microstrip antennas," *IEEE Press*, New York, 1995.

[3] D. H. Schaubert and F. G. Farrar, "Some conformal printed circuit antenna design," *Proc. Workshop Printed Antenna Technology*, New Mexico Stat University, Las Cruces, NM, Oct. 1979, pp. 5/1-5/21.

[4] G. Kumar and K. C. Gupta, "Directly coupled multiple resonator wide-band Microstrip antennas," *IEEE Trans. On Antennas and Propagation*, vol. 33, No. 6, pp. 588-593,1985.

[5] C. H. Tsao, Y. M. Hwang, F. Kilburg and F. Dietrich, "Aperture-coupled patch antennas with widebandwidth and dual polarization capabilities," *IEEE Antennas and Propagation Symp. Digest*, 1988, pp. 936-939.

[6] A. Ittipiboon, B. Clarke and M. Cuhaci, "Slot-coupled stacked Microstrip antennas," *IEEE Antennas and Propagation Symp. Digest*, 1990, pp. 1108-1111.

[7] F. Croq and D. M. Pozar, "Millimeter-wave design of wide-band aperture-coupled stacked Microstrip antennas," *IEEE Trans. On Antennas and Propagation*, 1991, vol. 39, No. 12, pp. 1770-1776.

[8] S. D. Targonski, R. B. Waterhouse and D. M. Pozar, "Millimeter-wave design of wideband aperture-coupled stacked Microstrip antennas," *IEEE Trans. On Antennas and Propagation*, 1998, vol. 46, No. 9, pp. 1245-1251.

[9] D. Heberling et al., "Simple feeding technology for stacked Microstrip antennas," *in Proceedings 19 th European Microwave Conference, London,* UK, September 1989, pp. 155-160.

[10] R. T. Cock and C. G. Christodoulu, "Design of a two-layer capacitively coupled microstrip patch antenna element for broadband applications," *IEEE, AP(S)* 1987, pp. 936-939.

[11] F. Croq, "Stacked resonators for bandwidth enhancement: A comparison of two feeding techniques," *IEE Proceedings*, Part H, vol. 140, No. 4, 1993, pp. 303-309.

[12] J. P. Damiano et al. "Study of multiplayer Microstrip antennas with radiating elements of various geometry," *IEEE Proceedings*, Part H, vol. 137, No. 3, 1990, pp. 163-170.

[13] S. Yano and A. Ishimaru, "Broadbanding of Microstrip antennas by orthogonal polarizations," *IEEE Antennas and Propagation Symp. Digest*, 1981, pp. 363-365.

[14] Y. L. Chow, Z. N. Chen, K. F. Lee, and K. M. Luk, "A design theory on broadband patch antennas with slot," *IEEE, AP(S),* 1998, pp. 1124-1127.

[15] T. Huynh and K. F. Lee, "Single-layer single patch wideband Microstrip antenna," *Electron. Lett.*, vol. 31, 1995, pp. 1310-1312.

[16] K. F. Lee, K. M. Luk, K. F. Tong, S. M. Shum, T. Huynh, and R. Q. Lee, "Experimental and simulation studies of coaxially fed U-slot rectangular patch antenna," *Inst. Elect. Eng. Proc. Microwave Antennas Propagat.*, 144, 1997, pp. 354-358.

[17] R. Bahalla and L. Shafai, "Resonance behavior of single U-slot Microstrip patch antenna," *Microwave Opt. Technol. Lett.*, vol. 32, No. 5, 2002, pp. 333-335.

[18] G. Dubost, Flat radiating dipoles and applications to arrays, Research studies press, New York, 1981.

[19] H. F. Pues and A. R. Van de Capelle, "An impedance matching technique for increasing the bandwidth for microstrip antennas," *IEEE Transactions on Antennas and Propagation*, vol. 37, No. 11, 1989, pp. 1345-1354.

[20] D. A. Paschen, "Practical examples of integral broadband matching of Microstrip antenna elements," *Proc. Antenna Applications Symp.*, 1986, pp. 199-217.

[21] N. Herscovici, "A wideband single layer patch antenna," *IEEE Transactions on Antennas and Propagation*, 1998, vol. 46, No. 4, pp. 471-474.

[22] K. L. Wong and Y. F. Lin, "Microstrip line fed compact Microstrip antenna with broadband operation," *IEEE Antennas and Propagation Symp. Digest*, 1998, pp. 1120-1123.

[23] K. R. Carver and J. W. Mink, "Microstrip antenna technology," *IEEE Trans. On Antennas and Propagation*, vol. Ap-29, pp. 2-24, Jan. 1981.

[24] D. M. Pozar, "Microstrip antenna aperture coupled to a microstrip line," *Electron. Lett.*, vol. 21, pp. 49-50, Jan. 1985.

[25] J-F. Zürcher, F. Gardiol, "Broadband Patch Antennas," Artech House, 1995.

[26] F. Croq and A. Papiernik, "Large Bandwidth Aperture-Coupled Microstrip Antenna," *Electronics Letters*, 26, August 1990, pp. 1293-1294.

[27] G. S. Kirov, A. Abdel-Rahman and A. S. Omar, "Wideband Aperture Coupled Microstrip Antenna," *IEEE, AP-S, 2003,* vol. 2.

[28] R. Q. Lee, K. F. Lee and J. Bobinchack, " Characteristics of a two layer electromagnetically coupled rectangular microstrip antenna," *Electron. Lett.,* vol.23, no. 20, pp.1017-1072,Sept.1987.

[29] N. Alexopoulos and D. Jackson, "Fundamental superstrate (cover) effect on printed Circuit Antennas," *IEEE Transactions on Antennas and Propagation*, vol. Ap-32, pp. 807-816, Aug. 1984.

[30] Y. Sugio, T. Makimoto, S. Nishimura, and H. Nakanishi, "Analysis for gain enhancement of multiple-relection line antenna with with dielectric plates," *IEEE Trans. IECE,* pp. 80-112, Jan. 1981.

[31] D. Jackson and N. Alexopoulos,"Gain Enhancement Methods for Printed Circuit Antennas," *IEEE Transactions on Antennas and Propagation*, vol. AP-33, no. 9, pp. 976-987, Sep. 1985.

[32] H. Yang and N. Alexopoulos, "Gain Enhancement Methods for Printed Circuit Antennas Through Multiple Superstrates," *IEEE Transactions on Antennas and Propagation*, vol. AP-35, no. 7, pp. 860-863, July1987.

[33] D. Jackson and A. Oliner, "A Leaky–wave Analysis of the High Gain Printed Antenna Configuration," *IEEE Transactions on Antennas and Propagation*, vol. AP-36, no. 7, pp. 905-909, July 1988.

[34] F. Zavosh and James T. Aberle, " Design of high gain microstrip antenna," *Microwave Journal,* vol. 42, No. 9, pp. 138-148, Sept. 1999.

[35] A. Abdel-Rahman, A. K. Verma, G. S. Kirov and A. S. Omar, "Aperture Coupled Microstrip Antenna With Quasi-Planner Surface Mounted Horn," *in Proceedings 33 th European Microwave Conference, Munich*, Oct. 2003. pp. 1377-1380.

[36] A. Abdel-Rahman, A. K. Verma and A. S. Omar, "Gain Enhancement of Microstrip Antenna Array Using Surface Mounted Horn," *in Proceedings 34 th European Microwave Conference, Amsterdam*, Oct. 2003. pp. 1377-1380.

[37] D. Ahn et al, "A Design of the Low-pass Filter using the Novel Microstrip Defected Ground Structure," *IEEE Trans. Microwave Theory Tech.*, vol. 49, No. 1, Jan. 2001, pp. 86-91.

[38] F.R. Yang, Y. Qian and T. Itoh, "A novel uniplanar compact PBG structures for filter and mixer applications," *IEEE Microwave Theory Tech. Symposium, MTT (S)-1999,* pp. *919-922.*

[39] J.S. Lim, C.S. Kim, Y.K. Lee, D. Ahn and S. Nam, "A spiral-shaped defected ground plane structure for coplanar Waveguide," *IEEE Microwave Wireless component Lett.,* vol.12, no. 9, pp. 330-312, Sept. 2002.

[40] W. Schwab, F. Boegelsack, and W. Menzel " Multilayer suspended stripline and coplanar line filters," *IEEE Trans. Microwave Theory Tech.*, vol. 42, pp. 1404-1407, July 1993.

[41] C. Quendo, E. Rius, C. Person, and M. Ney, " Integration of optimized low-pass filters in a bandpass filter for out-of-band improvement," *IEEE Trans. Microwave Theory Tech.*, vol. 49, pp. 2376-2383, Dec. 2001.

[42] T. Kim and C. Seo, " A Novel Photonic Bandgap Structure for Low-pass Filter of Wide Stopband," *IEEE Microwave and Guided Wave Letters*, vol. 10, No. 1, Jan. 2000, pp. 13-15.

[43] C. Kim, et al, "A Novel 1-D Periodic Defected Ground Structure for Plane on Circuits," *IEEE Trans. Microwave and Guided Wave Letters*, vol. 10, No. 4, Apr. 200, pp. 131-133.

[44] M. A. G. Laso. T. Lopetegi, M. J. Erro. D. Benito, M. J. Garde, and M. Sorolla, " Multiple-frequency-tuned photonic bandgap microstrip structures," *IEEE Microwave Guided Wave Lett.*, vol. 10, pp. 220-222, June 2000.

[45] D. Sievenpiper, L. Zhang, R. F. J. Broas, N. G. Alexopoulos, and E. Yablonovitch, "High-impedance electromagnetic surface with a forbidden frequency band," *IEEE Trans.,* MTT-47, Nov. 1999, pp. 2059-2074.

[46] V. Radisic, Y. Qian, R. Coccioli and T. Itoh, " Novel 2-D Photonic Bandgap Structure for Microstrip Lines," *IEEE Microwave and Guided Wave Letters*, vol. 8, No. 2, Feb. 1998, pp. 69-71.

[47] T. J. Ellis and G. M. Rebeiz, "MM-wave tapered slot antennas on micromachined photonic bandgap dielectrics," *IEEE MTT-S Int. Microwave Symp. Dig.*, June 1996, pp. 1157-1160.

[48] V. Radisic, Y. Qian, and T. Itoh, "Broadband Power Amplifier using Dielectric Photonic Bandgap Structure," *IEEE Microwave Guide Wave Lett.*, vol. 8, pp. 13-14, Jan. 1998.

[49] M. P. Kesler, J. G. Maloney, and B. L. Shirley, "Antenna design with the use of photonic bandgap material as all dielectric planar reflectors," *Microwave Opt. Technol. Lett.*, vol. 11, no. 4, pp. 169-174, Mar. 1996.

[50] Y. Qian and T. Itoh, "Planar Peroidic Structures for microwave and millimeter wave circuit applications," *IEEE MTT-S Int. Microwave Symp. Dig.*, June 1999, pp. 1533-1536.

[51] K.-P. Ma, J. Kim, F.-R. Yang, Y. Qian, and T. Itoh, "Leakage suppression in stripline circuits using a 2-D photonic bandgap lattice," *IEEE Microwave Theory Tech. Symposium,* MTT (S)-1999, pp. 73-76.

[52] T. Yun and K. Chang, "One-Dimensional Photonic Bandgap Resonators and Varactor Tuned Resonators," *IEEE MTT-S Int. Microwave Symp. Dig.*, June 1999, pp. 1629-1632.

[53] T. Y. Yn and K. Chang, "An electrically tunable photonic bandgap resonator controlled by piezoelectric transducer," *IEEE Microwave Theory Tech. Symposium, IEEE MTT-S Int. Microwave Symp. Dig.*, June *2000,* pp. 1445-1447.

[54] W. J. Chappell, M. P. Little, and L. P. B. Katehi, " High Q two dimensional defect resonators – Measured and Simulated," *IEEE Microwave Theory Tech. Symposium,* MTT (S)-2000*,* pp. 1437-1440.

[55] E. Yablonovitch, " Photonic bandgap Atructures," *J. Opt. Soc. Amer. B, Opt. Phys.*, vol. 10, pp. 283-295, Feb. 1993.

[56] Y. Qian, F. R. Yang, and T. Itoh, "Characteristics of Microstrip lines on a uniplanar compact PBG ground plane," *Asia-Pacific Microwave Conf. Dig.*, Dec. 1998, pp. 589-592.

[57] Y. Qian, V. Radisic, and T. Itoh, " Simulation and Experiment of Photonic Bandgap Structures for Microstrip Circuits," *in Proc. AMPC'97*, pp. 585-588.

[58] R. Qiang, Wang and D. Chen, " Anovel Microstrip Bandpass Filter with Two Cascaded PBG Structures," *IEEE AP-S Digest*, 2001, pp. 510-513.

[59] J. P. Kim and W. S. Park, " Microstrip lowpass Filter with Multislots on Ground Plane," *Electronic Letters*, vol. 37, No. 25, 6 Dec. 2001.

[60] J. Yun, et al, " A design of the Novel Coupled Line Bandpass Filter Using Defected Ground Structure," *IEEE MTT-S Digest*, 2000, pp. 327-330.

[61] M. Kahrizi, T. Sarkar and Z. Maricevic, " Dynamic Analysis of a Microstrip line Over a Perforated Ground Plane," *IEEE Trans. Microwave Theory Tech.*, vol. 42, No. 5, May 1994, pp. 820-825.

[62] X. Yi, P. Yeh and J. Hong, "Photonic Bandgap Structure in Thin Film Waveguides," *SBMO/IEEE MTT-S IMOC 99 Proceedings*, pp. 451-453.

[63] S. Jeong, et al, " Amplifier Design USING λ/4 High Impedance Bias Line with Defected Ground Structure (DGS) ," *IEEE MTT-S Digest*, 2002, pp. 1161-1163.

[64] F. Yang, K. Ma, Y. Qian, and T. Itoh, " A Uniplanar Compact Photonic-Bandgap (UC-PBG) Structure and Its Applications for Microwave Circuits," *IEEE Trans. Microwave Theory Tech.*, vol. 47, No. 8, Aug. 1999, pp. 1509-1513.

[65] D. M. Pozar, Microwave Engineering, 2nd ed., John-Wiley & Sons, 1998, pp. 422-496.

[66] A. Abdel-Rahman, A. K. Verma, A. Boutejdar and A. S. Omar, "Control of Band Stop Response of Hi-Low Microstrip Lowpass Filter Using Slot in Ground

Plane," *IEEE Trans. Microwave Theory Tech*., vol. 52, No. 3, pp. 1008-1013, Mar. 2004.

[67] A. Abdel-Rahman, A. Boutejdar, A. K. Verma, G. Nadim and A. S. Omar, "Improved Circuit Model for DGS based Lowpass Filte," *AP-S 2004*, pp. 998-1001.

[68] G. L. Matthaei, L. Young, and E. M. T. Jones, Microwave Filters, Impedance Matching Networks and Coupling Structures. Norwood, MA: Artech House, 1980, pp. 217-228.

[69] G. J., Cunningham, P. A. Blenkinsope, and J. H. Palmer, "Microstrip end-coupled filter design at MM-Wave frequencies," Procedings of the 19th *European Microwave Conference, London*, Sept. 1989, pp. 1210-1213.

[70] C-Kc. Tzuang et al., "Design of a quasi-planar broadside end-coupled bandpass filter," *IEEE Microwave Theory Tech. Symposium, MTT (S)-1990, Digest of papers,* pp. *407-410.*

[71] I. J. Bahl, "Broadbanding Microstrip Filters Using Capacitive Compensation," *Applied Microwave,* 1989.

[72] G. Kompa, and R. Mehran, "Microstrip Filter Analysis using a Microstrip waveguide model," Radio and Electronic Engineer, 50, No. ½, January/February 1980, 54-58.

[73] C. Y. Chang and T. Itoh, "A modified parallel-coupled filter structure that improves the upper stopband rejection and response symmetry," *IEEE Trans. Microwave Theory Tech.*, MTT-39, Feb. 1991, pp. 310-314.

[74] J. F. Mara, and J. B. Schappacher, "Broadband microstrip parallel-coupled filters using multi-line sections," *Microwave Journal*, April 1979, pp. 97-99.

[75] K. K. Pang, "Design of microwave filters by sine-plane approach," *IEEE Trans. Microwave Theory Tech.*, MTT-21, No. 10, October 1973, pp. 607-611.

[76] C-Kc. Tzuang, and W-T. Lo, "Printed circuit realization of tapped combline bandpass filter," *IEEE Microwave Theory Tech. Symposium,* MTT (S)-1990, Digest of papers, pp. 131-134.

[77] E. G. Cristal and S. Frankel, "Design of hairpin-line and hybrid hairpin-parallel-coupled-line filters," *IEEE Microwave Theory Tech. Symposium,* MTT (S)-1990, Digest of papers, pp. 12-13.

[78] J. S. Hong and M. J. Lancaster, Microstrip Filters for RF/Microwave Applications, Wiley, New York, 2001.

[79] S. B. Cohn, " Parallel-coupled transmission line resonator filter, " IRE Trans. Microwave Theory Tech., vol. 6, pp. 223-231, Apr., 1958.

[80] W. Schwab, " Full wave design of parallel coupled Microstrip bandpass filters with aligned input and output lines," *Proc. 26th Eur. Microwave Conf.*, pp. 418-421, 1996.

[81] R. W. Rhea, HF filter design and computer simulation, McGwar-Hill, New York, 1995.

[82] J.S. Park, J. Kim, J. Lee, S. Myung, "A novel equivalent circuit and modeling method for defected ground structure and its application to optimisation of a DGS lowpass filter," *IEEE Microwave Theory Tech. Symposium Dig.,* pp. 417-420, MTT (S)-2002.

[83] J. S. Yun, G. Y. Kim, J.S. Park, D. Ahn, K. W. Kang and J. B. Lim, "A design of the novel coupled line bandpass filter using defected ground structure," *IEEE Microwave Theory Tech. Symposium,* MTT (S)-2000.

[84] F. R. Yang, R. Coccioli, Y. Qian and T. Itoh, "Analysis and application of coupled microstrips on periodically patterned ground plane," *IEEE Microwave Theory Tech. Symposium,* MTT (S)-2000.

[85] A. Abdel-Rahman, A. K. Verma, A. Boutejdar and A. S. Omar, "Compact Stub Type Microstrip Bandpass Filter Using Defected Ground Plane," *IEEE Microwave Wireless Comp. Lett*., vol. 14, NO. 4, pp. 136-138, April 2004.

[86] G. A. Deschamp, " Microstrip Microwave Antennas", Proc. 1953 Antenna Applications Symp., Sept. 1953.

[87] H. Gutton and G. Baissinot, " Flat Aerial for Ultra High Frequencies", French patent No. 703113, 1955.

[88] Munson, R. E., " Conformal Microstrip Antennas and Microstrip Phased Arrays," *IEEE Trans. On Antennas and Propagation*, 1974, vol. 22, No. 1, pp. 74-78.

[89] D. M. Pozar, and B. Kaufmann, " Increasing the Bnadwidth of a Microstrip Antenna by Proximity Coupling," *Electron. Lett.*, 1987, vol.23, No. 8, pp. 368-369.

[90] D. M. Pozar, "A review of Aperture Coupled Microstrip Antennas: History, Operation, Development, and Applications," University of Massachusetts at Amherst, Amherst, MA 01003, May 1996, 12 p.

[91] http://www.eutelsat.com, Summary Characteristics of the Eurobird™ Satellite.

[92] Rogers Corporation, High Frequency Circuit Materials Product Selector Guide, 1991-2002.

[93] R. A. Sainati, CAD of Microstrip Antenna for Wireless Applications, Artech House, Boston. London, 1996.

[94] C. A. Balanis, Antenna Theory Analysis and Design, John Willy & Sons, 2nd Ed., 1997, Chap. 14.

[95] E. O. Hammerstadt, "Equations for Microstrip Circuit Design," *Proc. 5th European Microwave Conf.*, Sept. 1975, pp. 268-272.

[96] H. A. Wheeler, "Transmission Line Properties of Parallel Strips Strips Separated by a Dielectric Sheet," *IEEE Trans. On Microwave Theory and Tech.*, 1965, vol. 13, No. 2, pp. 172-185.

[97] D. R. Jackson, and N. G. Alexopoulos. "Simple Approximate Formulas for Input Resistance, Bandwidth, and Efficiency of a Resonant Rectangular Patch," *IEEE Trans. On Antennas and Propagation*, 1991, vol. 39, No. 3, pp. 407-410.

[98] E. Lier, and K. R. Jacobson, "Rectangular Microstrip Patch Antenna with Infinite and Finite Ground Plane Dimensions," *IEEE Trans. On Antennas and Propagation*, 1983, vol. 31, No. 6, pp. 978-984.

[99] J. Huang, " The finite Ground Plane Effect on the Microstrip Antenna Radiation Pattern," *IEEE Trans. On Antennas and Propagation*, 1983, vol. 31, No. 4, pp. 649-653.

[100] K. C. Gupta, R. Garge, I. Bahl, and P. Bhartis, Microstrip Lines and Slotlines, Second Edition, Artech House, Boston, 1996.

[101] I. J. Bahl, and R. Garge, "Simple and Accurate Formulas for Microstrip with Finite Strip Thickness," *Proc. IEEE*, 1977, vol. 65, pp. 1611-1612.

[102] R. K. Hoffmann, Handbook of Microwave Integrated Circuit, Artech Hous, 1987.

[103] D. H. Schrader, Microstrip Circuit analysis, Washington State University, Printice-Hall, Inc., 1995.

[104] M. Kirschning, and R. H. Jansen, "Accurate Model for Effective Dielectric Constant of Microstrip with Validity up to Millimeter-Wave Frequencies," *Electron. Lett.*, 1982, vol. 18, No. 6, pp. 272-273.

[105] R. Jansen, and M. Kirsching, "Arguments and an Accurate Mathematical Model for the Power Current Formulation of Microstrip Characteristic Impedance," *Arch. Elek. Übertragung.*, 1983, Band 37, Heft ¾, s. 108-112.

[106] K. C. Gupta, R. Garge, and I. J. Bahl, Microstrip Lines and Slotlines, Norwood, MA: Artech House, 1979.

[107] P. L. Sullivan, and D. H. Schaubert, "Analysis of an Aperture Coupled Microstrip Antenna," *IEEE Trans. On Antennas and Propagation*, 1986, vol. 34, No. 8, pp. 977-984.

[108] D. M. Pozar, "A reciprocity Method of Analysis for Printed Slot and Slot-Coupled Microstrip Antennas," *IEEE Trans. On Antennas and Propagation*, 1986, vol. 34, No. 12, pp. 1439-1446.

[109] Computer Simulation Technology MicroWave Studio™, Version 3 and 4.

[110] M. Kirschning, R. H. Jansen, N. H. L. Koster, "Accurate Model for Open End Effect of Microstrip Lines," *Electron. Lett.*, 1981, vol. 17, No. 3, pp. 123-125.

[111] T. Weiland, "A Discretization Method for the Solution of Maxwell's Equations for Six-Component Fields," *Electronics and Communication*, (AEÜ), 1977, vol. 31, pp. 116-120.

[112] G. Kossiavas, F. Croq, D. L. S. Luk, and A. Papiernik, "Large Bandwidth Stacked Printed Antennas," *Proc. ISAP'*89, Tokyo, 1989, pp. 21-24.

[113] H. D. Hristov, G. S. Kirov, "Short Backfire Antenna," *Certificat of Invention of P. R. Bulgaria.* No 44 853, December 1987.

[114] R. S. Elliot, *An Introduction to Guided Waves and Microwave Circuits,* Prentice-Hall Inc., New Jersey, 1993.

[115] H. Hristov, E. Altimirski, *Radio-Engineering Electrodynamics and Propagation of the Electromagnetic Waves,* Technika, Sofia, 1990.

[116] *Microwave Office*, 2002.

[117] A. Abdel-Rahman and A. S. Omar, "Improving the Radiation and Matching Characteristics of Antenna Arrays for Satellite Communication with Moving Vehicles," *IEEE, AP-S 2002*, pp. 656-659.

[118] A. Abdel-Rahman and A. K. Verma and A. S. Omar, "High Gain Wideband Compact Microstrip Antenna with Quasi-Planner Surface Mount Horn," *IEEE, MTT-S 2003*, pp. 571-574.

[119] Rod B. Waterhouse, D. Novak, A. Nirmalathas, and C. Lim, "Broadband Printed Sectorized Coverage Antennas for Millimeter-Wave Wireless Applications," *IEEE Trans. AP. 2002*, vol. 50, NO. 1, pp. 12 – 16.

[120] E. Chang, S. A. Long, and W. F. Richards, "An experimental investigation of electrically thick rectangular microstrip antennas," *IEEE Trans, Antennas and Propagation*, vol. AP-34, No. 6, pp. 767-772, June 1986.

[121] A. K. Bahattacharyya, and L. Shafai, "Surface Wave Coupling Between Circular Patch Antennas," *Electronics Letters*, vol. 22, 1986, pp. 1198-1200.

[122] J. R. James, P. S. Hall, and C. Wood, Microstrip Antenna Theory and Design, *Electromag. Waves Series* 12, Peregrinus, 1981.

[123] E. Hammerstadt, " Computed-Aided Design of Microstrip Couplers with Accurate Discontinuity Models," *IEEE MTT-S Int. Microwave Symp. Dig.*, 1981, pp. 54-56.

[124] A. Abdel-Rahman, A. K. Verma and A. S. Omar, "Compact High Gain Microstrip Array for Satellite Communication And Automotive Radar Applications," *Proc. Russian Scient. Conf., The Contemporary Problems of Physics and the High Technologies*, Tomsk, Russia, Oct. 2003, pp. 333-336.

Curriculum Vitae

05.08.1968	Born in Aswan, Egypt
Mai 1991	*B. Sc*. Electronics and Communication Engineering Department, Faculty of Engineering-Assiut University, Egypt
June 1993-	Assistant Lecturer, High Institute of Energy, Aswan, Egypt.
August 1998	*M. Sc.* Electrical Engineering-Title: "Design of Robust Prescribed Eigenstructure Controller for Interconnected Power System". Electrical Engineering Department, Faculty of Engineering-Assiut University, Egypt
November 1999-	*Ph.D* student *at* Microwave and Communication Engineering Department, FEIT, IESK, University of Magdeburg, Magdeburg, Germany.

Publications

[1] A. Abdel-Rahman and A. S. Omar, "Improving the Radiation and Matching Characteristics of Antenna Arrays for Satellite Communication with Moving Vehicles," *IEEE, AP-S 2002*, pp. 656-659.

[2] A. Abdel-Rahman and A. K. Verma and A. S. Omar, "High Gain Wideband Compact Microstrip Antenna with Quasi-Planar Surface Mount Horn," *IEEE, MTT-S 2003*, pp. 571-574.

[3] A. Abdel-Rahman, A. K. Verma, G. S. Kirov and A. S. Omar, "Aperture Coupled Microstrip Antenna With Quasi-Planar Surface Mounted Horn," *in Proceedings 33 th European Microwave Conference, Munich*, Oct. 2003. pp. 1377-1380.

[4] G. S. Kirov, A. Abdel-Rahman and A. S. Omar, "Wideband Aperture Coupled Microstrip Antenna," *IEEE, AP-S 2003*.

[5] A. Abdel-Rahman, A. K. Verma, A. Boutejdar and A. S. Omar, "Control of Band Stop Response of Hi-Low Microstrip Lowpass Filter Using Slot in Ground

Plane," *IEEE Trans. Microwave Theory Tech*., vol. 52, No. 3, pp. 1008-1013, Mar. 2004.

[6] A. Abdel-Rahman, A. K. Verma and A. S. Omar, "Compact High Gain Microstrip Array for Satellite Communication And Automotive Radar Applications," *Proc. Russian Scient. Conf., The Contemporary Problems of Physics and the High Technologies*, Tomsk, Russia, Oct. 2003, pp. 333-336.

[7] G. S. Kirov, A. S. Omar and A. Abdel-Rahman, "Receiving Antennas for Satellite Communications with Mobile Vehicles," *Proc. Russian Scient. Conf. " Physic of Radiowaves*", 23-28 Sept. 2002, Tomsk, Russia, pp. VII.5 –VII.8.

[8] A. Abdel-Rahman, A. K. Verma, A. Boutejdar and A. S. Omar, "Compact Stub Type Microstrip Band-pass Filter Using Defected Ground Plane," *IEEE Microwave Wireless Comp. Lett*., vol. 14, NO. 4, pp. 136-138, April 2004.

[9] A. Abdel-Rahman, A. K. Verma and A. S. Omar, "Gain Enhancement of Microstrip Antenna Array Using Surface Mounted Horn," accepted for publication *in 34 th European Microwave Conference, Amsterdam*, Oct. 2004 PP. 1345-1348.

[10] A. Abdel-Rahman, A. Boutejdar, A. K. Verma, G. Nadim and A. S. Omar, "Improved Circuit Model for DGS based Low-pass Filter," *IEEE, AP-S 2004*, pp. 998-1001.

[11] A. S. Slavova, A. Abdel-Rahman, A. S. Omar, "Bandwidth Enhancement of an Aperture-Coupled Microstrip Patch Antenna," *IEEE, AP-S 2004*, pp. 3737-3740.

[12] G. S. Kirov, A. Abdel-Rahman, G. Nadim and A. S. Omar, "Impedance Matching Improvement for A Classs of Wideband Antennas," *IEEE Antennas and Propagation Magazine,* vol. 46, NO. 6, pp. 98-101, December 2004.

[13] A. Abdel-Rahman, A. R. Ali, S. Amari and A. S. Omar "Compact Bandpass Filters Using Defected Ground Structure (DGS) Coupled Resonators," accepted for publication in *IEEE, MTT-S 2005.*

Magdeburg, 28.02.2005

MSc. Adel Abdel-Rahman